博士論文

Entropy of Hawking radiation in entangled disjoint universes and the island formula

(エンタングルした分離宇宙におけるホーキング放射のエントロピーとアイランド公式)

宮田晃宏

Contents

1 Introduction

The black hole information paradox is one of the most important problems in quantum gravity. The starting point of the paradox is the entropy of a black hole, that is, the Bekenstein-Hawking entropy [1–4],

$$S_{BH} = \frac{A}{4G_N}, \tag{1.1}$$

where A denotes the area of the black hole horizon. The existence of such an entropy suggests that a black hole looks like a thermal object and thus has a temperature, which is called the Hawking temperature. This temperature means that a black hole radiates, and such radiation is known as the Hawking radiation [1, 2]. Through Hawking radiation, a black hole evaporates. Hawking argued that quantum information inside a black hole would be destroyed during the (formation and) evaporation process of the black hole, and thus the von Neumann entropy of the system increases without bound under the process. Such an increase of the entropy (or loss of quantum information) is contradicted with the unitary time evolution of quantum gravity, and the contradiction is known as the black hole information paradox. In other words, such an increase of the entropy implies that a quantum state of the system evolves from a pure state to a mixed state eventually, which cannot be achieved by unitary evolution.

Since the discovery of Hawking radiation, many people have studied the von entropy of Hawking radiation. In the progress of the study, by using a toy model, Page showed that the von Neumann entropy of the Hawking radiation initially should increase and after some critical time, which is called the Page time, the entropy should decrease [5][1]. The entropy behavior is known as the Page curve. If the entropy follows the Page curve, we do not naively encounter the information paradox. Therefore we are interested in how we derive the Page curve by using a semi-classical description of gravity, not the toy model. The recent developments show that the island formula, which we mainly focus on in this thesis, enables us to derive the Page curve using a semi-classical description.

To introduce the island formula, we should go back to Ryu-Takayanagi/Hubeny-Ryu-Takayanagi formula and their generalizations [6–10] in the AdS/CFT correspondence [11]. We can calculate the entanglement entropy of a region in a CFT living in the boundary of anti-de Sitter spacetime (AdS). The entanglement entropy is defined by the von Neumann entropy of the reduced

[1]For some types of black holes, after the Page time the entropy should remain unchanged. We will see this behavior in section 2.1.

density matrix for the region and is also known as the fine-grained entropy. In the AdS/CFT correspondence, by using the Ryu-Takayanagi formula, we can also calculate the entropy semi-classically on anti-de Sitter spacetime. This formula tells us that the entropy of a sub-system (subregion) on the AdS boundary, say A, is calculated by finding the minimal extremal surface[2] that extremize and minimize the generalized entropy

$$S_{gen.} = \frac{\text{Area}(\gamma)}{4G_N} + S_{\text{eff}}(\mathcal{E}_A), \tag{1.2}$$

and the generalized entropy evaluated by using the surface gives the von Neumann entropy of the sub-system. Here $\text{Area}(\gamma)$ denotes the area of the surface, and $S_{\text{eff}}(\mathcal{E}_A)$ denotes the von Neumann entropy by using an effective field theory on the background spacetime in the region $\mathcal{E}_A$ bounded by the surface γ and the sub-system A, i.e., $\partial\mathcal{E}_A = \gamma \cup A$. The domain of dependence of the region $\mathcal{E}_A$ is called the entanglement wedge of A. See figure 1.

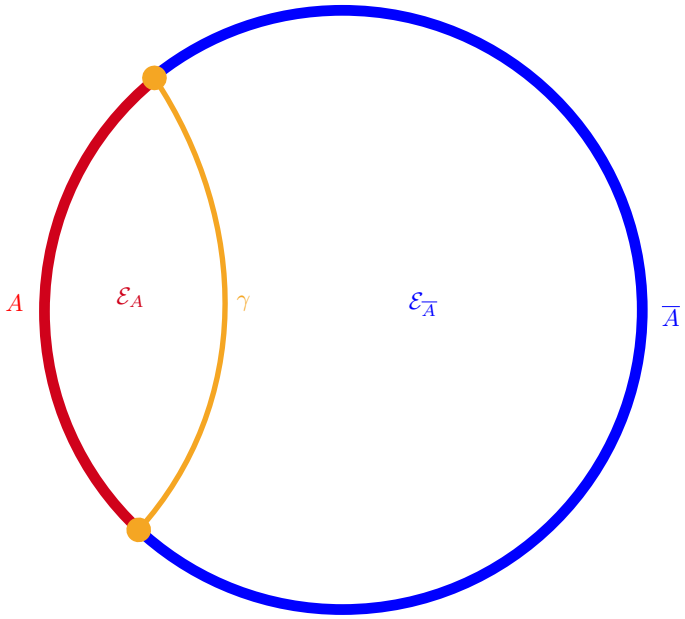

Figure 1: Time slice of AdS spacetime with a boundary region A (red arc) and its complement $\bar{A}$ (blue arc). The minimal extremal surface γ is represented by the orange line. The region bounded by the boundary region A and the extremal surface γ is $\mathcal{E}_A$, and its bulk complement region is $\mathcal{E}_{\overline{A}}$.

In the papers [12, 13], by using such a formula, the authors obtained the von Neumann entropy of a black hole that follows the Page curve within

[2] The extremal surface must satisfy the homology constraint, which means that there is a surface smoothly interpolating between the boundary region and the extremal surface.

the semi-classical gravitational description. Note that the entropy is equal to that of the Hawking radiation since the total state is pure in their setups. Therefore, it turns out that such a formula can be used to calculate the entropy of the Hawking radiation, which does not imply the black hole information paradox and is consistent with the quantum gravity.

An essential ingredient in the calculation is contributions from inside the black hole. In the process of Hawking radiation, entangled Hawking quanta are created inside and outside the black hole horizon. In such a naive picture, as the black hole evaporates, there are many Hawking quanta inside the black hole. They are entangled with the quanta outside the horizon, leading the entropy of the Hawking radiation beyond the Bekenstein-Hawking entropy of the black hole. The behavior implies the black hole information paradox. In such a case, the naive von Neumann entropy of the Hawking radiation measures the *apparent* entanglement between Hawking quanta inside and outside the black hole. However, the calculations of the entropy [12, 13] showed that in calculating the entropy, we must include the contribution from inside the black hole after the Page time, at which the von Neumann entropy of the Hawking radiation is equal to that of the black hole. Such an inclusion implies that, after the Page time, interior degrees of freedom of the black hole, such as the Hawking quanta inside the black hole, are encoded into the Hawking quanta outside the black hole, more precisely the early Hawking radiation, which is the radiation before the Page time. By including such a contribution into the calculation of the entropy, the von Neumann entropy of the Hawking radiation does measure the *true* entanglement between the black hole and the Hawking radiation, not the *apparent* entanglement between Hawking quanta inside and outside the black hole.

As explained above, the contribution from the interior of the black hole is significant. In calculating the entropy of the Hawking radiation, such a contribution is incorporated in what is called the island. It was proposed that the von Neumann entropy $S[R]$ of the Hawking radiation R can be calculated by the following so-called island formula [14][3]

$$S[R] = \mathrm{Min}_I \left\{ \mathrm{Ext}_I \left[\frac{\mathrm{Area}(\partial I)}{4G} + S_{\mathrm{eff}}[R \cup I] \right] \right\}, \tag{1.3}$$

where $\mathrm{Area}(\partial I)$ means the area of the endpoint ∂I of the island I, $S_{\mathrm{eff}}[R \cup I]$ is the von Neumann entropy calculated semi-classically of the region $R \cup I$, $\underset{I}{\mathrm{Ext}}$ means that we choose the regions I which extremize the functional of the region in the square brackets, and $\underset{I}{\mathrm{Min}}$ means that if there are some

[3] See also [15] for a nice review of this formula.

candidates for the region I, then we choose the region I which gives the minimum value of the functional between the candidates I. In later sections, we will explain this formula in detail. For example, as explained in section 2, we can apply this formula to the AdS black hole coupled to the heat bath (see figure 2), and get the von Neumann entropy following the Page curve.

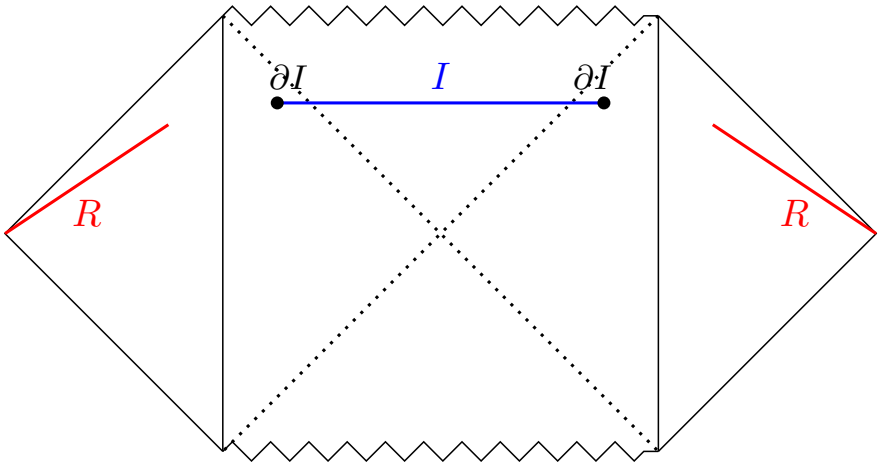

Figure 2: The Penrose diagram of the AdS black hole coupled to the flat bath spacetimes with the regions R (red region) and I (blue region). Before the Page time, the island region is empty. After the Page time, the island region I becomes non-empty.

Let us briefly explain why we can get the von Neumann entropy following the Page curve by using the island formula. Before the Page time, by the extremization and minimization in the island formula, we get the *empty* island region. In this case, since there is no contribution from the region I, the island formula (1.3) becomes $S[R] = S_{\text{eff}}[R]$, and this implies the Hawking-like growth of the entropy. If the story ends here, we run into the black hole information paradox again, but that is not the case. After the Page time, after which the island contribution becomes essential, by the extremization and minimization in the island formula, we obtain the *non-empty* island region, and the island formula (1.3) becomes $\text{Area}(\partial I)/4G + S_{\text{eff}}[R \cup I]$, where the island region I almost covers the region behind the black hole horizon[4]. In this case, because the endpoint of the island region almost coincides with the location of the black hole horizon, we can approximate the area term $\text{Area}(\partial I)/4G$ as the Bekenstein-Hawking entropy S_{BH} [5]. Moreover, because

[4]The detail properties of the island region depend on the model what we consider, but typically the non-empty island cover the region behind the black hole horizon.

[5]If we consider a two-sided black hole as figure 2, the black hole entropy is given by

the spatial region $R \cup I$ covers almost all of a Cauchy slice, the von Neumann entropy $S_{\text{eff}}[R \cup I]$ becomes very small compared to the Bekenstein-Hawking entropy; thus, we can neglect this von Neumann entropy. Therefore, after the Page time, the island formula becomes $S[R] = S_{BH}$. In summary, before the Page time, the island region I is empty, and thus the von Neumann entropy increases, but after the Page time, the island region is no longer empty, and thus the von Neumann entropy does not increase, and it is given by the Bekenstein-Hawking entropy. In later sections, we will see that the actual calculations correspond to the description given above in specific settings.

As noted above, the black hole interior degrees of freedom are encoded into the early Hawking radiation after the Page time. In other words, after the Page time, we can access the interior degrees of freedom from the early Hawking radiation. We can see this statement more explicitly by using the entanglement wedge reconstruction (conjecture) [15–17][6]. To explain entanglement wedge reconstruction, we consider the situation depicted in figure 1. In this situation, the entanglement wedge states that bulk operators in the region $\mathcal{E}_A$ (or $\mathcal{E}_{\overline{A}}$) can be expressed in terms of operators in the region A (or $\overline{A}$). The relation between operators in two regions would be very complicated generally, but there are some proposals for the relation, e.g., the Petz map [20,21], the modular flow [22,23]. By applying this entanglement wedge reconstruction to a black hole setup, operators in the (bulk) island region I, which corresponds to the region $\mathcal{E}_A$, can be expressed in terms of operators in the region R, which corresponds to the region A. In the paper, [24], using a simple gravitational model, the authors considered the entanglement wedge reconstruction to explicitly reconstruct operators in the island region from the Hawking radiation.

The island formula seems to have solved the black hole information paradox in the sense that it can derive the Page curve within a semi-classical description, but the island formula does not reveal all of the paradox. For example, it does not yet reveal the structure of the quantum state of a black hole system, such as matrix elements of the density matrix of the Hawking radiation. Therefore, we need to further investigate the black hole information paradox, in addition to the island formula itself, from various perspectives.

---

the twice the Bekenstein-Hawking entropy $2S_{BH}$, since there are two horizons in such a black hole.

[6]This conjecture is a "quantum" version of the HKLL bulk reconstruction [18, 19] in the AdS/CFT correspondence.

Outline of this thesis

In this thesis, we study the island formula, the entropy of Hawking radiation, and also the entropy of a black hole from two perspectives. Below we briefly explain them and their results.

Disjoint universe setup in Asymptotically Flat Black Hole

Firstly we focus on a disjoint setup for a black hole in asymptotically flat two-dimensional dilaton gravity, and under the setup, we will study the von Neumann entropy. We need to explain the disjoint setup firstly. The disjoint setup is firstly introduced in the papers [25, 26] and the authors consider black holes in AdS spacetime [25] and dS spacetime [26]. The disjoint setup is thought to be an idealized version of the evaporation of a black hole by Hawking radiation. In the setup, we consider two universes, say A and B, and assume that the universe A is non-gravitating, B is gravitating and contains a black hole, and the matter states on two universes A and B are entangled with each other. The entanglement of matter states between the two universes mimics the entanglement between a black hole and its Hawking radiation.

In this thesis, we use the setup for a black hole in asymptotically flat two-dimensional dilaton gravity based on our paper [27]. For concreteness, we consider the CGHS model [28] as the gravitational sector. In the setup, we will study the von Neumann entropy of the universe A or the universe B, which corresponds to the entropy of the Hawking radiation or that of the black hole, respectively. The resulting von Neumann entropy follows the Page curve as a function of the strength of the entanglement between the two universes[7].

We also investigate how the von Neumann entropy is modified when the entanglement between the universes is changed by an operation called local quench in the universe B. The resulting von Neumann entropy shows that the local quench "accelerates" the evaporation of the black hole in our setup.

The Island formula and Baby Universes

Next, based on our paper [29], we reconsider an ensemble of states appearing in a semi-classical description of a black hole by introducing new degrees

[7]The Page curve as a function of the strength of the entanglement is close to the original work by Page [5].

of freedom, which we call the baby universe, and discuss the relationship between the island formula and the baby universe. We also discuss some physical implications of the baby universe.

The introduction of the baby universe is related to the chaotic dynamics of a black hole. In the semi-classical description of a system consisting of a black hole and its Hawking radiation, the dynamics of a black hole are so chaotic that it is natural to describe the state of the system by an ensemble of semi-classically indistinguishable states. Indeed, such an ensemble description of the state of the system is used to derive the Page curve for typical states in the original Page's paper [5].

If we accept the existence of the ensemble literally, the naive von Neumann entropy does not follow the Page curve, and we get Hawking's result that implies the black hole information paradox. To get the Page curve, we need to consider a different way of treating the ensemble when calculating the von Neumann entropy.

We can consider such a treatment of the ensemble by introducing new auxiliary systems, which we call the baby universe. By introducing the baby universe, we can purify the original system consisting of the black hole and the Hawking radiation. Then we can get the von Neumann entropy following the Page curve by dividing the system, which includes the baby universe, into two parts appropriately.

Besides the fact that the entropy following the Page curve can be obtained by introducing the baby universe, there are several other implications. For example, we can consistently consider the gravitational dressing of operators in the island region, as explained later. In general, in the paper [30], it was proposed that such gravitational dressing would be inconsistent with the island formula. However, our prescription using the baby universe avoids the paradox.

Organization of this thesis

In section 2, we briefly review the recent progress of the information paradox and its resolution by the island formula in an AdS/CFT setup. In section 3, we consider a black hole in asymptotically flat two-dimensional dilaton gravity by using the disjoint setup, and we calculate the von Neumann entropy of the universe A (B). We also study the von Neumann entropy of the universe A (B) under local quench and discuss its physical interpretation. In section 4, we reconsider the treatment of an ensemble of states in a black hole plus Hawking radiation system by introducing the baby universe, and we calcu-

late the von Neumann entropy under the presence of the baby universe and discuss the relationship between the baby universe and the island formula. We also explain some physical implications. In section 5, we summarize our results and suggest future directions.

2 The Black Hole Information Paradox and the Island formula

In this section, we review the recent progress of the black hole information paradox. In particular, we see that the correctly calculated entropy of Hawking radiation follows the Page curve, not the Hawking result.

For simplicity, to calculate the entropy of Hawking radiation explicitly, in 2.1 we consider the setup discussed in the paper [31][8]. We consider AdS spacetime coupled to two external flat spacetimes in the setup.

2.1 AdS_2 Black Hole coupled to Non-gravitating Baths CFT_2

The gravitational model which we consider is two dimensional Jackiw-Teitelboim gravity, whose action is given by

$$I_{JT} = \frac{1}{16\pi G_N}\int d^2x\sqrt{-g}\left[\Phi R + 2\left(\Phi-\phi_0\right)\right], \tag{2.1}$$

where ϕ_0 is a just constant corresponding to the extremal entropy. The boundary conditions of the dilaton ϕ and the metric $g_{\mu\nu}$ are given by the usual ones [35]

$$\begin{aligned}\left(\Phi-\phi_0\right)|_{bdy} &= \frac{\phi_r}{\varepsilon_{\text{cut}}}\\ g_{uu}|_{bdy} &= -\frac{1}{\varepsilon^2_{\text{cut}}},\end{aligned} \tag{2.2}$$

where ε_{cut} is a cutoff, ϕ_r is a just constant corresponding to the renormalized dilaton value, u is a physical boundary time.

A two-dimensional matter CFT lives on the gravitational system and couples to the metric, but not the dilaton. The CFT matter plays the role of Hawking quanta. For simplicity and convenience, we assume that the matter

[8]See also, e.g., [32–34] for the related discussions.

CFT is holographic, whose central charge is large $c \gg 1$ and whose CFT spectrum is sparse [36].

The same CFT also lives in two external flat spacetimes, which are non-gravitating and coupled to the gravitational system at the AdS boundaries with the transparent boundary condition[9]. See figure 3. The two external flat spacetimes play a role of a heat bath in equilibrium with the black hole. The boundary condition allows the CFT matter to move freely between two spacetimes.

Then the total action is given by

$$I = I_{JT}[g_{\mu\nu}, \Phi] + I_{CFT}[g_{\mu\nu}, \chi], \tag{2.3}$$

where we denote the CFT field by χ. Using this setup and a semi-classical description of gravity, we consider an eternal AdS black hole coupled to the two external flat spacetimes. The CFT matter state on this background spacetime is the Hartle-Hawking state. See figure 3 again. They mimic an eternal black hole in asymptotically flat spacetime. In the combined system, we calculate the von Neumann entropy of Hawking radiation, which is also often called the entanglement entropy.

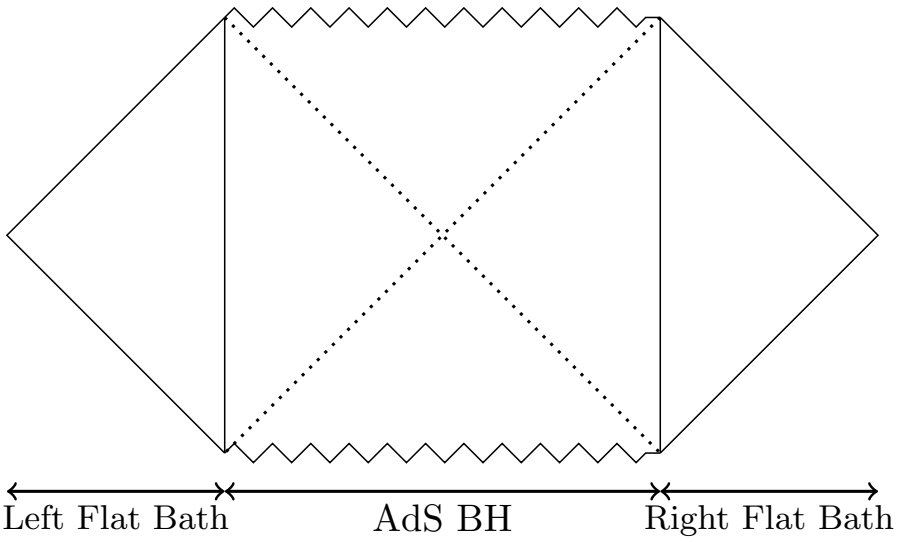

Figure 3: Penrose diagram of the AdS eternal black hole coupled to the baths, which are half of Minkowski spacetime.

[9]Note that, in usual AdS/CFT setups, we usually impose the reflecting boundary condition, by which matters on AdS spacetime are reflected back to the AdS spacetime.

2.1.1 Black hole in Jackiw-Teitelboim gravity

To introduce the black hole solution, we need to focus on the equations of motion for (2.3) given by

$$R + 2 = 0, \tag{2.4}$$

$$\nabla_\mu \nabla_\nu \Phi - g_{\mu\nu} \nabla^2 \Phi + g_{\mu\nu}(\Phi - \phi_0) = 8\pi G_N \langle T_{\mu\nu} \rangle, \tag{2.5}$$

where we defined the expectation value of the CFT stress-energy tensor by

$$\langle T_{\mu\nu} \rangle = \frac{2}{\sqrt{-g}} \frac{\delta}{\delta g^{\mu\nu}} \log Z_{\text{CFT}}. \tag{2.6}$$

The first equation (2.4) can be satisfied by taking the metric to be Poincare coordinates

$$\begin{aligned} ds^2 &= \frac{-dt^2 + dz^2}{z^2}, \\ &= \frac{4dx^+ dx^-}{(x^+ + x^-)^2}, \end{aligned} \tag{2.7}$$

where, in the second line, we introduced coordinates defined by $x^\pm = z \pm t$. The Poincare coordinates cover a part of AdS_2 spacetime, and, unlike the usual one, the coordinate z is negative $z < 0$, or equivalently $x^+ + x^- < 0$. See figure 4.

Since we are interested in an eternal black hole solution, we consider the case that the stress-energy tensor vanishes $\langle T_{\mu\nu} \rangle = 0$ for the coordinates in AdS spacetime. In this case, we can easily solve the second equation (2.5), and the general solution is given by [35, 37]

$$\Phi = \phi_0 + \frac{A + B(x^+ + x^-) + C x^+ x^-}{x^+ + x^-}, \tag{2.8}$$

where A, B, C are constants. For later convenience, by taking the constants to be $A = -2\phi_r$, $B = 0$, $C = -2\phi_r \left(\frac{\pi}{\beta}\right)^2$, and we consider the dilaton profile

$$\begin{aligned} \Phi &= \phi_0 - 2\,\phi_r \frac{1 + \left(\frac{\pi}{\beta}\right)^2 x^+ x^-}{x^+ + x^-} \\ &= \phi_0 - \phi_r \frac{1 - \left(\frac{\pi}{\beta}\right)^2 (t^2 - z^2)}{z}, \end{aligned} \tag{2.9}$$

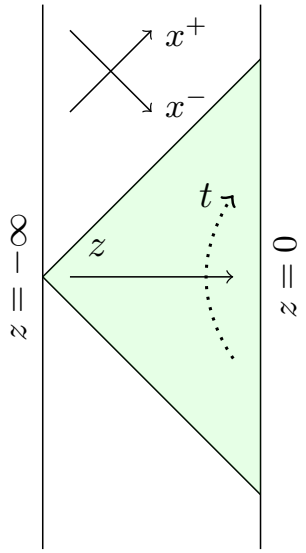

Figure 4: The Penrose diagram of the AdS_2 spacetime. The green shaded region is covered by the Poincare patch corresponding to the Poincare coordinates (2.7).

where β is a constant related the inverse temperature of the black hole. In the limit $z \to 0$, we can see that this dilaton profile is consistent with the boundary condition of the dilaton (2.2).

In JT gravity, the geometry of a black hole is characterized by the corresponding dilaton profile. From the dilaton profile (2.9), we check that it actually corresponds to an eternal black hole [37]. Before staring it, we note that in JT gravity (, or more generally two-dimensional dilaton gravity), the vector $\xi = \xi^\mu \partial_\mu = \epsilon^{\mu\nu} \partial_\nu \Phi \, \partial_\mu$ is a Killing vector for the metric [38], owing to the equation (2.5) with the vanishing stress-energy tensor.

At first, the location of the (Killing) horizon is a null surface on which the Killing vector ξ is null,

$$g_{\mu\nu} \xi^\mu \xi^\nu = 0 \quad \text{at the horizon,} \tag{2.10}$$

and the bifurcation surface is the fixed point of the Killing vector

$$\xi = 0 \qquad \text{at the bifurcation surface,} \tag{2.11}$$

or equivalently

$$\partial_\mu \Phi = 0 \qquad \text{at the bifurcation surface.} \tag{2.12}$$

Next, the the singularity is located at

$$\Phi = 0 \qquad \text{at the singularity.} \tag{2.13}$$

For the dilaton profile (2.9), the bifurcation surface is located at

$$x_H^{\pm} = -\frac{\beta}{\pi} \qquad \Longleftrightarrow \qquad t_H = 0,\ z_H = -\frac{\beta}{\pi}, \tag{2.14}$$

the horizons at $x^+ = -\frac{\beta}{\pi}$ and $x^- = -\frac{\beta}{\pi}$. The locus of the singularity is given by

$$\left(x^+ - \frac{\phi_0}{2\phi_r}\left(\frac{\beta}{\pi}\right)^2\right)\left(x^- - \frac{\phi_0}{2\phi_r}\left(\frac{\beta}{\pi}\right)^2\right) = \left(\frac{\beta}{\pi}\right)^2\left(1 + \left(\frac{\beta\phi_r}{2b\phi_r}\right)^2\right). \tag{2.15}$$

These discussions give the Penrose diagram for the eternal black hole described by the dilaton profile (2.9), see figure 5.

In considering the black hole, it is convenient to introduce the static coordinates, which cover the exteriors of the black hole. They are related to the Poincare coordinates through

$$x^{\pm} = \frac{\beta}{\pi}\tanh\frac{\pi y^{\pm}}{\beta}, \tag{2.16}$$

and this coordinates system covers the right exterior of the black hole[10]. We note that, in the static coordinates, the inequality $x^+ + x^- < 0$ implies $y^+ + y^- < 0$. Using this coordinate system, the metric and the dilaton become

$$ds^2 = \left(\frac{2\pi}{\beta}\right)^2 \frac{dy^+ dy^-}{\sinh^2\left(\frac{\pi}{\beta}(y^+ + y^-)\right)}, \tag{2.18}$$

$$\Phi = \phi_0 - \frac{2\pi}{\beta}\phi_r \frac{1}{\tanh\left(\frac{\pi}{\beta}(y^+ + y^-)\right)}, \tag{2.19}$$

and the horizons are at $y^+ = -\infty$ and $y^- = -\infty$. The singularity is not covered by the static patch.

[10]The coordinates that cover the left exterior is given by

$$x^{\pm} = -\frac{\beta}{\pi}\frac{1}{\tanh\frac{\pi y^{\pm}}{\beta}}. \tag{2.17}$$

Note that in the left exterior of the black hole, $y^+ + y^- > 0$.

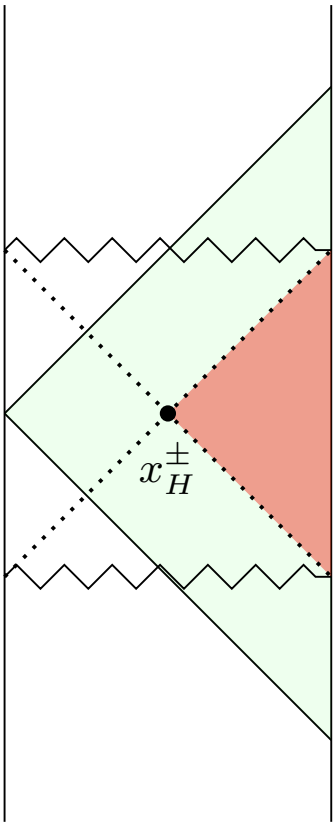

Figure 5: The Penrose diagram of the black hole in AdS_2. The dotted lines are the horizons, the black dot ($x_H^{\pm}$)is the bifurcation horizon, and the wavy lines are singularities. The Poincare patch (2.7) (green shaded region) covers a part of the black hole. The right exterior of the black hole (red shaded region) is covered by the static or the Schwarzschild patches (2.18) or (2.21).

We can also express the dilaton profile in terms of the so-called Schwarzschild coordinates. The Schwarzschild coordinates $r, t_{\rm Sch}$ are related to the static coordinates (2.18) by

$$\tanh\left(\frac{2\pi}{\beta}\sigma\right) = \frac{\beta}{2\pi}r, \qquad \tau = t_{\rm Sch}, \tag{2.20}$$

where $y^{\pm} = \sigma \pm \tau$. In the Schwarzschild coordinates, the metric and the

dilaton become

$$ds^2 = -\left(r^2 - \left(\frac{2\pi}{\beta}\right)^2\right) dt_{\text{Sch}}^2 + \frac{dr^2}{r^2 - \left(\frac{2\pi}{\beta}\right)^2} \tag{2.21}$$

$$\Phi = \phi_0 + \phi_r\, r, \tag{2.22}$$

and the horizons are at $r = \frac{2\pi}{\beta}$, which is the Schwarzschild radius. In the Schwarzschild coordinates, the singularity is also not covered by the patch again.

Since, as we saw above, we determined the location of the horizons, we can evaluate the Bekenstein-Hawking entropy of the black hole (or the black hole entropy), which is given by the dilaton value at the horizon in JT gravity,

$$\begin{aligned} S_{\text{BH}} &= \frac{\Phi|_{\text{Horizon}}}{4G_N} \\ &= \frac{\phi_0 + \frac{2\pi}{\beta}\phi_r}{4G_N}. \end{aligned} \tag{2.23}$$

$\frac{\phi_0}{4G_N}$ is called the extremal entropy, and $\frac{\frac{2\pi}{\beta}\phi_r}{4G_N}$ is called the near-extremal entropy.

Dual description of the Black Hole

In the above analysis, we consider JT gravity in AdS_2. Using the AdS/CFT correspondence, more precisely $NAdS_2/NCFT_1$ [39], we can describe it holographically. The holographic dual is given in this setup by the two quantum mechanical (QM) systems living in the two AdS_2 boundaries. We do not explain it explicitly here.

2.1.2 Coupling to the Baths

Next, we introduce the baths and couple them to the black hole explained above. We note that the two-dimensional matter CFT lives in the bath and black hole regions. We also note that we impose the transparent boundary condition at the boundaries of two regions.

Since the bath we consider here is non-gravitating and flat, we fix the metric to be

$$ds^2 = \frac{dy^+ dy^-}{\varepsilon_{\text{cut}}^2}, \tag{2.24}$$

where we consider the regions $y^+ + y^- = 2\sigma < 0$ and $y^+ + y^- = 2\sigma > 0$ corresponding the left and the right bath respectively, and we introduced the cutoff $\varepsilon_{\rm cut}$ to glue the bath to AdS spacetime with the boundary condition (2.2). At the present stage, these coordinates $y^\pm$ in the bath region are not related to the static coordinates $y^\pm$ (2.18) in the black hole region. However, as we will see, they are related.

Because we are interested in the case that the baths have a temperature and interacts with the black hole, we take the CFT state of the bath region to be in a thermal state in the coordinates $y^\pm$, and thus the stress-energy tensor becomes thermal one, that is,

$$\langle T_{y^\pm y^\pm} \rangle = \frac{\pi c}{12\beta^2} \qquad \text{in the bath region.} \tag{2.25}$$

On the other hand, when we introduced the dilaton profile (2.9) corresponding to the eternal black hole in the Poincare coordinates $x^\pm$, we took the stress-energy tensor to be zero in the black hole region

$$\langle T_{x^\pm x^\pm} \rangle = 0 \qquad \text{in the black hole region.}$$

Now we want to find the coordinate transformation $x^\pm(y^\pm)$ in the black hole region that brings the stress-energy tensor to the thermal one, $\langle T_{y^\pm y^\pm} \rangle = \frac{\pi c}{12\beta^2}$. By using the transformation of the stress-energy tensor

$$\left(\frac{\partial x^\pm}{\partial y^\pm}\right)^2 \langle T_{x^\pm x^\pm} \rangle = \langle T_{y^\pm y^\pm} \rangle + \frac{c}{24\pi} \left\{ x^\pm, y^\pm \right\}, \tag{2.26}$$

we get the condition for the coordinate transformation

$$\left\{ x^\pm(y^\pm), y^\pm \right\} = -\frac{2\pi^2}{\beta^2}, \tag{2.27}$$

where $\{f(x), x\} = -\frac{1}{2}\frac{f''^2}{f'^2} + \left(\frac{f''}{f'}\right)'$ is a Schwarzian derivative. The coordinate transformation (2.16) satisfies the condition (2.27)[11], thus we can use the coordinate transformation (2.16), and the coordinates $y^\pm$ are continued from the bath region into the black hole region. The continued coordinates cover the right exterior of the black hole and the bath regions (see figure 6). By using the coordinates the metric is expressed as

$$ds^2_{\rm right} = \begin{cases} \left(\dfrac{2\pi}{\beta}\right)^2 \dfrac{dy^+ dy^-}{\sinh^2\left(\frac{\pi}{\beta}(y^+ + y^-)\right)} & \text{for} \quad y^+ + y^- < 0, \\ \dfrac{dy^+ dy^-}{\varepsilon^2_{\rm cut}} \quad \text{for} \quad y^+ + y^- > 0. \end{cases} \tag{2.28}$$

[11] A more general solution can be obtained by using the SL(2,$\mathbb{R}$) symmetry, and thus it is given by $\frac{ax^\pm(y^\pm)+b}{cx^\pm(y^\pm)+d}$ with $ad - bc = 1$, where $x^\pm(y^\pm)$ is given by (2.16).

By a similar arguments as above, we can get the expression for the left

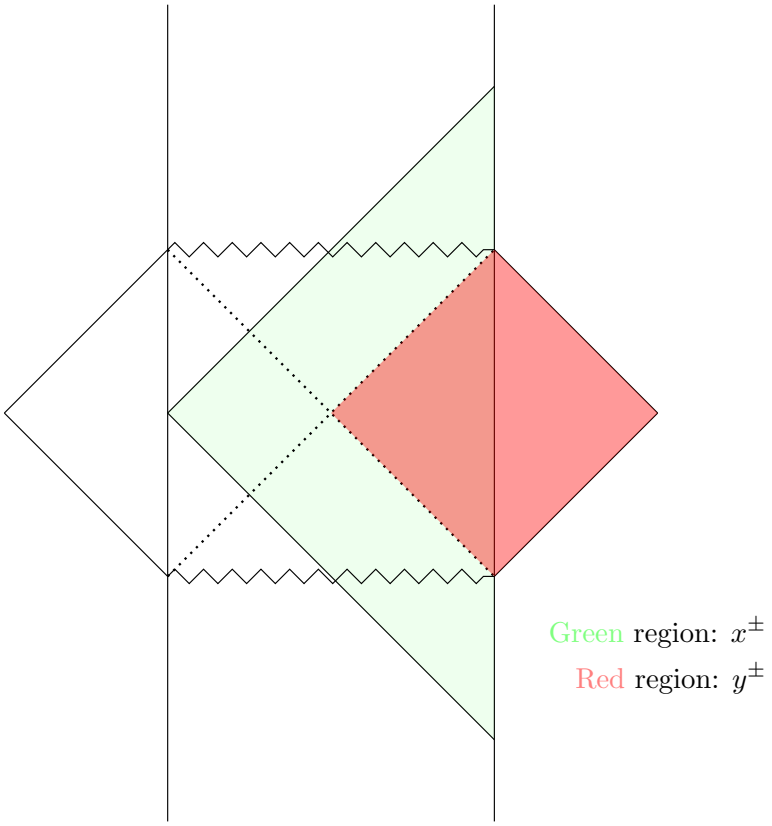

Figure 6: The Penrose diagram of the AdS black hole coupled to the flat bath spacetimes. The Penrose coordinates $x^{\pm}$ cover the green shaded region. The $y^{\pm}$ coordinates (2.28) cover the right exterior of the black hole and the right bath regions (red shaded region). The combined region (red shaded region) is similar to the right Rindler wedge of Minkowski spacetime.

exterior of the black hole and the left bath,

$$ds^2_{\text{left}} = \begin{cases} \left(\dfrac{2\pi}{\beta}\right)^2 \dfrac{dy^+ dy^-}{\sinh^2\left(\frac{\pi}{\beta}(y^+ + y^-)\right)} & \text{for} \quad y^+ + y^- > 0, \\ \dfrac{dy^+ dy^-}{\varepsilon^2_{\text{cut}}} & \text{for} \quad y^+ + y^- < 0. \end{cases} \tag{2.29}$$

Although we got the coordinates that cover the right exterior of the black hole and the right bath regions and that for left, it is more convenient to introduce the coordinates that cover both left and right black hole plus bath

regions in calculating the von Neumann entropy of the Hawking radiation. By considering each black hole plus bath region as each Rindler wedge of Minkowski space, we can get such coordinates. In particular, we can get the coordinates $w^{\pm}$ by the coordinate transformation

$$w^{\pm} = \begin{cases} \exp\left(\dfrac{2\pi y^{\pm}}{\beta}\right) & \text{for the right BH-Bath region,} \\ -\exp\left(-\dfrac{2\pi y^{\pm}}{\beta}\right) & \text{for the left BH-Bath region.} \end{cases} \tag{2.30}$$

In the $w^{\pm}$ coordinates, the region $w^{+} > 0$, $w^{-} > 0$ corresponds to the right black hole plus bath region, and $w^{+} < 0$, $w^{-} < 0$ does to the left one. By using the $w^{\pm}$ coordinates, the metric is given by

$$ds^2 = \begin{cases} \dfrac{4dw^{+}dw^{-}}{\left(1 - w^{+}w^{-}\right)^2} & \text{for the black hole region,} \\ \dfrac{1}{\varepsilon_{\text{cut}}^2}\left(\dfrac{\beta}{2\pi}\right)^2 \dfrac{dw^{+}dw^{-}}{w^{+}w^{-}} & \text{for the bath region,} \end{cases} \tag{2.31}$$

and the dilaton profile is given by

$$\Phi = \phi_0 + \frac{2\pi}{\beta}\phi_r \frac{1 + w^{+}w^{-}}{1 - w^{+}w^{-}}. \tag{2.32}$$

We note that the horizons in the coordinates are at $w^{+} = 0$ and $w^{-} = 0$. See figure 7.

Using the relation (2.26) for $w^{\pm}$ and $y^{\pm}$, we can see that the stress-energy tensor in the $w^{\pm}$ coordinates vanishes

$$\langle T_{w^{\pm}w^{\pm}} \rangle = 0 \qquad \text{in the whole region.}$$

Thus in the $w^{\pm}$ coordinates, the CFT state is not a thermal state but a vacuum one. In this case, on calculating the von Neumann entropy, we can use a simple expression by using the coordinates, as we will see later.

Dual description of the coupling of the black hole with the baths

The black hole coupled to the baths is also holographically described in terms of the quantum mechanical system and the bath CFT_2, which are coupled to each other. In the holographic description, the dual state is given by the thermo-field double (TFD) state on the left and right QM-CFT_2 systems

$$|TFD\rangle = \frac{1}{\sqrt{Z(\beta)}} \sum_n e^{-\beta E_n/2} |E_n\rangle_{\text{Left QM-Bath}} \otimes |E_n\rangle^{*}_{\text{Right QM-Bath}}, \tag{2.33}$$

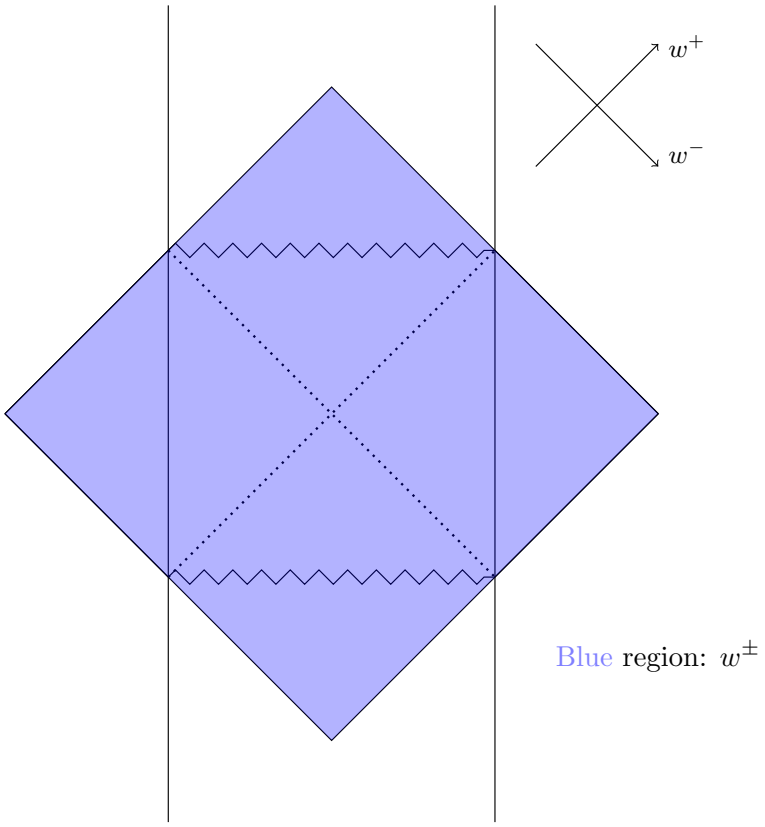

Figure 7: The Penrose diagram of the AdS black hole coupled to the flat bath spacetimes covered by the $w^\pm$ coordinates. The $w^\pm$ coordinates cover both left and right black hole plus bath regions.

where $|E_n\rangle_{\text{Left QM-Bath}} \in H_{\text{Left QM-Bath}}$, $|E_n\rangle_{\text{Right QM-Bath}} \in H_{\text{Right QM-Bath}}$ are the energy eigenstates of the left and right QM-CFT_2 systems with the energy E_n, and $Z(\beta)$ is the normalization factor.

Through the AdS/CFT correspondence, the time evolution of the black hole and the bath systems is expected to be described by the unitary time evolution of this dual state.

2.1.3 the von Neumann entropy of the Hawking radiation

Now that we introduced the setup, we start to calculate the von Neumann entropy of the Hawking radiation. As explained above, by using the $w^\pm$ coordinates, we can simplify the calculation. In particular, after calculating the von Neumann entropy in the $w^\pm$ coordinates, by using the coordinate

transformation (2.30) we transform the result into the one in the physical coordinate $y^{\pm}$.

Before starting the calculation of the von Neumann entropy of the Hawking radiation, we need to specify the region where we calculate the von Neumann entropy. Since we couple the black hole to the baths in thermal equilibrium, the Hawking quanta emitted from the black hole move to the bath region, and they are stored in the bath regions; thus, the black hole appears to lose some energy by the Hawking radiation. However, owing to the thermal equilibrium between the black hole and the baths, the baths provide the black hole with energy which cancels the loss of the energy by the Hawking radiation. Therefore the bath and the black hole exchange the Hawking radiation, leading to the large entanglement between the two systems.

By calculating the von Neumann entropy associated with a bath spatial subregion R, we can study the von Neumann entropy of the Hawking radiation emitted from the black hole. In particular, we take the region R to be semi-infinite and symmetric between the left and right regions, see figure 8. In the $y^{\pm}$ coordinates, let the endpoint of the region ∂R to be $(\tau, \sigma = -b)$ for the left one and $(\tau, \sigma = b)$ for the right one, where b is a positive constant. Fixing the constant b, we consider the time variation of the von Neumann entropy of the Hawking radiation R. We note that since, on a full Cauchy slice, the CFT matter state is pure, which is given by the Hartle-Hawking state as explained at the beginning of this section 2, the von Neumann entropy of the compliment region $\bar{R}$ is equal to that of the original region R.

The above choice of the spatial subregion R on the entire Cauchy slice corresponds to the tensor factorization of a total Hilbert space H into two Hilbert spaces $H = H_R \otimes H_{\bar{R}}$, where $\bar{R}$ is the complement of R. The von Neumann entropy or equivalently the entanglement entropy of the Hawking radiation R (or the complement $\bar{R}$) measures the entanglement between the two systems (regions) R and $\bar{R}$. In other words, it measures the entanglement between the black hole in the region $\bar{R}$ and the Hawking quanta stored in the one R *naively*.

In the holographic description, we can factorize the Hilbert space $H = H_{\text{Left QM-Bath}} \otimes H_{\text{Right QM-Bath}}$ into $H_{\text{Bath Rad }(R)} \otimes H_{\text{QM-Bath Rad }(\bar{R})}$ similarly. We note that in the holographic description, the region $\bar{R}$ does not mean the complement region of the region R on the full Cauchy slice in the black hole plus the bath spacetime, but the region on the quantum mechanical plus the bath spacetimes, see figure 9. The Hilbert space $H_{\text{Bath Rad }(R)}$ corresponds to the radiation region R, which does not include the quantum mechanical systems, in the QM plus the bath CFT_2 system, and $H_{\text{QM-Bath Rad }(\bar{R})}$ does to

its complement region, which includes the quantum mechanical systems. We note that since $H_{\text{QM-Bath Rad }(\bar{R})}$ includes the black hole degrees of freedom, we can call the region associated with the Hilbert space $H_{\text{QM-Bath Rad }(\bar{R})}$ the black hole (region) $BH = \bar{R}$.

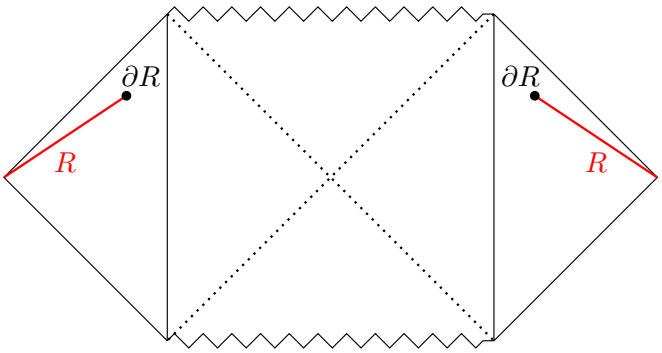

Figure 8: The Penrose diagram of the AdS black hole coupled to the flat bath spacetimes with the region R. The end points of the region ∂R are by the black dots. In the $y^{\pm}$ coordinates, the left endpoint is given by $(\tau, \sigma = -b)$,and the right one is given by $(\tau, \sigma = b)$.

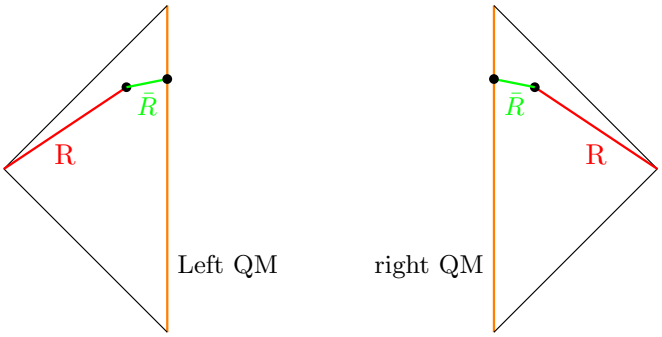

Figure 9: Schematic picture of the subregions R and $\bar{R}$ on the quantum mechanical plus the bath spacetimes. The quantum mechanical systems are are represented by the orange vertical lines. $\bar{R}$ contains the quantum mechanical systems, implying that the region $\bar{R}$ should be regarded as the black hole region $BH = \bar{R}$

Under the above factorization $H_{\text{Bath Rad }(R)} \otimes H_{\text{QM-Bath Rad }(BH)}$, we focus on the von Neumann entropy of the reduced density matrix associated with the Hilbert space $H_{\text{Bath Rad }(R)}$ (or $H_{\text{QM-Bath Rad }(BH)}$). The von Neumann entropy of the Hawking radiation R is given by

$$S(\rho_R) = -\text{tr}_{H_{\text{Bath Rad }(R)}}[\rho_R \log \rho_R], \tag{2.34}$$

where ρ_R is defined for the state (2.33) by tracing out the remaining degrees of freedom

$$\rho_R = \mathrm{tr}_{H_{\text{QM-Bath Rad }(BH)}} \left[U \left| TFD \right\rangle \left\langle TFD \right| U^\dagger \right] . \tag{2.35}$$

Here U is a unitary time evolution operator on the QM plus the bath CFT_2 system. This von Neumann entropy is also called the fine-grained entropy. We note that this von Neumann entropy $S(\rho_R)$ is equal to that of the black hole $S(\rho_{BH})$, where ρ_{BH} is defined by tracing out the Hawking radiation degrees of freedom.

We evaluate the above von Neumann entropy $S(\rho_R)(= S(\rho_{BH}))$ on the gravity side, i.e., by using a semi-classical description of gravity on the AdS plus bath system. We will see that a naive computation of the entropy leads us to a Hawking-like result inconsistent with quantum gravity. As we will see later, we need to introduce the island formula to get the entropy consistent with quantum gravity. Using it, we will check that the entropy of the Hawking radiation is consistent with quantum gravity, i.e., it follows the Page curve.

At first, we calculate the von Neumann entropy of the Hawking radiation R naively for the matter CFT. As noted above, the von Neumann entropy of the region R is equal to that of the complement region consisting of the interval between two points $(\tau, \sigma = -b)$ and $(\tau, \sigma = -b)$. In the $w^\pm$ coordinates with the general metric $ds^2 = \Omega^{-2} dw^+ dw^-$, the CFT von Neumann entropy on the interval $[w_1, w_2]$ is given by

$$S_{\text{CFT}}[w_1, w_2] = \frac{c}{6} \log \left[\frac{|w_{12}|^2}{\varepsilon_{UV}^2 \Omega(w_1^+, w_1^-) \Omega(w_2^+, w_2^-)} \right] , \tag{2.36}$$

where ε_{UV} is a UV cutoff different from one in the JT gravity boundary conditions (2.2), and $|w_{12}|^2$ is defined by $|w_{12}|^2 = \left| (w_1^+ - w_2^+)(w_1^- - w_2^-) \right|$. Note that the CFT von Neumann entropy here means the von Neumann entropy of the matter CFT calculated semi-classically. In appendix A.1, we give the derivation of (2.36). See also, e.g., [13] for another derivation. By using the coordinate transformation (2.30) and the metric (2.31), we can calculate the CFT von Neumann entropy of the Hawking radiation R. For the interval between two points $(\tau, \sigma = -b)$ and $(\tau, \sigma = -b)$, the factors

$w_1,\ w_2,\ \Omega_1,\ \Omega_2$ are given by

$$w_1^{\pm} = -\exp\left(-\frac{2\pi}{\beta}(-b \pm \tau)\right), \qquad w_2^{\pm} = \exp\left(\frac{2\pi}{\beta}(b \pm \tau)\right) \tag{2.37}$$

$$\Omega(w_1^+, w_1^-) = \varepsilon_{\rm cut}\frac{2\pi}{\beta}\sqrt{w_1^+ w_1^-} = \varepsilon_{\rm cut}\frac{2\pi}{\beta}\exp\left(\frac{2\pi}{\beta}b\right), \tag{2.38}$$

$$\Omega(w_2^+, w_2^-) = \varepsilon_{\rm cut}\frac{2\pi}{\beta}\sqrt{w_2^+ w_2^-} = \varepsilon_{\rm cut}\frac{2\pi}{\beta}\exp\left(\frac{2\pi}{\beta}b\right), \tag{2.39}$$

and thus we obtain

$$S_{\rm CFT}[R] = \frac{c}{6}\log\left(\frac{1}{\varepsilon_{UV}^2\varepsilon_{\rm cut}^2}\left(\frac{\beta}{\pi}\right)^2\cosh^2\left(\frac{2\pi}{\beta}\tau\right)\right). \tag{2.40}$$

Naively we expect that this von Neumann entropy $S_{\rm CFT}[R]$ is equal to the entropy $S(\rho_R)$, but this is not correct as we will see below.

We can see that, for late times $\tau \gg \beta$, the CFT von Neumann entropy on the Hawking radiation R linearly growths

$$S_{\rm CFT}[R] = \frac{c}{6}\log\left(\frac{1}{\varepsilon_{UV}^2\varepsilon_{\rm cut}^2}\left(\frac{\beta}{\pi}\right)^2\cosh^2\left(\frac{2\pi}{\beta}\tau\right)\right) \longrightarrow \frac{2\pi}{3}c\frac{\tau}{\beta} + \cdots \qquad \text{for } \tau \gg \beta \tag{2.41}$$

where $\cdots$ are constants which are not depend on time. This linear growth is consistent with the physical intuition that the baths and the black hole exchange the Hawking radiation, and thus the exchange gives the entanglement between the Hawking quanta stored in the baths and the black hole, leading us to the linear growth.

However, the linear growth for sufficiently late times is problematic and implies the black hole information paradox. This is because the *correct* entropy of the complement region $BH(=\bar{R})$, which is equal to that of the Hawking radiation R, must be bounded by the Bekenstein-Hawking entropy of the black hole, $S_{\rm BH}$.

To put it another way, if the entropy is not bounded by the Bekenstein-Hawking entropy, but it linearly grows, then it implies that the initial pure state, which is given by the state (2.33) holographically, becomes a mixed state or a thermal state at a sufficiently late time, leading to linear growth of the von Neumann entropy. Such a time evolution is not unitary, and it is inconsistent with the unitarity of quantum gravity.

Island formula

We need to consider the island formula to get a correct entropy, bounded by the Bekenstein-Hawking entropy. The island formula is given by

$$S(\rho_R) = \underset{I}{\text{Min}} \left\{ \underset{I}{\text{Ext}} \left[\frac{\text{Area}(\partial I)}{4G_N} + S_{\text{CFT}}[R \cup I] \right] \right\}, \tag{2.42}$$

where $\text{Area}(\partial I)$ means the area of the endpoint ∂I of a new region I called the island, $S_{\text{CFT}}[R \cup I]$ is the CFT von Neumann entropy associated with the region $R \cup I$, $\underset{I}{\text{Ext}}$ means that we choose the regions I which extremize the functional of the region in the square brackets, and $\underset{I}{\text{Min}}$ means that if there are some candidates for the region I, then we choose the region I which gives the minimum value of the functional among the candidates I. In JT gravity, the area of the endpoint ∂I is given by the dilaton value at the points.

We note that for the complement region of the radiation region, i.e., BH, we have the quantum extremal surface (QES) formula[12]

$$S(\rho_{BH}) = \underset{\gamma}{\text{Min}} \left\{ \underset{\gamma}{\text{Ext}} \left[\frac{\text{Area}(\gamma)}{4G_N} + S_{\text{CFT}}[\mathcal{E}_{BH}] \right] \right\}, \tag{2.43}$$

where $\text{Area}(\gamma)$ means the area of a codimension two surface γ called the quantum extremal surface (QES), which is homologous to the black hole region BH on the QM plus CFT system, $S_{\text{CFT}}[\mathcal{E}_{BH}]$ means that the CFT von Neumann entropy of the region $\mathcal{E}_{BH}$ bounded by the QES surface γ and the black hole region BH on the QM plus CFT system, and $\underset{\gamma}{\text{Min}}\underset{\gamma}{\text{Ext}}$ means that we choose the QES surface which extremizes the functional in the square brackets and gives the minimal value between some candidates. This entropy is similar to the generalized entropy of the black hole, which is defined by the sum of the Bekenstein-Hawking entropy and the (CFT) matter von Neumann entropy of the region outside the black hole horizon. We note that if the total state is pure, then after the extremalization and the minimization, the resulting island region and the QES surface have properties that $\gamma = \partial I$ and $\overline{(R \cup I)} = \mathcal{E}_{BH}$, which ensure that the entropies derived from the island formula and the QES formula coincide. We use either the island formula (2.42) or the QES formula (2.43) as necessary, which gives the same result in the current setup.

Since if the island region is empty (no island phase), then the island formula is equal to the CFT von Neumann entropy of the region R, $S_{\text{no-island}} =$

[12]We note that if we focus only on a similar formula which includes only the area part, not the CFT von Neumann entropy part, the QES reduced to the so-called classical extremal surface (CES).

$S_{\rm CFT}[R]$, (see figure 10), we consider the case that the island is non-empty (island phase). Although there is a possibility that the island region consists of multiple regions, because in such cases, the area contribution becomes large, we simply consider a region consisting of a single interval. We assume that the endpoints ∂I are symmetric between the left and right regions since the radiation region is symmetric between the left and right ones. See figure 11. In the $y^{\pm}$ coordinates, let the endpoint of the region ∂I to be $(\tau_a, \sigma = a)$ for the left one and $(\tau_a, \sigma = -a)$ for the right one, where a is a positive constant, which is determined by the extremalization and the minimization in the island (or QES) formula.

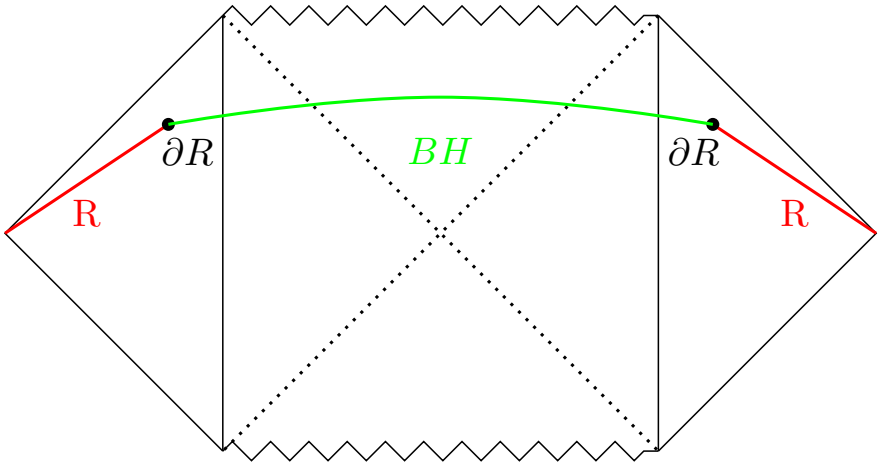

Figure 10: The Penrose diagram of the AdS black hole coupled to the flat bath spacetimes with the regions R (red region), BH (green region) in the empty island case.

Since we need to consider two intervals $R \cup I$ or equivalently BH (see figure 11) by the appearance of the non-empty island region, we can no longer use the expression (2.36). In this case we need to consider the CFT von Neumann entropy on two intervals, whose expression depends on the CFT we consider and is non-universal (see, e.g., [40]). For simplicity we consider the c free Dirac fermions theory, and in the $w^{\pm}$ coordinates with the general metric $ds^2 = \Omega^{-2} dw^+ dw^-$, the CFT von Neumann entropy on the two intervals $[w_1, w_2] \cup [w_3, w_4]$ is given by [41]

$$S_{\rm Fermi.}[w_1, w_2; w_3, w_4] = \frac{c}{6} \log \left[\frac{|w_{12} w_{23} w_{34} w_{14}|^2}{\varepsilon_{UV}^4 \, |w_{13} w_{24}|^2 \, \Omega(w_1^+, w_1^-) \Omega(w_2^+, w_2^-) \Omega(w_3^+, w_3^-) \Omega(w_4^+, w_4^-)} \right]. \tag{2.44}$$

In the w coordinates, the endpoints of two intervals $R \cup I$ (or equivalently

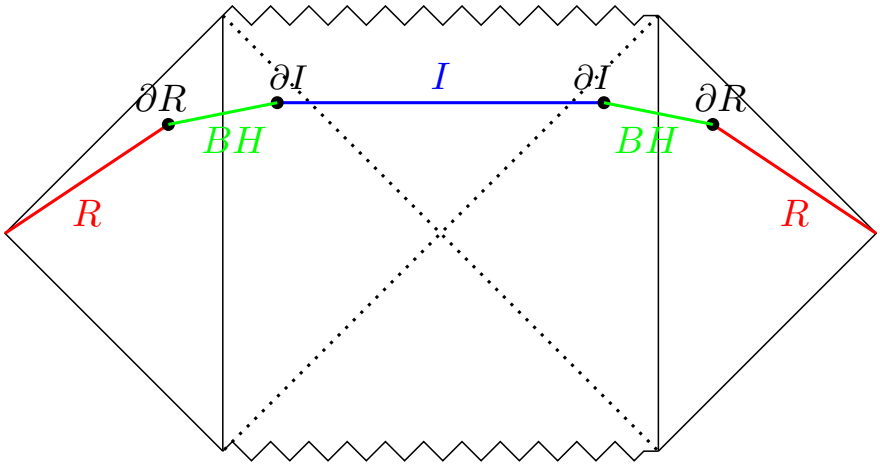

Figure 11: The Penrose diagram of the AdS black hole coupled to the flat bath spacetimes with the regions R (red region), BH (green region), and I (blue region). In the $y^{\pm}$ coordinates, the left endpoint of the island is given by $(\tau_a, \sigma = -a)$,and the right one is given by $(\tau_a, \sigma = a)$.

BH), are given by

$$w_1^{\pm} = -\exp\left(-\frac{2\pi}{\beta}(-b \pm \tau)\right), \qquad w_2^{\pm} = -\exp\left(-\frac{2\pi}{\beta}(a \pm \tau_a)\right) \tag{2.45}$$

$$w_3^{\pm} = \exp\left(\frac{2\pi}{\beta}(-a \pm \tau_a)\right), \qquad w_4^{\pm} = \exp\left(\frac{2\pi}{\beta}(b \pm \tau)\right), \tag{2.46}$$

where w_1, w_2 are at the left bath region and the left black hole region respectively, and w_3, w_4 are at the right black hole region and the right bath region respectively. By using the expression (2.44), (2.46) and the metric (2.31), we can calculate the CFT von Neumann entropy on the region $R \cup I$ (or BH) [13], and by using the result, we can evaluate the island formula (2.42). However, at late times $\tau \gg \beta$ when the CFT von Neumann entropy $S_{\rm CFT}[R]$ exceeds the Bekenstein-Hawking entropy, and the island phase is expected to dominate, the cross-ratio $|w_{23}w_{14}|/|w_{13}w_{24}|$ approaches to one, and the CFT

[13]The CFT von Neumann entropy on the region $R \cup I$ is explicitly given by

$$S_{\rm Fermi.}[I \cup R] = \frac{c}{3}\log\left[\frac{2\cosh\left(\frac{2\pi}{\beta}\tau_a\right)\cosh\left(\frac{2\pi}{\beta}\tau\right)\left|\cosh\left(\frac{2\pi}{\beta}\left(\tau_a - \tau\right)\right) - \cosh\left(\frac{2\pi}{\beta}(a+b)\right)\right|}{\sinh\left(\frac{2\pi}{\beta}a\right)\cosh\left(\frac{2\pi}{\beta}\left(\frac{a+b-\tau_a-\tau}{2}\right)\right)\cosh\left(\frac{2\pi}{\beta}\left(\frac{a+b+\tau_a+\tau}{2}\right)\right)}\right] + \cdots,$$

where $\cdots$ are constant independent of the parameters τ, b, τ_a, a.

entropy for the two intervals reduces to twice the single interval expression

$$\begin{aligned} S_{\text{Fermi.}}\left[R\cup I\right] &\approx S_{\text{CFT}}\left[w_1,w_2\right]+S_{\text{CFT}}\left[w_3,w_4\right] \\ &= 2S_{\text{CFT}}\left[w_3,w_4\right], \end{aligned} \qquad \text{at late times} \tag{2.47}$$

where in the second line we used the fact that the two intervals are symmetric between the left and right regions. This simplification is expected to occur in general CFTs, thus we use the simplified expression rather than the original two interval result. In this case, by using the expressions (2.36), (2.46), and the metric (2.31), we get the simpler expression

$$\begin{aligned} S_{\text{Fermi.}}\left[R\cup I\right] &\approx 2S_{\text{CFT}}\left[w_3,w_4\right] \\ &= \frac{c}{3}\log\left(\frac{4\beta}{\pi\varepsilon_{\text{cut}}\varepsilon_{UV}^2}\frac{\left|\cosh\left(\frac{2\pi}{\beta}\left(\tau_a-\tau\right)\right)-\cosh\left(\frac{2\pi}{\beta}(a+b)\right)\right|}{\sinh\left(\frac{2\pi}{\beta}a\right)}\right). \end{aligned} \tag{2.48}$$

Now we can evaluate the island formula for island phase. The functional $S_{\text{gen.}}(a,\tau_a)$ of the island, which is specified by the parameters τ_a, a, is given by

$$\begin{aligned} S_{\text{gen.}}(a,\tau_a) &= \frac{\Phi(w_2^+,w_2^-)}{4G_N}+\frac{\Phi(w_3^+,w_3^-)}{4G_N}+S_{\text{Fermi.}}[w_1,w_2;w_3,w_4] \\ &\approx 2\left(\frac{\Phi(w_3^+,w_3^-)}{4G_N}+S_{\text{CFT}}\left[w_3,w_4\right]\right) \\ &= 2\Bigg[\frac{\phi_0}{4G_N}+\frac{\pi\phi_r}{2G_N\beta}\frac{1}{\tanh\left(\frac{2\pi}{\beta}a\right)} \\ &\qquad +\frac{c}{6}\log\left(\frac{4\beta}{\pi\varepsilon_{\text{cut}}\varepsilon_{UV}^2}\frac{\left|\cosh\left(\frac{2\pi}{\beta}\left(\tau_a-\tau\right)\right)-\cosh\left(\frac{2\pi}{\beta}(a+b)\right)\right|}{\sinh\left(\frac{2\pi}{\beta}a\right)}\right)\Bigg], \end{aligned} \tag{2.49}$$

where in the second line we used the fact that the two intervals are symmetric between the left and right regions and the approximation (2.48), and in the third line we used the dilaton profile (2.19). The extremality conditions for the island I are given by

$$\partial_{\tau_a}S_{\text{gen.}}(a,\tau_a)=0, \qquad \partial_a S_{\text{gen.}}(a,\tau_a)=0. \tag{2.50}$$

From the first condition $\partial_{\tau_a}S_{\text{gen.}}(a,\tau_a)=0$, we get

$$\tau_a=\tau. \tag{2.51}$$

By using the result, from the second condition $\partial_a S_{\text{gen.}}(a,\tau)=0$, we get the one for the parameter a

$$\frac{1}{\sinh\frac{2\pi a}{\beta}}=\frac{G_N c\beta}{3\pi\phi_r}\frac{\sinh\frac{\pi(a-b)}{\beta}}{\sinh\frac{\pi(a+b)}{\beta}}. \tag{2.52}$$

The above equation determines a, that is, the location of the endpoints of the island I. We note that while the location of the black hole horizon is at $y^+=-\infty$ and $y^-=-\infty$ as we saw in the analysis of the dilaton profile, the endpoint of the island is at a (or $-a$), which is finite; thus the endpoints of the island are outside the horizon for the eternal black hole [31]. This fact means that the island region contains the region behind the horizon, i.e., the black hole interior region[14].

In the high temperature limit $\frac{\phi_r}{G_N c\beta}\gg 1$ where the near extremal entropy $\frac{2\pi}{\beta}\phi_r/4G_N$ becomes large compared to the central charge c and the effect of the Hawking radiation becomes small, the condition (2.52) reduces to

$$a\approx b+\frac{\beta}{2\pi}\log\left(\frac{6\pi\phi_r}{G_N c\beta}\right)\qquad\text{at the high temperature limit }\frac{G_N\phi_r}{c\beta}\gg 1. \tag{2.53}$$

In this case, the value of the functional $S_{\text{gen.}}(a,\tau_a)$ is given by

$$\begin{aligned} S_{\text{island}}\equiv S_{\text{gen.}}(a,\tau_a)&\approx 2\left\{\frac{\phi_0+\frac{2\pi}{\beta}\phi_r}{4G_N}+\frac{c}{6}\log\left(\frac{\beta}{\pi\varepsilon_{\text{cut}}\varepsilon_{UV}^2}e^{\frac{2\pi}{\beta}b}\right)\right\}\\ &\approx 2\left\{S_{BH}+\frac{\pi c}{3\beta}b\right\}, \end{aligned} \tag{2.54}$$

where in the second line we used the previous result (2.23) and dropped terms, which is independent of the parameter b, in the CFT von Neumann entropy. In this expression, the CFT von Neumann entropy is very small compared to the no-island result (2.41) at late times. This is because the Hawking quanta, which are store in R entangled with their pairs inside the black hole interior is purified by the inclusion of the island region.

By combining the above results and using the island formula (2.42), we get

$$\begin{aligned} S(\rho_R)&=\text{Min}\left\{S_{\text{no-island}},S_{\text{island}}\right\}\\ &\approx\text{Min}\left\{\frac{2\pi}{3}c\frac{\tau}{\beta},\ 2S_{BH}\right\}, \end{aligned} \tag{2.55}$$

[14]For an evaporating black hole, not eternal, the endpoint of the island is little bit $\mathcal{O}(G_N)$ inside the event horizon, see, e.g., [12].

where in the second line we used the approximations (2.41) and (2.54) and further we dropped subdominant terms. The time when the transition from the no-island phase to the island one happens is called the Page time, τ_{Page}. Roughly speaking, the Page time is given by $\tau_{Page} \sim \frac{\beta S_{BH}}{c}$. The above discussion gives the Page curve for the eternal black hole. See figure 12.

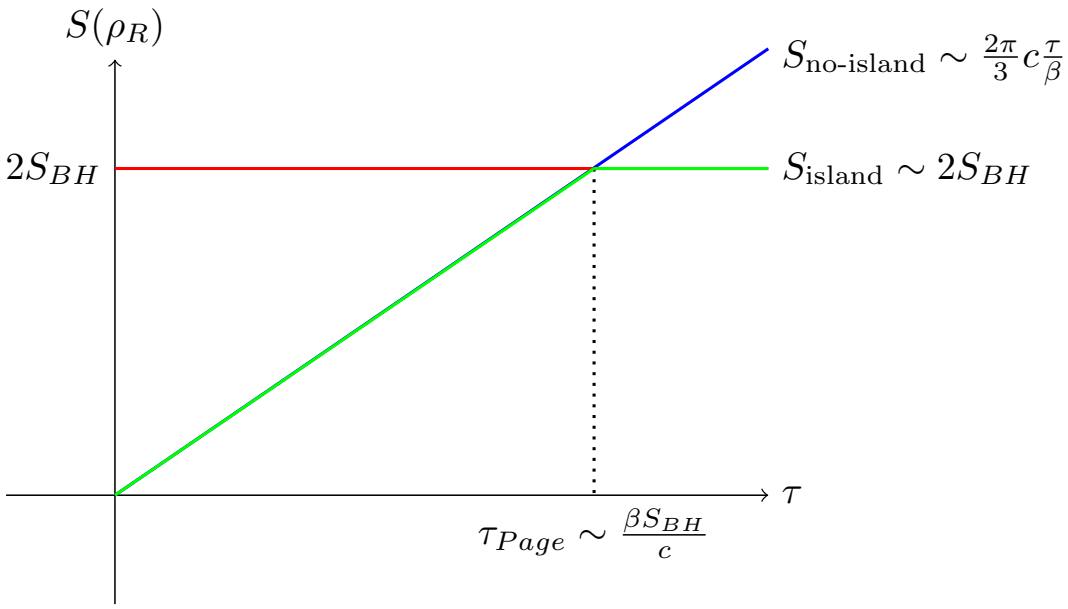

Figure 12: Schematic picture of the Page curve for the eternal black hole. The von Neumann entropy of the Hawking radiation gives the Page curve. The Page curve (green curve) is given by the smaller value between the two curves $S_{\text{no-island}}$ (blue curve), S_{island} (red curve).

The entropy of the Hawking radiation calculated by the island formula follows the Page curve and does not exceed the Bekenstein-Hawking entropy. Thus, we do not encounter the information paradox.

2.2 The Island formula

In the previous subsection 2.1, we considered the AdS_2 eternal black hole coupled to the flat baths, by using the island formula we computed the von Neumann entropy of the Hawking radiation (or equivalently the black hole), and we checked that it gives the Page curve. In this subsection, we give some more explanation on the island formula.

Firstly, the calculation of the island formula suggests that after the Page time, we need to treat the degrees of freedom on (the entanglement wedge

of) the island region I as that on (the entanglement wedge of) the Hawking radiation R. This implies that the *true* Hawking radiation, which is described by the QM and CFT system holographically in the current setup, consists of the union of the Hawking radiation region R and the island region I in the semi-classical gravitational description. Roughly speaking, this means that the degrees of freedom on the black hole interior are encoded into the Hawking radiation region R in a very complicated manner. We can make this statement more precise by using the entanglement wedge reconstruction (conjecture) [12] in the AdS/CFT correspondence, which states that local operators on the entanglement wedge on the island region I can be expressed (reconstructed) by operators on that of the radiation region R. Here we do not explain such directions.

Next, we can apply the island formula not only an AdS black hole coupled to a bath system but also a black hole in asymptotically flat spacetime, e.g., [42–45]. Furthermore, we can apply the island formula to the de Sitter space with some modifications, e.g., [26, 46, 47]. Thus, the island formula is used to solve information paradoxes in various situations. In the next section 3, we will consider the island formula in different modeling of the evaporation of a black hole.

In the previous subsection 2.1, we considered the case that the matter theory is the holographic CFT, but it is not necessarily required for the application of the island formula. We generally consider the effective field theory on a curved spacetime, not necessarily conformal, and compute the QFT von Neumann entropy instead of the CFT von Neumann entropy. In such a case, the island formula is given by

$$S(\rho_R) = \underset{I}{\mathrm{Min}} \left\{ \underset{I}{\mathrm{Ext}} \left[\frac{\mathrm{Area}(\partial I)}{4G} + S_{\mathrm{eff}}[R \cup I] \right] \right\}, \tag{2.56}$$

where $S_{\mathrm{eff}}[R \cup I]$ is the QFT von Neumann entropy on the interval $R \cup I$ by using the effective field theory on the background spacetime.

Replica Wormhole and the Island formula

We briefly explain the derivation of the island formula. The complete derivation can be founded in [32], see also [24][15]. We use the setup in the previous subsection 2.1.

The starting point is the replica trick for the von Neumann entropy of

[15] See also [45] for the derivation on the island formula in two-dimensional asymptotically flat spacetime.

the Hawking radiation

$$\begin{aligned} S(\rho_R) &= -\mathrm{tr}_R[\rho_R \log \rho_R] \\ &= -\lim_{n\to 1} \partial_n \mathrm{tr}_R\left[\rho_R^n\right], \end{aligned} \tag{2.57}$$

thus we need to evaluate $\mathrm{tr}_R\left[\rho_R^n\right]$. We note that the reduced density matrix ρ_R is defined holographically by (2.35), and through the AdS/CFT correspondence $\mathrm{tr}_R\left[\rho_R^n\right]$ can be evaluated in the gravity side with the semi-classical limit, $G \to 0$.

In evaluating the quantity $\mathrm{tr}_R\left[\rho_R^n\right]$, we prepare n copies of the original spacetime, and need to consider the (Euclidean) gravitational path integral on the n copied spacetime.

The naive gravitational saddle is the disconnected n spacetimes (disconnected saddle) since it is topologically trivial. However, this leads to the no-island result.

Thus we need to consider other gravitational saddles, which are topologically non-trivial and non-perturbative contributions. Such gravitational saddles are given by wormholes connecting some of or all of the n copied spacetimes, called replica wormholes (replica wormhole saddle). The dominant replica wormhole is given by the one connecting all the n copied spacetimes. After the Page time, the replica wormhole becomes the dominant saddle instead of the disconnected saddle. By considering the replica wormhole, we get the island formula in the limit $n \to 1$ through the replica trick (2.57).

3 Asymptotically Flat Black Hole in Disjoint Universes setup

In this section, we consider different modeling of the evaporation of a black hole, sometimes called the disjoint (universes) setup. In particular, we focus on a black hole in asymptotically flat spacetime under the disjoint setup[16].

In the disjoint setup, we introduce two universes A and B, and assume that the universe A is non-gravitating, the universe B is gravitating and contains a black hole, and the matter state on the two universes is given by an entangled pure state $|\Psi\rangle_{AB}$, which we explain later.

[16]There are also studies of black holes in asymptotically flat spacetime that do not use the disjoint setup. See e.g., [42–45] for the discussions.

Intuitively, we can consider the setup as follows: we consider an evaporating black hole in a gravitating universe, collect all Hawking quanta, and put them in the other non-gravitating universe (the auxiliary universe). This results in the entanglement between the two universes represented by the state $|\Psi\rangle_{AB}$, which has a similar structure to the Hartle-Hawking state on a black hole. See figure 13.

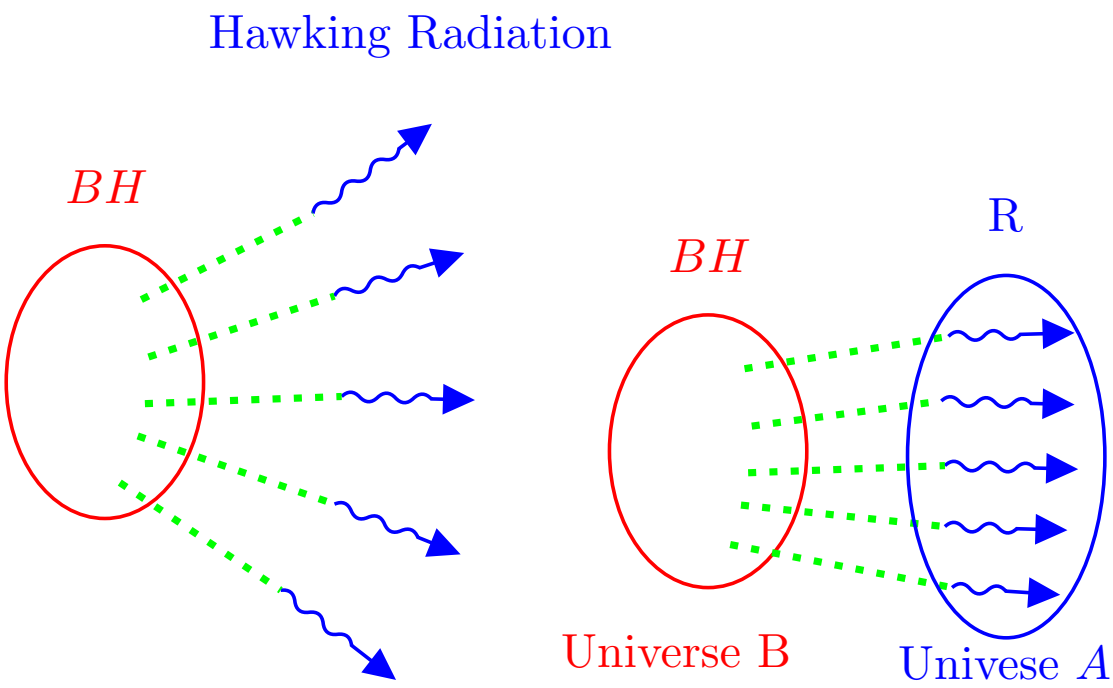

Figure 13: Schematic picture of the preparation of the disjoint setup. **Left**: A black hole (in the universe B) emits Hawking quanta by Hawking radiation, which are entangled with the black hole. Green dotted lines imply the entanglement between the black hole and the Hawking radiation. **Right**: We collect the Hawking quanta and put them into the auxiliary non-gravitating universe A. In this case, the universe B is entangled with the universe A. Green dotted lines also imply the entanglement between (black hole in) the universe B and (the Hawking radiation in) the universe A.

In the papers [25, 26], by using the disjoint setup for two-dimensional black holes in AdS and dS spacetime, the authors studied the entropy of the Hawking radiation by using a modified version of the island (or HRT) formula, and checked that the von Neumann entropy of the Hawking radiation on the universe A, which is equal to the von Neumann entropy of the universe B, obeys a Page curve as a strength of the entanglement between the two universes A, B, not the time like the previous section.

In this section, as noted above, we consider an evaporating black hole in asymptotically flat spacetime by using the disjoint setup, and calculate the von Neumann entropy of the Hawking radiation on the universe A[17], or the von Neumann entropy of the universe B, by using a modified version of the island (or HRT) formula, which we will explain later. We note that the von Neumann entropy of the universe B, which contains the black hole, corresponds to the von Neumann entropy of the black hole on the universe.

After the calculation, we will consider a perturbation of the entangled state by a local quench, which we will explain later, and study the von Neumann entropy of the universe A or B.

3.1 Setup

3.1.1 Two disjoint asymptotically flat universes

We explain the disjoint setup in more detail. At first, we introduce two disjoint universes, A and B which are asymptotically flat (see figure 14). For simplicity, we consider two-dimensional spacetimes. Next, we define two identical CFTs, on each universe A and B, and we assume that on the universe B, we have a semi-classical gravitational description. Thus the effective actions on the universes A, B are given by

$$\log Z_A = \log Z_{\mathrm{CFT}}, \quad \log Z_B = -I_{\mathrm{grav}} + \log Z_{\mathrm{CFT}}. \tag{3.1}$$

As the gravitational sector I_{grav} of the above effective action, we consider the CGHS action [28],

$$I_{\mathrm{grav}} = \frac{1}{16\pi G_N} \int dx^2 \sqrt{-g} \left(\Phi R - \Lambda\right), \tag{3.2}$$

which is two-dimensional dilaton gravity in (asymptotically) flat space. The action contains the dilaton Φ in addition to the metric $g_{\mu\nu}$. Also, we introduced a parameter Λ, which is negative, and similar to, but different from, the cosmological constant.

The Hilbert space of the system is given by $H_A \otimes H_B$, which is bipartite. Because the two universes A, B are disjoint, classical information can not be exchanged between them, but CFT matter states on the universes A, B can be quantum mechanically entangled with each other. We are interested in

[17] We sometimes call the entropy the von Neumann entropy of the universe A, and similarly for B.

the structure of the entanglement between states on the two Hilbert space. To study the structure explicitly, we will consider the thermo-field double (TFD) state on the system

$$|\Psi\rangle = \sum_{i=0}^{\infty} \sqrt{p_i}\, |i\rangle_A\, |\psi_i\rangle_B, \quad p_i = \frac{e^{-\beta E_i}}{Z(\beta)}, \tag{3.3}$$

where $Z(\beta)$ is a normalization factor, which ensure the normalization condition $\langle\Psi|\Psi\rangle = 1$, $|i\rangle_A$ is a CFT energy eigenstate on the non-gravitating universe A, and $|\psi_i\rangle_B$ is the same energy eigenstate on the gravitating universe B. Although they are same states, since, on the universe B gravity is turned on, and properties of the states are affected by the fact, thus we write them in different notations. The parameter β in (3.3) characterizes the strength of the entanglement between the two universes, not the temperature of a black hole. For this reason, sometimes $1/\beta$ is called the entanglement temperature.

3.1.2 Islands in the setup

In the papers [25, 26], for the TFD state (3.3), the von Neumann entropy on the non-gravitating universe A, $S(\rho_A)$ was studied. This quantity is defined by

$$S(\rho_A) = -\mathrm{tr}\rho_A \log \rho_A, \quad \rho_A = \mathrm{tr}_B |\Psi\rangle\langle\Psi|. \tag{3.4}$$

The above von Neumann entropy is evaluated by the replica trick [25] as noted in the previous section. In this disjoint setup case, the dominant replica wormhole saddle is the replica wormhole connecting all the copies of the universe B with given consistent boundary conditions. Such a replica wormhole leads to the following formula for the von Neumann entropy [25]

$$S(\rho_A) = \mathrm{Min}\{S_{\mathrm{no-island}}, S_{\mathrm{island}}\}. \tag{3.5}$$

$S_{\mathrm{no-island}}$ in the above formula is equal to the CFT thermal entropy $S_{\mathrm{no-island}} = S_\beta(B)$ given by

$$S_{\mathrm{th}}(B) = -\sum_i p_i \log p_i, \tag{3.6}$$

where p_i is defined in (3.3). More explicitly, it is given by

$$S_{\mathrm{th}}(B) = \frac{c}{3} \log\left(\frac{\beta}{\pi} \sinh\left(\frac{\pi^2}{\beta}\right)\right), \tag{3.7}$$

in the coordinates (3.10) which we will explain later. One can obtain this expression from (A.7) with $l = \pi$.

On the other hand, S_{island} in the above formula is given by

$$S_{\text{island}} = \underset{\bar{C}}{\text{Ext}} \left[\frac{\Phi(\partial \bar{C})}{4G_N} + S_\beta[\bar{C}] - S_{\text{vac}}[\bar{C}] \right] \equiv \underset{\bar{C}}{\text{Ext}}\ S_{\text{gen}}[\bar{C}], \tag{3.8}$$

where $\underset{\bar{C}}{\text{Ext}}$ means that we choose the configuration that extremize the generalized entropy among all possible intervals $\bar{C}$ in the gravitating universe B. $\Phi(\partial \bar{C})/4G_N$ is the area term of the generalized entropy, which is given by the sum of the dilaton values at the endpoints of the interval $\bar{C}$. $S_\beta[\bar{C}]$ is the von Neumann entropy for thermal states on $\bar{C}$, and $S_{\text{vac}}[\bar{C}]$ is that of the vacuum state. Because the TFD state is pure on the two universe A, B, the generalized entropy has the property that $S_{\text{gen}}[\bar{C}] = S_{\text{gen}}[AC]$. This implies the interval C in the gravitating universe B can be identified with the island in current setup. We note that, although the term $S_{\text{vac}}[\bar{C}]$ does not appear in the island formula (2.42) (or (2.56)) of the previous section, the appearance of the term results from the disjointness between the two universes [25].

We are interested in the behavior of the entropy $S(\rho_A)$ as we vary the entanglement temperature $1/\beta$, in particular when the gravitating universe B contains a black hole. In the papers [25, 26], it was argued that, in the low entanglement temperature $1/\beta \ll 1$, because $S_{\text{no-island}} < S_{\text{island}}$ the von Neumann entropy (3.5) is equal to the CFT thermal entropy $S_{\text{th}}(B)$, which is analog of the Hawking's result for the von Neumann entropy of the Hawking radiation. This also implies that the entropy linearly grows as we increase the entanglement temperature $1/\beta$. For sufficiently high temperature $S_{\text{no-island}}$ becomes larger than S_{island}. Thanks to the formula (3.5), in that case, the von Neumann entropy is given by S_{island}, not the naive Hawking-like entropy $S_{\text{no-island}}$. Furthermore, in the limit $1/\beta \gg 1$, S_{island} almost coincides with the Bekenstein-Hawking entropy in the gravitating universe B. In this way, we can get the Page curve of a black hole in the current setup.

3.1.3 Embedding of two universes

One can study the above setup by embedding the system into larger Minkowski spacetime M (see figure 14). Each universe is a Rindler wedge in the larger Minkowski spacetime. The non-gravitating universe A is the left Rindler wedge of M, and the gravitating one B is the right one. More specifically,

we define the light-cone coordinates $x^{\pm} = x \pm t$ on each universe[18]. Also, for the right Rindler wedge, we define the coordinates (w^+, w^-) of the larger Minkowski space M through

$$w^{\pm} = e^{\frac{2\pi}{\beta} x^{\pm}}, \tag{3.9}$$

and for the left one we define $w^{\pm} = -e^{\frac{2\pi}{\beta} x^{\pm}}$.

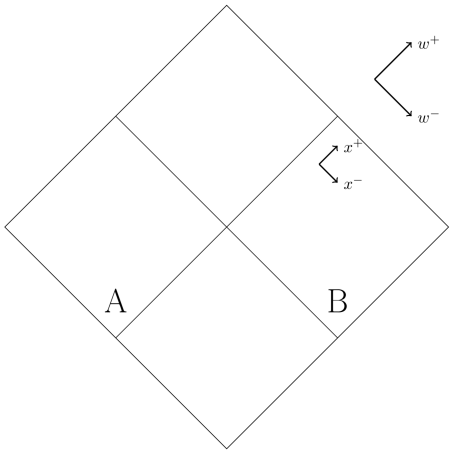

Figure 14: The system with two disjoint asymptotically Minkowski spacetimes, A and B. In this figure, these spacetimes (universes) are embedded into the larger Minkowski spacetimes.

The non-gravitating universe A corresponds to the left Rindler wedge of M, $w^{\pm} < 0$, and the gravitating universe B does to the right one of M, $w^{\pm} > 0$. Also, the thermo-field double state on the universes A, B is mapped to the (Minkowski) vacuum of M. This situation is similar to the one in the previous section 2.1.2.

3.2 An asymptotically flat black hole and its radiation entropy

To use the island formula (3.5), we need to determine the dilaton profile Φ, which appears in the generalized entropy (3.8). Because the TFD state leads to the thermal expectation value of the stress-energy tensor $\langle \Psi | T_{\pm\pm} | \Psi \rangle$ on

[18]We note that clearly, the light-cone coordinates are different from the Poincare coordinates for the AdS spacetime in the previous section. We can distinguish which coordinate we use from the context.

the gravitating universe B, the dilaton profile is affected by it through the equations of motion.

In the CGHS model with the action (3.2), we fix the metric to be the flat one, since by the variation of the action with respect to Φ we get $R = 0$. It is convenient to use the compact coordinates (x^+, x^-) with the flat metric given by

$$ds^2 = \frac{dx^+ dx^-}{\cos^2 x^+ \cos^2 x^-}, \quad -\frac{\pi}{2} \leq x^\pm \leq \frac{\pi}{2}. \tag{3.10}$$

The above coordinates are related to the usual coordinates (X^+, X^-) with the metric $ds^2 = dX^+ dX^-$, where $X^\pm = \tan x^\pm$. In the x coordinates, the asymptotic infinities of the spacetime correspond to $x^+ = \pm\frac{\pi}{2}$ and $x^- = \pm\frac{\pi}{2}$.

Next, by varying the effective action on the universe B with respect to the metric, we get the equations of motion for the dilaton

$$\nabla_a \nabla_b \Phi - g_{ab} \nabla^2 \Phi = \frac{\Lambda}{2} g_{ab} - 8\pi G_N \, \langle \Psi | T_{ab} | \Psi \rangle. \tag{3.11}$$

Generally, in the conformal gauge, the metric is in the form

$$ds^2 = e^{2\omega} dx^+ dx^-, \tag{3.12}$$

and using this metric, the above equations of motion becomes

$$-e^{2\omega} \partial_\pm \left[e^{-2\omega} \partial_\pm \right] \Phi = 8\pi \, G_N \langle \Psi | \, T_{\pm\pm} | \Psi \rangle, \quad \partial_+ \partial_- \Phi = 8\pi \, G_N \, \langle \Psi | T_{+-} | \Psi \rangle - \frac{\Lambda}{4} e^{2\omega}. \tag{3.13}$$

The Sourceless solution

Firstly we discuss the dilaton profile for the case that the stress-energy tensor vanishes $\langle \Psi | T_{ab} | \Psi \rangle = 0$. For the current setup, this happens in the limit that the entanglement temperature is very low, $\beta \to \infty$. It leads us to the dilaton profile

$$\Phi_0 = \phi_0 + \frac{|\Lambda|}{4} \tan x^+ \tan x^-, \tag{3.14}$$

where Λ is the parameter of the CGHS model (3.2). As we will see later, the dilaton profile corresponds to an eternal black hole in asymptotically flat spacetime, whose Penrose diagram is identical to the usual eternal black hole (see the left panel of Fig. 15).

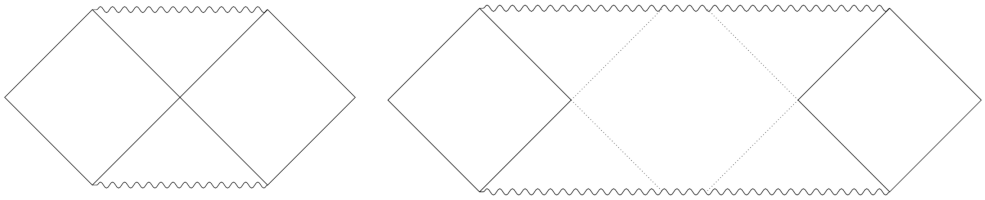

Figure 15: **Left**: The Penrose diagram of the black hole without the back-reaction. **Right**: The Penrose diagram of the black hole with the back-reaction of the source (3.15). It develops a long wormhole region in its interior.

The Solution with the source

As we increase the entanglement temperature $1/\beta$, we can not ignore the back-reaction of the stress-energy tensor to the dilaton profile. The expectation value of the stress-energy tensor for the TFD state (3.3) is given by

$$\langle \Psi | T_{\pm\pm} | \Psi \rangle = \frac{\pi c}{12\beta^2} \equiv \langle T \rangle_\beta, \qquad \langle \Psi | T_{\pm\mp} | \Psi \rangle = 0. \tag{3.15}$$

In this case, we can solve the equations (3.13) for Φ, and we obtain

$$\Phi_\beta = \phi_0 + \frac{|\Lambda|}{4} \tan x^+ \tan x^- - X_\beta \left(x^+ \tan x^+ + x^- \tan x^- \right), \quad X_\beta \equiv 4\pi G \langle T \rangle_\beta. \tag{3.16}$$

The above solution corresponds to an eternal black hole, which has a long interior region (the right panel of Fig. 15).

3.2.1 Penrose diagrams

Now that we have obtained the dilaton profile (3.16), which we are interested in, we discuss the causal structure of the spacetime corresponding to the dilaton profile. Because it turns out that the dilaton profile corresponds to an eternal black hole, we consider the location of the singularity and the event horizon of the black hole. Like in the previous subsection 2.1.1, at the black hole singularity, the dilaton vanishes $\Phi = 0$, and the bifurcation surface of the black hole is given by the point that satisfies the conditions $\partial_\pm \Phi = 0$. The Bekenstein-Hawking entropy is given by the dilaton value at the horizon divided by $4G_N$.

The sourceless solution

As a warm-up, we firstly consider the causal structure of the dilaton profile (3.14) for the vanishing stress tensor. In this case, the locus of the singularity satisfies

$$\Phi_0 = 0 \leftrightarrow \tan x^+ \tan x^- = -\frac{4\phi_0}{|\Lambda|}. \tag{3.17}$$

In the coordinates (X^+, X^-), the locus of the singularity is just a hyperbola $X^+X^- = -4\phi_0/|\Lambda|$, which is expected. The singularity intersects with the right future null infinity $x^+ = \frac{\pi}{2}$ at $x^- = 0$, and it also intersects with the left one $x^- = -\frac{\pi}{2}$ at $x^+ = 0$. By the observation, we can fix the location of the event horizon to $x^+ = 0$ and $x^- = 0$. This is consistent with the location of the bifurcation surface; that is, the black hole has only one bifurcation surface at $x^\pm = 0$. The dilaton value at the surface is given by $\Phi(0) = \phi_0$, which is related to the entropy of the black hole, and does not depend on the parameter Λ.

The solution with the source

Next we consider the dilaton profile Φ_β (3.16) for the case that the stress tensor is non-vanishing. In this case, the geometry of the black hole is eventually deformed by the stress-energy tensor (3.15), due to the back-reaction. Like the above simple case, we can study the location of the singularity in the deformed spacetime from the dilaton profile Φ_β. Near the the right future null infinity $x^+ = \frac{\pi}{2}$, we can approximate the dilaton profile as

$$\Phi_\beta = \frac{\Lambda}{4} \tan x^+ \left(\tan x^- - \frac{2\pi X_\beta}{|\Lambda|} \right), \quad x^+ \to \frac{\pi}{2}, \tag{3.18}$$

where we dropped the extremal entropy term ϕ_0. From the above equation, the singularity intersects with the future infinity at $x^- = x_c^-$ which satisfies

$$\tan x_c^- = \frac{2\pi X_\beta}{|\Lambda|}. \tag{3.19}$$

As we increase the entanglement temperature $1/\beta \to \infty$, X_β in the right hand side becomes larger, and the intersecting point goes to right spatial infinity, $x_c^- \to \frac{\pi}{2}$ with $x^+ = \frac{\pi}{2}$. Similarly, the singularity intersects with the left future null infinity $x^- = -\frac{\pi}{2}$ at $x^+ = x_c^+$ satisfing

$$\tan x_c^+ = -\frac{2\pi X_\beta}{|\Lambda|}, \tag{3.20}$$

and in the limit $1/\beta \to 0$, it goes to $x_c^+ \to -\frac{\pi}{2}$, so this intersecting point goes to the left spatial infinity. Because the dilaton profile (3.16) is a time reflection symmetric $x^+ \leftrightarrow x^-$, the singularity also intersects with the past null infinity similarly, i.e., the singularity intersects with the right past null infinity $x^- = \frac{\pi}{2}$ at $x^+ = -x_c^+$ satisfying (3.20) and the left past null infinity $x^+ = -\frac{\pi}{2}$ at $x^- = -x_c^-$, (3.19). As a result, as we increase the entanglement temperature $1/\beta \to \infty$, the singularity approaches to the reflection symmetric slice $x^+ = x^-$, in other words the $t = 0$ time slice.

The above discussion also determines the location of the event horizon. The right future horizon is at $x^- = x_c^-$ satisfying (3.19). Similarly the left future horizon is at $x^+ = -x_c^+$. Because these two future horizons do not intersect on the reflection symmetric slice $x^+ = x^-$, the black hole have a region in its interior, which is inaccessible causally from asymptotic spatial infinities (the right panel of figure 15) . Such a region is called the causal shadow region. The fact that the black hole singularity approaches the reflection symmetric slice $x^+ = x^-$ as we increase the entanglement temperature $1/\beta \to \infty$ means that the causal shadow region becomes larger in the limit.

We can also check the above observation by considering locations of the bifurcation surfaces (x_H^+, x_H^-) from the conditions $\partial_\pm \Phi_\beta = 0$. Due to the symmetry $x^+ \leftrightarrow x^-$ of the dilaton profile (3.16), the locations of the bifurcation surfaces satisfy $x_H^+ = x_H^- \equiv y$, and the following condition

$$\frac{|\Lambda|}{4} \tan y - X_\beta \left(\cos y \sin y + y\right) = 0. \tag{3.21}$$

In the high entanglement temperature limit $1/\beta \to \infty$, the equation (3.21) reduces to

$$\tan y_\pm = \frac{4 X_\beta y_\pm}{|\Lambda|}. \tag{3.22}$$

These bifurcation surfaces approach to the spatial asymptotic infinities, $y_\pm \to \pm\frac{\pi}{2}$ in the high temperature limit $1/\beta \to \infty$. Also, in the limit $1/\beta \to \infty$, the dilaton value at the bifurcation surfaces becomes

$$\Phi_\beta(x_H^\pm) = \phi_0 - \frac{(\pi X_\beta)^2}{|\Lambda|}. \tag{3.23}$$

We note that the dilaton value at the horizons, $\Phi_\beta(x_H^\pm)$, becomes smaller as we increase the entanglement temperature $1/\beta$. The fact implies that, as we increase the entanglement between the two universes $\beta \to 0$, the black hole horizon becomes smaller by the back-reaction from the stress-energy tensor. The behavior is closely related to the fact that a black hole in flat spacetime

evaporates through the emission of Hawking quanta. Our current setup (the disjoint setup) indeed can be interpreted as a model of the black hole plus a radiation system. The degrees of freedom of the Hawking radiation corresponds to the CFT degrees of freedom in our setup, and the entanglement of the TFD state (3.3) between the two universes A and B corresponds to the entanglement in the Hartle-Hawking state. Thus the increase of the entanglement between the two universes, (which we do by hand), emulates the physics of the actual black hole evaporation process at late times, and as the entropy of the black hole in our current setup becomes small or zero like an actual evaporating black hole in asymptotically flat spacetime.

However, at the final stage that the black hole has almost evaporated, we can not trust a semi-classical description of the black hole. This is because, in a sufficiently large entanglement temperature regime, the two future and past singularities get close to the reflection symmetric slice $x^+ = x^-$, and in the end, they touch the slice. We can determine the critical temperature from the dilaton values at the bifurcation surfaces (3.23), at which it becomes zero.

3.2.2 Quantum extremal surface

Now we will compute the von Neumann entropy $S(\rho_A)$ of the universe A by using the island formula (3.5) with (3.8). To do so, we need to consider the extremalization of the generalized entropy over all possible regions $\bar{C}$, whose endpoints are identified with QES surfaces. In the consideration, we assume that the region $\bar{C}$ is located on the reflection symmetric slice $x^+ = x^-$ and it is given by the union of two regions $\bar{C} = \bar{C}_1 \cup \bar{C}_2$, $\bar{C}_1 : -\frac{\pi}{2} < x^+ \leq -\frac{\pi x}{2}$, $\bar{C}_2 : \frac{\pi x}{2} \leq x^+ < \frac{\pi}{2}$ with $0 < x < 1$. Further, we assume that, when the island phase dominates, the CFT von Neumann entropy of the union of the two regions can be written as the sum of the CFT von Neumann entropies of the single region $\bar{C}_1$ and that of $\bar{C}_2$ as the discussion in (2.47). Then the generalize entropy reduces to a function of the variable x,

$$S_{\rm gen}(x) = 2\cdot\frac{\Phi_\beta(x)}{4G_N} + \frac{2c}{3}\log\left[\frac{\beta}{\pi\varepsilon_{\rm UV}}\sinh\frac{\pi^2}{2\beta}(1-x)\right] - \frac{2c}{3}\log\left[\frac{1}{\varepsilon_{\rm UV}}\sin\frac{\pi}{2}(1-x)\right], \tag{3.24}$$

where $\varepsilon_{\rm UV}$ is the UV cutoff. One can obtain the above CFT entropy part by using (A.7) and (A.8) with $l = \pi$, $L = \pi$. We give a plot of the above generalized entropy in the top panel of figure 17.

In the high entanglement temperature limit $\beta \to 0$, the location of the quantum extremal surfaces almost approaches that of the classical bifurcation

surfaces of the black hole. This is because the quantum extremal surfaces get close to the asymptotic spatial infinities, and thus, in the limit, the CFT von Neumann entropy part in the generalized entropy becomes almost zero. Therefore, we can regard the island region C as the causal shadow region in the black hole interior (figure 16).

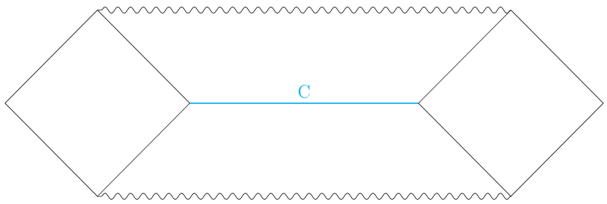

Figure 16: The location of the island C in the black hole with the back-reaction, denoted by the blue line.

From above results, we can approximate the von Neumann entropy $S(\rho_A)$ like the discussion of the expression (2.55) and get the following expression

$$S(\rho_A) = \begin{cases} S_{\text{no-island}} = \frac{\pi^2 c}{3\beta} & \beta > \beta_c \\ S_{\text{island}} = \frac{1}{2G_N}\left[\phi_0 - \frac{(\pi X_\beta)^2}{|\Lambda|}\right] & \beta < \beta_c, \end{cases} \tag{3.25}$$

where β_c is the critical inverse entanglement temperature, which is determined by $S_{\text{no-island}} = S_{\text{island}}$. We give the plot of the Page curve for the above expression (3.25) in the bottom panel of figure 17. Note that in this section we consider a evaporating black hole in asymptotically flat spacetime, not an eternal black hole in AdS spacetime, thus the resulting Page curve (the bottom panel of figure 17) is different from the one (figure 12) in previous subsection 2.1.

3.3 Black hole interior in the presence of shock wave

We have checked that, as we make the entanglement between two universes stronger, the size of the interior region of the black hole in the gravitating universe B becomes larger. Thus we can interpret this interior region as the one that is created by the entanglement between the degrees of freedom in the gravitating universe B and those in the other universe A. In this subsection, we investigate the interpretation further by considering local operations in the gravitating universe B. Such local operations would "perturb" the entanglement between two universes. One can model such local operations by local

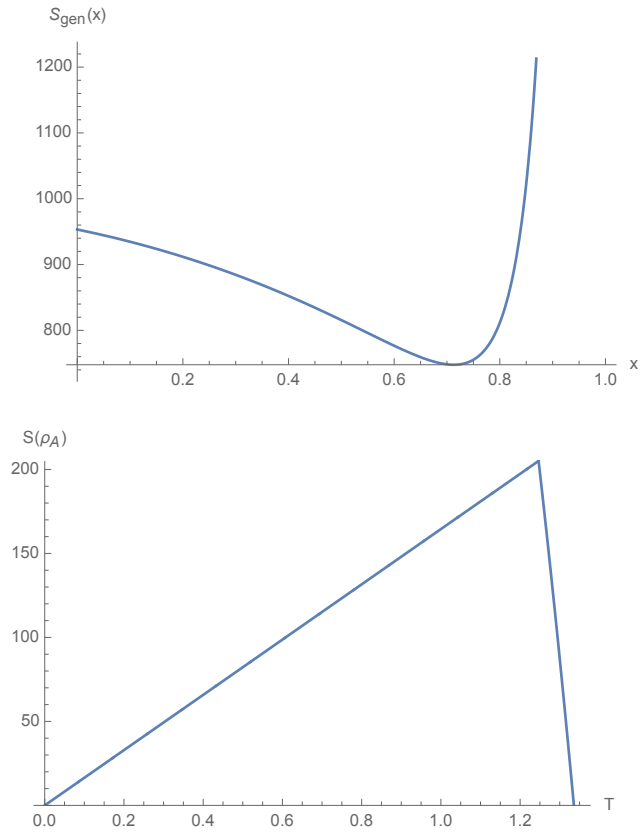

Figure 17: **Top**: Plot of the generalized entropy $S_{\rm gen}(x)$ as a function of the size (or the location of the endpoint) of the island in the interior. **Bottom**: The resulting Page curve as a function of the entanglement temperature $T = 1/\beta$. Here we set the parameters to be $\phi_0 = 1700$, $|\Lambda| = 500$, $c = 50$ in both figures and $\beta = 1$ for left figure. (These plots were obtained in our paper [27] and we show them.)

operator quench on the gravitating universe B. The local operator quench on B means that we insert a local operator into the region we are interested in on the gravitating universe B. The insertion of the local operator induces shock waves in the two null directions on the universe B, along which the stress-energy tensor has a delta-function-like peak. Through the equations of motion (3.13), it can change the geometry of the black hole described by the dilaton profile.

At first we consider a state $|\Psi\rangle$ on the universes A, B, which we prepare by applying a local operator $\mathcal{O}$ in the gravitating universe B into the TFD

state

$$|\Psi\rangle = (1_A \otimes \mathcal{O}|_B)|TFD\rangle = \frac{1}{\sqrt{Z(\beta)}} \sum_{i=0}^{\infty} e^{-\frac{\beta}{2}E_i} \, |i\rangle_A \, \otimes \mathcal{O} \, |\psi_i\rangle_B \, . \tag{3.26}$$

We will consider the von Neumann entropy $S(\rho_A)$ for the above state by using the island formula (3.5). Because the insertion of the local operator $\mathcal{O}$ does not change the no-island case $S_{\text{no-island}}$[19], we focus on the non-empty island case S_{island} given by the generalized entropy,

$$S_{\text{gen}} = \text{Ext}_{\bar{C}} \left[\frac{\Phi(\partial \bar{C})}{4G_N} + S_{\beta,E}[\bar{C}] - S_{\text{vac}}[\bar{C}] \right], \tag{3.27}$$

where $S_{\beta,E}[\bar{C}]$ means the CFT von Neumann entropy calculated by using the state (3.26).

Let (x_0^+, x_0^-) be the insertion point of the local operator $\mathcal{O}$. Then we get the reduced density matrix of the universe B

$$\rho_B = \frac{\text{tr}_A |\Psi\rangle\langle\Psi|}{\text{tr}_{A\cup B} \, |\Psi\rangle\langle\Psi|} = \frac{1}{Z_{\mathcal{O}}} \, e^{-\varepsilon H} \mathcal{O}(x_0^+, x_0^-) \rho_\beta \, \mathcal{O}^\dagger(x_0^+, x_0^-) \, e^{-\varepsilon H}, \tag{3.28}$$

where to make the density matrix normalizable we introduced the UV regulator ε different from the UV cutoff ε_{UV} in the CFT von Neumann entropy, and the normalization factor $Z_{\mathcal{O}}$ is given by

$$Z_{\mathcal{O}} = \langle \mathcal{O}(2i\varepsilon)\mathcal{O}(0)\rangle_\beta, \tag{3.29}$$

where we introduced the notation $\langle \cdots \rangle_\beta \equiv \text{tr}[\rho_\beta \cdots]$.

The insertion of the local operator $\mathcal{O}$ affects the expectation value of the stress-energy tensor, thus changes the dilaton profile through the equations of motion (3.13). The expectation value of the stress-energy tensor is given by the three point functions $\text{tr}[\rho_\beta T_{\pm\pm}\mathcal{O}\mathcal{O}]$, and it is given explicitly by (e.g., [48, 49]) in the $\varepsilon \to 0$ limit

$$\begin{aligned} \langle \Psi | T_{++}(x^+) | \Psi \rangle &= \frac{\pi c}{12\beta^2} + E_{\text{Shock}} \, \delta(x^+ - x_0^+), \\ \langle \Psi | T_{--}(x^-) | \Psi \rangle &= \frac{\pi c}{12\beta^2} + E_{\text{Shock}} \, \delta(x^- - x_0^-), \end{aligned} \tag{3.30}$$

[19]The fact that the entropy for the no-island case is unchanged in the presence of the local quench in the universe B can be understood by the direct calculation of the entropy using the techniques explained in appendix B.

where E_{Shock} is the constant related to the conformal dimension Δ of the local operator

$$E_{\text{Shock}} = \frac{\Delta}{\varepsilon}. \tag{3.31}$$

Thus, the local quench creates a pair of shock waves in the spacetime, one of which is left moving, the other is right moving. The delta functions in the expectation value of the CFT stress-energy tensor manifest the existence of these shocks. For notational convenience, we write $E \equiv E_{\text{Shock}}$ below.

3.3.1 Dilaton part

We consider the effect of the shock waves on the dilaton profile Φ in detail. In the current case with the stress tensor (3.30), the equations of motion (3.13) become

$$\begin{aligned} -e^{2\omega}\partial_{\pm}\left(e^{-2\omega}\partial_{\pm}\Phi\right) &= 2X_{\beta} + 8\pi G_N E\,\delta\left(x^{\pm} - x_0^{\pm}\right), \\ \partial_{+}\partial_{-}\Phi &= -\frac{\Lambda}{4}e^{2\omega}. \end{aligned} \tag{3.32}$$

We can solve the above equations, and we get the dilaton profile in the presence of shock wave,

$$\begin{aligned} \Phi = \phi_0 + \frac{|\Lambda|}{4}\tan x^{+}\tan x^{-} - X_{\beta}(x^{+}\tan x^{+} + x^{-}\tan x^{-}) \\ - 8\pi G_N E\cos^2 x_0^{+}(\tan x^{+} - \tan x_0^{+})\theta(x^{+} - x_0^{+}) \\ - 8\pi G_N E\cos^2 x_0^{-}(\tan x^{-} - \tan x_0^{-})\theta(x^{-} - x_0^{-}), \end{aligned} \tag{3.33}$$

where $\theta(x)$ is the Heaviside step function,

$$\theta(x) = \begin{cases} 1 & x > 0 \\ 0 & x < 0. \end{cases} \tag{3.34}$$

3.3.2 Classical extremal surfaces

Next, we determine the classical extremal surfaces in the black hole described by the dilaton profile (3.33). We will see that the locations of the classical extremal surfaces highly depend on that of the local operator instead. In the right wedge of the operator insertion point $x^{\pm} > x_0^{\pm}$, the dilaton profile is

equal to the one $\Phi_{\beta,E}$ defined by

$$\Phi_{\beta,E} = \phi_0 + \frac{|\Lambda|}{4}\tan x^+ \tan x^- - X_\beta(x^+ \tan x^+ + x^- \tan x^-) \\ - 8\pi G_N E \cos^2 x_0^+ (\tan x^+ - \tan x_0^+) - 8\pi G_N E \cos^2 x_0^- (\tan x^- - \tan x_0^-). \tag{3.35}$$

On the other hand, in the left wedge $x^\pm < x_0^\pm$, it coincide with the original dilaton profile $\Phi = \Phi_{\beta,E=0} \equiv \Phi_\beta$ (3.16), see figure 18. We note that if there is no shock wave, i.e., $E = 0$, a causal shadow region exists in the interior of the black hole, thus there are two bifurcation surfaces in the black hole. Even in the presence of the shock wave, the dilaton profile (3.33) has also two critical points, one of which is located near the left asymptotic spatial infinity $(x^+, x^-) = (-\frac{\pi}{2}, -\frac{\pi}{2})$ and the other is located near the right one $(x^+, x^-) = (\frac{\pi}{2}, \frac{\pi}{2})$. In this subsection, we consider only the local operator insertions which do not change the location of the left horizon (or the left bifurcation surface) of the original dilaton profile Φ_β. To consider such a situation, we simply consider the restriction of the range of the operator insertion point to $0 < x_0^+ + x_0^-$. Under the restriction, we can consider only the change of the right critical point below. We can discuss operator insertions in the region $x_0^+ + x_0^- < 0$ similarly.

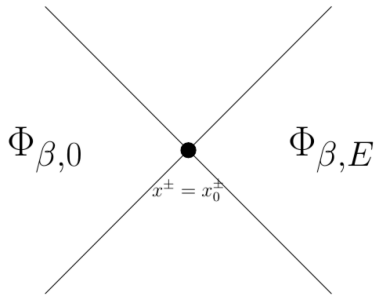

Figure 18: The dilaton profile (3.33) in the presence of the shock wave. In the right wedge of the local operator insertion point, $x^\pm > x_0^\pm$, we have $\Phi = \Phi_{\beta,E}$ with (3.35). On the left wedge, $x^\pm < x_0^\pm$, the dilaton profile coincides with $\Phi_{\beta,0}$, which is identical to (3.16) .

To specify the right classical extremal surface, it is useful to introduce characteristic two critical points of the dilaton profile Φ. We denote by $x^\pm = x_H^\pm(0)$ the first critical point of the undeformed dilaton profile $\Phi_\beta(x^\pm)$,i.e.,

$$\partial_\pm \Phi_\beta|_{x^\pm = x_H^\pm(0)} = 0 \to \tan\ x_H^\pm(0) = \frac{2\pi}{|\Lambda|} X_\beta. \tag{3.36}$$

The other critical point is the one $x^{\pm} = x_H^{\pm}(E)$ of the deformed dilaton profile $\Phi_{\beta,E}$ (3.35), which satisfies

$$\tan\ x_H^{\pm}(E) = \frac{4}{|\Lambda|}\left(\frac{\pi}{2}X_\beta + 8\pi G_N E\cos^2 x_0\right). \tag{3.37}$$

These critical points are candidates for the classical extremal surfaces of the full dilaton (3.33), and depending on the operator insertion point $x^{\pm} = x_0^{\pm}$, we choose one of them, which gives the smaller dilaton value.

For simplify of the below discussion, we consider the symmetric insertions $x_0^+ = x_0^- \equiv x_0$ instead of considering all possible cases. In such a case, from the symmetry the above two candidate extremal surfaces are symmetric too, that is, they are on the reflection symmetric slice : $x_H^+(0) = x_H^-(0) \equiv x_H(0)$, and $x_H^+(E) = x_H^-(E) \equiv x_H(E)$. Generally, we have the relation $x_H(0) < x_H(E)$ due to the effect of the shock wave. In the current setup, there are three possible cases for the operator insertion points (see figure 18), that is, the operator insertion points is (1) behind the original horizon $x_0 < x_H(0)$, (2) in the middle of two horizons, $x_H(0) < x_0 < x_H(E)$ and (3) in the exterior of the deformed horizon $x_H(E) < x_0$.

Case 1

In the case (1), we insert the local operator $\mathcal{O}$ into the left region of the original horizon : $x_0 < x_H(0)$ (top panel of figure 19). In this case, only the classical extremal surface is the critical point of the deformed dilaton profile $x^{\pm} = x_H(E)$ given by (3.37). This is because $x^{\pm} = x_H(0)$ is not a critical point of the full dilaton profile (3.33), since at this point $x^{\pm} = x_H(0)$ the full dilaton profile (3.33) becomes the deformed one $\Phi_{\beta,E}$ (3.35), due to the condition $x_0 < x_H(0)$. At the classical extremal surface the dilaton value is given by $\Phi(x_H(E)) = \Phi_{\beta,E}(x_H(E))$.

Case 2

In the case (2), we insert the local operator $\mathcal{O}$ into between the two would-be classical extremal surfaces $x_H(0) < x_0 < x_H(E)$ (middle panel of figure 19). In this case, both the two critical points $x^{\pm} = x_H^{\pm}(0)$ and $x^{\pm} = x_H^{\pm}(E)$ are classical extremal surfaces of the dilaton profile (3.33).

Case 3

In the case (3), we insert the local operator $\mathcal{O}$ into the right region of the deformed horizon $x_H(E) < x_0$ (bottom panel of figure 19). In this case, only the classical extremal surface is the critical point of the undeformed dilaton profile $x^{\pm} = x_H^{\pm}(0)$. Again this is because the critical point of the deformed dilaton profile $x^{\pm} = x_H^{\pm}(E)$ is not that of the full dilaton profile (3.33) in this region. At the classical extremal surface the dilaton value is given by $\Phi_\beta(x_H^{\pm}(0))$.

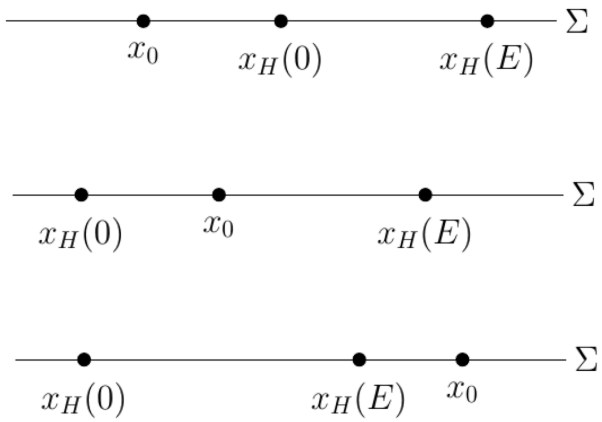

Figure 19: Three possible locations of the local operator $\mathcal{O}$ on the reflection symmetric slice $\Sigma : x^+ = x^-$. **Top** : When $x_0 < x_H(0) < x_H(E)$, the classical extremal surface is located at $x^{\pm} = x_H(E)$. **Middle** : When $x_H(0) < x_0 < x_H(E)$, both $x^{\pm} = x_H(0)$ and $x^{\pm} = x_H(E)$ are extremal. **Bottom**: When $x_H(0) < x_H(E) < x_0$, the classical extremal surface is located at $x^{\pm} = x_H(0)$.

3.3.3 CFT entropy part

To compute the generalized entropy (3.27) we need to give the expression of the CFT von Neumann entropy $S_{\beta,E}[\bar{C}]$ of the reduced density matrix (3.28) on the region $\bar{C}$ in the gravitating universe B. Since we are interested in the high entanglement temperature limit $1/\beta \to \infty$, the region $\bar{C}$ is the union of two disjoint pieces $\bar{C} = \bar{C}_1 \cup \bar{C}_2$, as in the discussion of the shockless case 3.2.2. Let the coordinates of $\bar{C}$ to be as follows;

$$\begin{cases} x_2^{\pm} = -\frac{\pi}{2}, \\ x_3^{\pm} = x_3 \pm t_3, \end{cases} \quad \text{for } \bar{C}_1$$

$$\begin{cases} x_5^{\pm} = x_5 \pm t_5, \\ x_6^{\pm} = \frac{\pi}{2}. \end{cases} \quad \text{for } \bar{C}_2$$

In the high entanglement temperature limit $\beta \to 0$ limit, $x_3^{\pm} \to x_2^{\pm}$ and $x_5^{\pm} \to x_6^{\pm}$ holds. Therefore, if there is no shock wave $E = 0$, the CFT thermal von Neumann entropy on the region $\bar{C} = \bar{C}_1 \cup \bar{C}_2$ at finite temperature β is given by

$$\begin{aligned} S_\beta[\bar{C}] =& \frac{c}{6} \log \left[\frac{\beta}{\pi \varepsilon_{UV}} \sinh \left(\frac{\pi}{\beta} \left(x_3^+ - x_2^+ \right) \right) \right] + \frac{c}{6} \log \left[\frac{\beta}{\pi \varepsilon_{UV}} \sinh \left(\frac{\pi}{\beta} \left(x_3^- - x_2^- \right) \right) \right] \\ &+ \frac{c}{6} \log \left[\frac{\beta}{\pi \varepsilon_{UV}} \sinh \left(\frac{\pi}{\beta} \left(x_6^+ - x_5^+ \right) \right) \right] + \frac{c}{6} \log \left[\frac{\beta}{\pi \varepsilon_{UV}} \sinh \left(\frac{\pi}{\beta} \left(x_6^- - x_5^- \right) \right) \right]. \end{aligned} \tag{3.38}$$

Also we need the CFT vacuum von Neumann entropy for $\bar{C} = \bar{C}_1 \cup \bar{C}_2$, and the entropy is given by

$$\begin{aligned} S_{\text{vac}}[\bar{C}] =& \frac{c}{6} \log \left[\frac{1}{\varepsilon_{UV}} \sin \left(x_3^+ - x_2^+ \right) \right] + \frac{c}{6} \log \left[\frac{1}{\varepsilon_{UV}} \sin \left(x_3^- - x_2^- \right) \right] \\ &+ \frac{c}{6} \log \left[\frac{1}{\varepsilon_{UV}} \sin \left(x_6^+ - x_5^+ \right) \right] + \frac{c}{6} \log \left[\frac{1}{\varepsilon_{UV}} \sin \left(x_6^- - x_5^- \right) \right]. \end{aligned} \tag{3.39}$$

CFT entropy for a single interval Next, we consider the CFT thermal von Neumann entropy $S_{\beta,E}[\bar{C}]$ in the presence of a local quench. This kind of von Neumann entropy (entanglement entropy) was discussed in [50], which we will review in appendix B. As a warmup, we study the simple case of the von Neumann entropy $S_{\beta,E}[\bar{C}]$ of the single interval,

$$\bar{C} : x_5^{\pm} < x^{\pm} < x_6^{\pm} = \frac{\pi}{2}, \tag{3.40}$$

whose endpoint is located at the asymptotic spatial infinity $x_6^{\pm} = \frac{\pi}{2}$. To introduce the CFT von Neumann entropy explicitly, we firstly fix the region $\bar{C}$, i.e., fix $x_5^{\pm}$.

This von Neumann entropy can be evaluated, at first writing the quantity $\text{tr}\rho_{\bar{C}}^n$ in terms of the four point function involving twist operators,

$$\text{tr}\rho_{\bar{C}}^n = \text{tr} \left[\rho_\beta \, \mathcal{O}^{\otimes n}(x_1) \sigma_n(x_5) \sigma_{-n}(x_6) \mathcal{O}^{\otimes n}(x_4) \right], \tag{3.41}$$

after the derivative of it with respect to n, and taking $n \to 1$ limit. Here x_1 and x_4 are given by (B.4), which are related to the operator insertion point x_0. When the CFT has the large central charge $c \gg 1$ and the sparse spectrum, the above four-point function can be approximated by the vacuum conformal block with an appropriate choice of branch [50]. We explain this computation in detail in appendix B.

The expression of the CFT von Neumann entropy is constrained by the causal relationship between the operator insertion point $x^{\pm} = x_0^{\pm}$ and the endpoint $x_5^{\pm}$ of the region $\bar{C}$ [48–59]. Indeed, the local operator insertion induces a pair of shock waves, one of which is left moving and the other is right moving, and roughly speaking, we can interpret the pair as an entangled pair of particles. In this interpretation, the CFT von Neumann entropy can be non-trivial only when one of the shock waves enters the domain of dependence of the region $D[\bar{C}]$ and its "partner" does not. Thus, for the fixed endpoint $x^{\pm} = x_5^{\pm}$ of the region $D[\bar{C}]$, there are four possible forms of the von Neumann entropy, depending on the relative position of the endpoint and the operator insertion point as in figure 20.

(1) When the endpoint x_5 is in the right wedge of the operator insertion point x_0, i.e., $x_5^{\pm} > x_0^{\pm}$, both left and right moving shock waves do not enter the domain of dependence $D[\bar{C}]$ of the region $\bar{C}$. Thus, the shock waves can not change the entanglement between the region $\bar{C}$ and its complement region, and the CFT von Neumann entropy of the region $\bar{C}$ is equal to that for the shockless case $S_\beta[\bar{C}]$ owing to causality.

(2) Similarly, when the endpoint x_5 is in the left wedge of the operator insertion point $x_0^{\pm} > x_5^{\pm}$, both left and right moving shock waves enter the domain of dependence $D[\bar{C}]$, and again owing to causality the von Neumann entropy is equal to that for the shockless case $S_\beta[\bar{C}]$.

(3) When the local operator is inserted in the causal future or past of the endpoint, the CFT von Neumann entropy can be changed by the shock waves. When the operator insertion point is inside the future light-cone of the endpoint x_5, i.e., $x_5^- > x_0^-$ and $x_0^+ > x_5^+$, then the left moving one of the shock waves contributes to the CFT von Neumann entropy non-trivially. In this case, the difference between the non-trivial CFT von Neumann entropy and the trivial one, $\Delta S \equiv S_{\beta,E}[\bar{C}] - S_\beta[\bar{C}]$, is given by [50]

$$\Delta S_F = \frac{c}{6} \log \left[\frac{\beta}{\pi\varepsilon} \frac{\sin \pi\alpha}{\alpha} \frac{\sinh \frac{\pi}{\beta}(x_0^+ - x_5^+) \sinh \frac{\pi}{\beta}(x_6^+ - x_0^+)}{\sinh \frac{\pi}{\beta}(x_6^+ - x_5^+)} \right]. \tag{3.42}$$

On the other hand, when the local operator is inserted inside the past light cone of the endpoint x_5, i.e., $x_0^- > x_5^-$ and $x_5^+ > x_0^+$, then only the right moving one of the shock waves contributes non-trivially, and the non-trivial part is given by

$$\Delta S_P = \frac{c}{6} \log \left[\frac{\beta}{\pi\varepsilon} \frac{\sin \pi\alpha}{\alpha} \frac{\sinh \frac{\pi}{\beta}(x_0^- - x_5^-) \sinh \frac{\pi}{\beta}(x_6^- - x_0^-)}{\sinh \frac{\pi}{\beta}(x_6^- - x_5^-)} \right]. \tag{3.43}$$

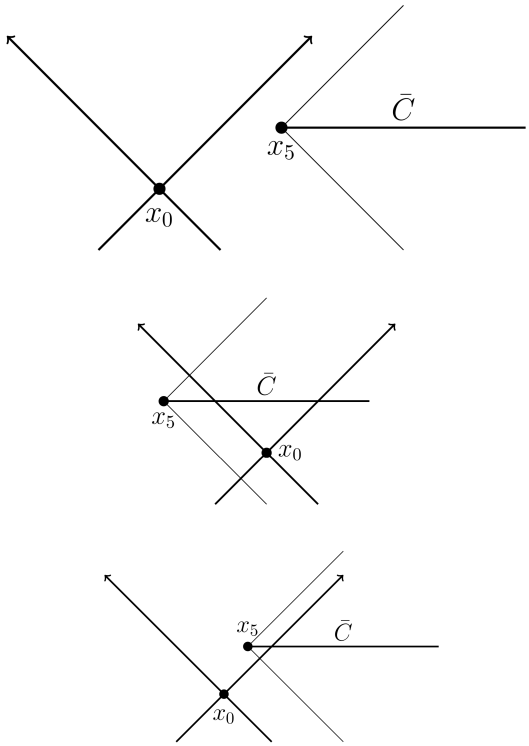

Figure 20: Three possible causal relations between the operator at $x^{\pm} = x_0^{\pm}$ and the interval $\bar{C}$. **Top** and **Middle** : The local operator is spatially separated from $\bar{C}$. In this case, the non-trivial part of the CFT entropy ΔS in the generalized entropy is vanishing owing to causality. **Bottom**: When the local operator and the $\bar{C}$ are causally connected, the right mover emitted by the quench can enter the causal diamond of $D[\bar{C}]$. Only in this case, ΔS is non vanishing. In particular, ΔS is given by (3.42).

CFT entropy for two disjoint intervals In evaluating the generalized entropy, we need to consider the CFT von Neumann entropy of two disjoint intervals $\bar{C} = \bar{C}_1 \cup \bar{C}_2$. The possible form for the CFT von Neumann entropy is constrained by causality. In the previous subsection, we saw that, as we increase the entanglement temperature $1/\beta \to \infty$, the size of two intervals become smaller $\bar{C}_1,\ \bar{C}_2 \to 0$. From the observation, it is reasonable to approximate the von Neumann entropy of two disjoint intervals by the sum of the von Neumann entropies of the single interval $\bar{C}_1$ and that of $\bar{C}_2$,

$$S[\bar{C}] \approx S[\bar{C}_1] + S[\bar{C}_2]. \tag{3.44}$$

Thus it is enough to consider the von Neumann entropy for a single interval in evaluating the generalized entropy in the high entanglement temperature limit $1/\beta \to \infty$. This discussion is very similar to that of (2.47).

For simplicity, we assume the shock waves do not enter the domain of dependence of the left interval $\bar{C}_1$, i.e., $x_0^{\pm} > x_3^{\pm}$, thus in this case only the von Neumann entropy of the right region $S[\bar{C}_2]$ can be changed by the shock waves non-trivially.

3.3.4 Quantum extremal surfaces

We will study the behavior of the dominant quantum extremal surface as we change the operator insertion point x_0. In particular, we will mainly study it in the high entanglement temperature limit, where the island contribution dominates, and in such a situation the classical extremal surface is located near the spatial asymptotic infinity $x^{\pm} = \frac{\pi}{2}$. We decompose the CFT von Neumann entropy $S_{\beta,E}[\bar{C}] - S_{\rm vac}[\bar{C}]$ in (3.27) , into the trivial part $S_{\beta}[\bar{C}] - S_{\rm vac}[\bar{C}]$ which does not contain the effect of the local quench, and the remaining one $\Delta S = S_{\beta,E}[\bar{C}] - S_{\beta}[\bar{C}]$. In this decomposition, in high entanglement temperature limit the former part does not give almost no contribution to the generalized entropy and we ignore the trivial part below. As we noted before in 3.2.2, under high entanglement temperature limit the classical extremal surfaces almost coincides with the bifurcation surfaces of the black hole. Thus, now we will mainly study the non-trivial part of the CFT von Neumann entropy to get the non-trivial quantum extremal surfaces. Before studying the case that the non-trivial part of the CFT von Neumann entropy does not give non-trivial contributions, we explain two limiting cases where the non-trivial part vanishes.

At first, when the local operator is inserted into the deep interior of the black hole $x_0 \sim 0$, the location of the quantum extremal surface almost coincides with that of the bifurcation surface of the black hole, which is deformed by the shock waves, i.e., $x^{\pm} = x_H^{\pm}(E)$ given by (3.37). The reason for the above coincidence is that we insert the local operator into the deep interior region of the black hole $x_0 \sim 0$, which is spatially separated from the bifurcation surface of the deformed black hole $x^{\pm} = x_H^{\pm}(E)$, thus, in this case, the non-trivial CFT entropy part ΔS vanishes owing to causality.

On the other hand, when the local operator is inserted into the exterior of the deformed black hole, i.e., $x_0 > x_H(E)$, because the non-trivial CFT entropy part ΔS vanishes in this case again, the location of the quantum extremal surface almost coincides that of the bifurcation surface of the original undeformed black hole at $x^{\pm} = x_H^{\pm}(0)$ given by (3.36). Below, we explain details of the above behavior of the quantum extremal surfaces.

Before the explanation, we note that the generalized entropy which we

consider have the contribution coming from the left quantum extremal surface, which is independent of the operator insertion point $x_0^{\pm}$ as long as we consider the operator insertion for the region $x_0^+ + x_0^- > 0$ (and $x_0^{\pm} > x_3^{\pm}$). In the high temperature limit, the contribution from the left quantum extremal surface is given by (3.23) divided by $4G_N$ and we denote the contribution by S_L.

Then, we have the following three cases for the generalized entropy from the above discussions.

Case 1

When we insert the local operator inside the original horizon $x_0 < x_H(0)$ (the top panel of figure 20), the location of the (right) quantum extremal surface almost coincides with that of the bifurcation surface of the black hole which is deformed by the shock waves. In this case, since the location of the quantum extremal surface is at $x^{\pm} = x_H(E)$ and the non-trivial CFT part vanishes $\Delta S = 0$, we obtain the following generalized entropy

$$\begin{aligned} S_{\text{gen}} &= \frac{\Phi_{\beta,E}(x_H(E))}{4G_N} + S_L \\ &= \frac{1}{4G_N}\left[\phi_0 - \frac{4}{|\Lambda|}\left[\left(\frac{\pi X_\beta}{2}\right)^2 + 8\pi^2 G_N X_\beta E\cos^2 x_0\right.\right. \\ &\qquad \left.\left. - \frac{128\pi^2 G_N^2}{|\Lambda|}E^2\cos^4 x_0 + 16\pi G_N E\cos^2 x_0\tan x_0\right]\right] + S_L. \end{aligned} \tag{3.45}$$

Case 2

When we insert the local operator in between two candidate quantum extremal surfaces (the middle panel of figure 20), $x_H(0) < x_0 < x_H(E)$, the

generalized entropy is given by

$$
\begin{aligned}
S_{\text{gen}} &= \text{Min}\left\{\frac{\Phi_\beta(x_H(0))}{4G_N},\ \frac{\Phi_{\beta,E}(x_H(E))}{4G_N}\right\} + S_L \\
&= \frac{1}{4G_N}\Bigg[\phi_0 - \frac{(\pi X_\beta)^2}{|\Lambda|} \\
&\qquad + \text{Min}\left\{0, -16\pi G_N E\cos^2 x_0\left(\frac{2\pi X_\beta}{|\Lambda|} + \frac{16\pi G_N}{|\Lambda|}E\cos^2 x_0 - \tan x_0\right)\right\}\Bigg] + S_L.
\end{aligned}
\tag{3.46}
$$

In this case, the non-trivial CFT entropy part vanishes again $\Delta S = 0$.

We can explicitly give the point $x_0^{\pm} = x_T$ at which the two contribution coincides satisfies the following equation

$$
\tan x_T = \frac{2\pi X_\beta}{|\Lambda|} + \frac{16\pi G_N}{|\Lambda|}E\cos^2 x_T. \tag{3.47}
$$

Case 3

When we insert the local operator outside the deformed horizon $x_H(E) < x_0$ (the bottom panel of figure 20), we have the following trivial generalized entropy

$$
\begin{aligned}
S_{\text{gen}} &= \frac{\Phi_\beta\left(x_H(0)\right)}{4G_N} + S_L \\
&= \frac{1}{4G_N}\left[\phi_0 - \frac{(\pi X_\beta)^2}{|\Lambda|}\right] + S_L.
\end{aligned}
\tag{3.48}
$$

Net result

From above results, we obtain the following generalized entropy as the function of the operator insertion point x_0 in the high temperature limit,

$$S_{\text{gen}}\ (x_0) = \begin{cases} \dfrac{1}{4G_N}\left[\phi_0 - \dfrac{(\pi X_\beta)^2}{|\Lambda|}\right. \\ \qquad \left. - 2E\cos^2 x_0\left(\dfrac{2\pi X_\beta}{|\Lambda|} + \dfrac{2}{|\Lambda|}E\cos^2 x_0 - \tan x_0\right)\right] + S_L \quad \text{for } x_0 < x_T \\ \dfrac{1}{4G_N}\left[\phi_0 - \dfrac{(\pi X_\beta)^2}{|\Lambda|}\right] + S_L \qquad \text{for } x_T < x_0. \end{cases} \tag{3.49}$$

We display the plots of the above generalized entropy for two different E cases in figure 21 [20].

The plots show that when the local operator is inserted outside the black hole horizon, the generalized entropy is not affected by the local operator and remains unchanged, while when it is inserted inside the black hole horizon, the generalized entropy is changed by it and decreases. The plots also show that as we insert the local operator into the deeper interior of the black hole, the generalized entropy becomes smaller significantly.

This is because if we insert the local operator inside of the horizon and create the shock waves at the insertion point, the resulting black hole have the longer interior wormhole region compared to the shockless case, which is seen from the relation $x_H(0) < x_H(E)$, and as a result the entropy of the black hole becomes smaller $\Phi_\beta(x_H(0))/4G_N > \Phi_{\beta,E}(x_H(E))/4G_N$. Thus, in some sense, what the shock waves do is to make the black hole further "evaporate". The black hole in the gravitating universe B has been evaporating owing to the entanglement between two universes A, B, and the local operator insertion accelerates the evaporation, which means that the entropy of the black hole decrease faster as a function of the entanglement temperature β.

We can get the actual von Neumann entropy of the universe A, $S(\rho_A)$, by using the formula (3.5), that is, the entropy is given by the minimum between two von Neumann entropy $S_{\text{no-island}}$ and $S_{\text{gen}}\ (x_0)$. The plot of the actual von Neumann entropy $S(\rho_A)$ is shown in figure 22. Because we are

[20] We obtained the plots in our paper [27] which show in this section by full numerical calculations through the faithful extremization of the generalized entropies, unlike analytical expressions appearing in the body of this section.

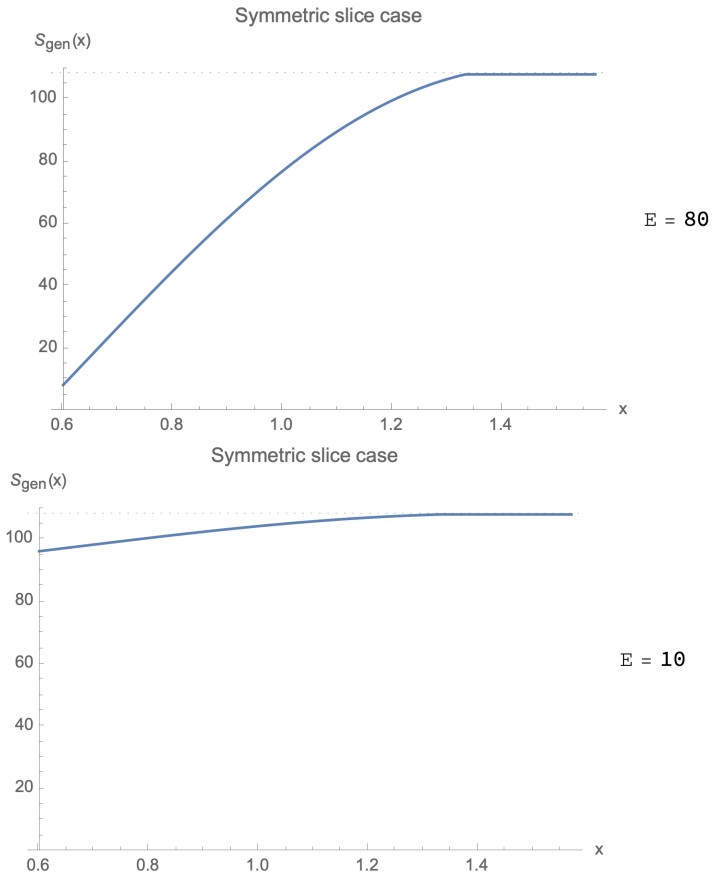

Figure 21: Plots of the generalized entropy S_{gen}, (3.49), as the function of x_0 $(0 \leq x_0 \leq \pi/2)$ with $\phi_0 = 1700$, $\beta = 1$, $|\Lambda| = 500$, $c = 50$, $\varepsilon = 0.1$. $\Delta = 8\,(E = 80)$(top) and $\Delta = 1\,(E = 10)$(bottom). The dotted line is the value of the entropy for the shock-less case, $\Delta = 0\,(E = 0)$. (These plots were also obtained in our paper [27] and we show them again.)

interested in the behavior of the von Neumann entropy $S(\rho_A)$ as a function of the entanglement temperature $1/\beta$, we give the plot (figure 22) as a function of $1/\beta$ with fixing the operator insertion point $x^{\pm} = x_0^{\pm}$. As the entanglement temperature becomes higher, the bifurcation surface of the black hole gets closer to the asymptotic spatial infinity, and the local operator initially located outside of the black hole horizon is absorbed into the black hole. Like the expression (3.25), we can again see that, above some critical temperature β_c, the dominant contribution to the von Neumann entropy $S(\rho_A)$ is given by the generalized entropy $S_{\text{gen}}(x_0)$ (3.49). In particular, in the high entanglement temperature limit $1/\beta \to \infty$, because the local operator goes into the deep interior of the black hole against to the black hole horizon of

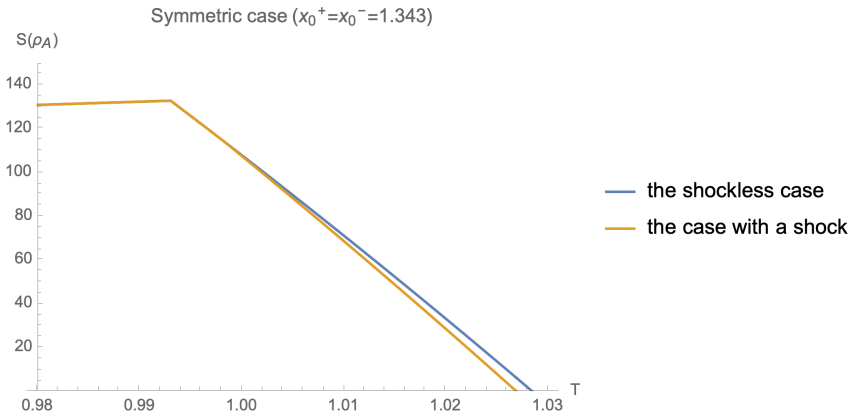

Figure 22: Plots of the Page curves corresponding to the shockless case (3.25) and the case with the shock (3.50) as the function of $T = 1/\beta$ with fixing the location of the operator, which we place on the reflection symmetric slice $x_0^+ = x_0^-$. $\phi_0 = 1700$, $|\Lambda| = 500$, $c = 50$, $\Delta = 10$, $\varepsilon = 0.01$, $x_0^+ = x_0^- = 1.343$. The island begins dominating at $T \simeq 0.993$ and the location of the corresponding QES is $x_H^+(0) = x_H^-(0) \simeq 1.328$. The von Neumann entropy with a shock decreases faster than the one without it. (These plots were also obtained in our paper [27] and we show them again.)

the low entanglement temperature regime, the generalized entropy $S_{\rm gen}(x_0)$ is given by the first line of (3.49). Thus an approximate expression for the von Neumann entropy is given by

$$S(\rho_A) = \begin{cases} S_{\rm no-island} = \dfrac{\pi^2 c}{3\beta} & \beta \gg \beta_c \\ S_{\rm gen}(x_0) = \dfrac{1}{4G_N}\left[\phi_0 - \dfrac{(\pi X_\beta)^2}{|\Lambda|}\right. & \\ \qquad \left. - 2E\cos^2 x_0 \left(\dfrac{2\pi X_\beta}{|\Lambda|} + \dfrac{2}{|\Lambda|} E\cos^2 x_0 - \tan x_0\right)\right] + S_L & \beta \ll \beta_c. \end{cases} \tag{3.50}$$

Since the above expression (3.50) is clearly different from the one (3.25) without the local operator insertion, we consider the difference between them.

In the previous case (3.25), above the critical temperature β_c, the von Neumann entropy decreases as

$$S_{\rm island} = \frac{1}{4G_N}\left[\phi_0 - \frac{(\pi X_\beta)^2}{|\Lambda|}\right] + S_L. \tag{3.51}$$

On the other hand, in the presence of the shock waves, the von Neumann entropy (3.50) decreases faster than the one without the shock waves (3.25) owing to the additional terms coming from the shock wave, which are proportional to the constant E. This also supports the point of view that the shock waves accelerate the evaporation of the black hole in our setup.

3.3.5 QESs with non-trivial CFT entropy

We have focused on the cases that the non-trivial part of the CFT von Neumann entropy $\Delta S = S_{\beta,E}[\bar{C}] - S_{\beta}[\bar{C}]$ vanishes by choosing the operator insertion point to be on the time reflection symmetric slice $x_0^+ = x_0^-$. We note that, in such cases, the quantum extremal surfaces and the local operator insertion point are spatially separated. As a result, the quantum extremal surfaces coincide with the classical extremal surfaces, which we can identify with the bifurcation surfaces of the black hole.

On the other hand, when the local operator is inserted into the causal future of the original horizon $x^{\pm} = x_H^{\pm}(0)$, i.e., $x_0^+ > x_H^+(0), x_0^- < x_H^-(0)$, then the non-trivial part of the CFT von Neumann entropy does not vanish.

Firstly, we determine the location of the classical extremal surface. The full dilaton profile is still given by (3.33), and since we expect that the new classical extremal surface is in the causal past of the local operator insertion point, we extremize

$$\begin{aligned}\Phi_R(x^{\pm}) = \phi_0 + \frac{|\Lambda|}{4}\tan x^+ \tan x^- - X_\beta(x^+ \tan x^+ + x^- \tan x^-) \\ - 8\pi G_N E \cos^2 x_0^- (\tan x^- - \tan x_0^-).\end{aligned} \tag{3.52}$$

From the above dilaton profile $\Phi_R(x^{\pm})$, we get the critical point $(x_{\mathcal{H}}^+(E), x_{\mathcal{H}}^-(E))$ satisfying

$$x_{\mathcal{H}}^-(E) = x_H^-(0), \quad \tan x_{\mathcal{H}}^+(E) = \tan x_H^+(0) + \frac{32\pi G_N E}{|\Lambda|}\cos^2 x_0^-. \tag{3.53}$$

We note that the above critical point $(x_{\mathcal{H}}^+(E), x_{\mathcal{H}}^-(E))$ is different from the one $(x_H^+(E), x_H^-(E))$ of $\Phi_{\beta,E}$ (3.35).

The shock wave induces the shift of the horizon along the x^+ direction. In order for the critical point $(x_{\mathcal{H}}^+(E), x_{\mathcal{H}}^-(E))$ to be in the causal past of the local operator insertion point, we need the condition

$$\tan x_H^+(0) + \frac{32\pi G_N E}{|\Lambda|}\cos^2 x_0^- < \tan x_0^+. \tag{3.54}$$

Next to determine the location of the quantum extremal surface $x^\pm = x^\pm_{Q_1}$ in the same situation, we consider the generalized entropy obtained from (3.42),

$$S_{\rm gen}(x^\pm) = \frac{\Phi_R(x^\pm)}{4G_N} + \frac{c}{6}\log\left[\frac{\beta}{\pi\varepsilon}\frac{\sin\pi\alpha}{\alpha}\frac{\sinh\frac{\pi}{\beta}(x_0^+ - x_5^+)\sinh\frac{\pi}{\beta}(x_6^+ - x_0^+)}{\sinh\frac{\pi}{\beta}(x_6^+ - x_5^+)}\right] + S_\beta[\bar{C}] - S_{\rm vac}[\bar{C}] + S_L \tag{3.55}$$

where S_L is the contribution from the left extremal surface, as in the discussion in 3.3.4. In the high temperature limit, $S_L \approx \Phi_\beta(x_H^\pm(0))/4G_N$ with (3.23).

We consider the critical point of the above generalized entropy (3.55). Because the non-trivial part of the CFT entropy ΔS does not contribute to its derivative with respect to x^-, $\tan x^+_{Q_1}$ is still given by

$$\tan x^+_{Q_1} = \tan x^+_H(0) + \frac{32\pi G_N E}{|\Lambda|}\cos^2 x_0^-. \tag{3.56}$$

On the other hand, the derivative with respect to x^+ is modified by ΔS. By ignoring the trivial CFT entropy part $S_\beta[\bar{C}] - S_{\rm vac}[\bar{C}]$, we obtain

$$\tan x^-_{Q_1} = \frac{4}{|\Lambda|}\left[\frac{\pi}{2}X_\beta + \frac{c\pi}{6\beta}\cos^2 x^+_{Q_1}\left(\frac{1}{\sinh\frac{\pi}{\beta}(x_0^+ - x^+_{Q_1})} - \frac{1}{\sinh\frac{\pi}{\beta}(x_6^+ - x^+_{Q_1})}\right)\right]. \tag{3.57}$$

Since the above conditions determine $x^\pm_{Q_1}$, by substituting the coordinates $x^\pm_{Q_1}$ into the generalized entropy we can give the expression of the generalized entropy (3.55).

There is also another quantum extremal surface, $x^\pm = x^\pm_{Q_2}$, which is located at the right wedge of the local operator insertion point $x^\pm_{Q_2} > x^\pm_0$. In this case, the non-trivial CFT entropy part ΔS vanishes, thus the quantum extremal surface $x^\pm_{Q_2}$ almost coincides with the bifurcation surface of the original black hole $x^\pm_{Q_2} = x^\pm_H(0)$.

Although there are two candidates for the quantum extremal surface at $x^\pm = x^\pm_{Q_1}$ and $x^\pm = x^\pm_{Q_2}$, they can not appear simultaneously owing to the non-symmetric insertion of the local operator. If the local operator is inserted into the causal future of the bifurcation surface of the original black hole $x_0^+ > x_H^+(0)$, $x_0^- < x_H^-(0)$, then the bifurcation surface is shifted to the point $(x^+_{\mathcal{H}}(E), x^-_{\mathcal{H}}(E))$. In this case, the candidate quantum extremal surface at $x^\pm_H(0) = x^\pm_{Q_2}$ is no longer extremal, and only the other candidate quantum

extremal surface $x^{\pm} = x^{\pm}_{Q_1}$ becomes the quantum extremal surface. On the other hand, if the local operator $x^{\pm}_0$ is inserted into the exterior of the original horizon $x^{\pm}_0 > x^{\pm}_H(0)$, then $x^{\pm} = x^{\pm}_{Q_2}$ becomes the quantum extremal surface. Thus, we obtain the generalized entropy

$$S_{\rm gen,E}(x^+_0, x^-_0) = \begin{cases} S_{\rm gen}(x^{\pm}_{Q_1}) & \text{for} \quad x^-_H(0) > x^-_0 \\ S_{\rm gen}(x^{\pm}_{Q_2}) & \text{for} \quad x^-_H(0) < x^-_0 . \end{cases} \tag{3.58}$$

In the high entanglement temperature limit, we can get the generalized entropy $S_{\rm gen}(x^{\pm}_{Q_1})$ by evaluating it at the point specified by (3.56) and (3.57) into the expression (3.55). $S_{\rm gen}(x^{\pm}_{Q_2})$ almost coincides with the entropy of the original black hole $\Phi_\beta(x^{\pm}_H(0))/4G_N$. From the formula (3.5), the von Neumann entropy is given by the minimum between the above generalized entropy and the thermal CFT von Neumann entropy $S_{\rm no-island}$,

$$S(\rho_A) = {\rm Min}\left\{S_{\rm no-island},\, S_{\rm gen,E}\right\}. \tag{3.59}$$

Plot of the result

We consider the case that although the location of the left moving shock wave is fixed $x^+ = x^+_0$, and we can change that of the right moving one as shown in figure 23. We consider the case $x^+_0 > x^+_H(E)$ so that the local operator insertion point can move between the interior and the exterior of the black hole. Under the above conditions, we plot the generalized entropy $S_{{\rm gen},E}(x^{\pm}_0)$ as a function of x^-_0 in figure 24.

As we decrease the value of x^-_0, the local operator is "falling" into the region behind the black hole horizon, and we are interested in the behavior of the von Neumann entropy as the local operator is falling to the black hole horizon and eventually enters the black hole interior.

This plot in figure 24 for the asymmetric local operator insertion is compared to the similar plot shown in figure 21, where we insert the local operator on the reflection symmetric slice (3.49), as in the top panel of figure 23.

The two plots (fig 24 and 21) have the common feature that when we insert the local operator outside the black hole horizon $x^- > x^-_H(0)$, the two generalized entropy almost coincides with the classical entropy of the original black hole, that is, the Bekenstein-Hawking entropy of the black hole, which is given by $\Phi_\beta(x^{\pm}_H(0))/4G_N$ with (3.23). This is because the non-trivial CFT entropy part ΔS vanishes owing to the space-like separation between the local operator insertion point and the quantum extremal surface.

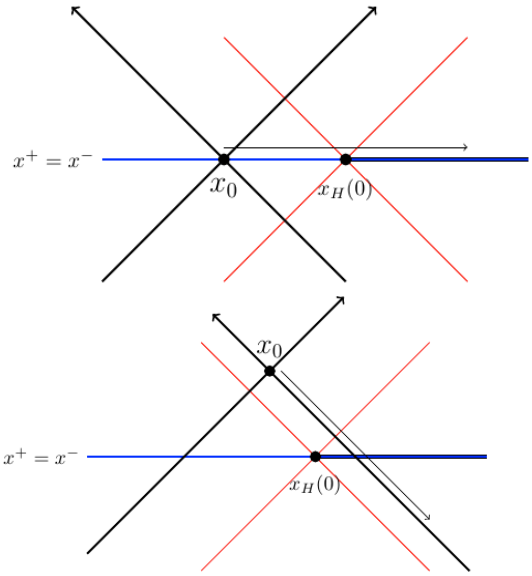

Figure 23: **Top**: The operator inserted on the time reflection symmetric slice (the blue line). In this case the operator is spatially separated from the bifurcation surface of the black hole at $x^{\pm} = x_H^{\pm}(0)$. (The black hole horizon is drawn by the red lines.) **Bottom**: The operator inserted on the non time reflection symmetric slice. In this case, the bifurcation surface can causally contact with the operator.

On the other hand, when we insert the local operator into the black hole interior $x_0^- < x_H^-(0)$, their behaviors of the generalized entropy are different. In particular, we can see that there is a bump in the plot for the asymmetric insertion (figure 24), however, for the symmetric insertion (figure 21), there is no such a bump. The presence of the bump is related to the fact that the quantum extremal surface for the asymmetric insertion is in the causal past of the local operator insertion point, i.e., the non-trivial CFT entropy part ΔS does not vanish. On the other hand, for the symmetric local operator insertion, owing to the space-like separation between the local operator insertion point and the quantum extremal surface, the non-trivial CFT entropy part ΔS vanishes.

We can interpret the bump in figure 24 as a result of the dynamics of the black hole. In order to explain the interpretation, it is useful to follow the plot backward in the x_0^- direction. As we decrease x_0^-, the black hole becomes larger owing to the absorption of the local operator, and this gives the sudden increase of the generalized entropy in the plot. After the increase of the black hole size, the black hole starts to evaporate again, and therefore, the generalized entropy starts decreasing.

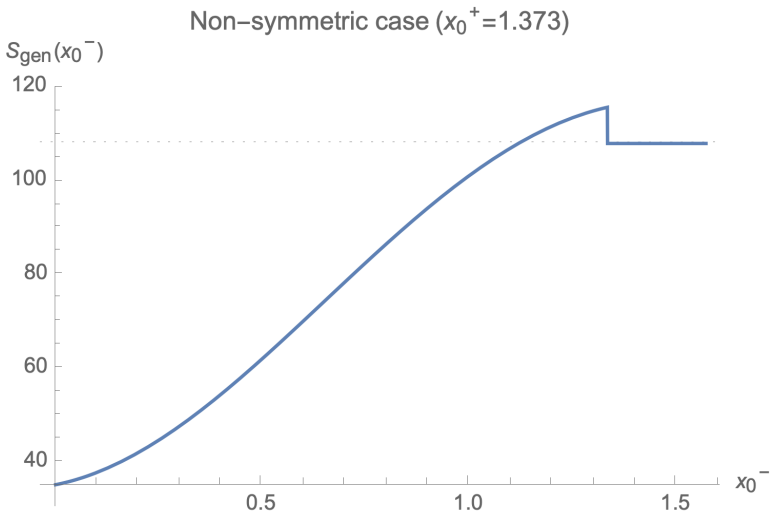

Figure 24: Plot of the generalized entropy given in (3.58) as a function of x_0^- with fixing x_0^+ (the case of the non-symmetric insertion), with the choice of parameters $\phi_0 = 1700$, $|\Lambda| = 500$, $c = 50$, $\beta = 1$, $\Delta = 7$, $\varepsilon = 0.1$, $x_0^+ = 1.373$. The dotted line corresponds to the shockless case $\Delta = 0$. (These plots were also obtained in our paper [27] and we show them again.)

One can regard the difference between these behaviors of the two generalized entropies as the difference in the ways of these two insertions. The symmetric operator insertion can be regarded as a local operation, since, in the symmetric case, the local operator is inserted in either the domain of dependence of the island region $D[C]$ (, which we can consider as a part of the radiation system on the non-gravitating universe A) or its causal complement region $D[\bar{C}]$ in the universe B, as in the top panel of figure 23. Because they are local operations, they can only decrease or unchanged the von Neumann entropy, not increase[21]. On the other hand, local operators inserted asymmetrically can enter a region that is behind the horizon and belong to neither of the two domains of dependence $D[C]$ and $D[\bar{C}]$ (the bottom panel of figure 23). Thus, these asymmetric operator insertions are not local operations, so they can increase the entanglement between two regions C and $\bar{C}$, leading to the bump in figure 24.

[21]This property is used to characterize entanglement in quantum information theory, see details in, e.g., [60].

3.3.6 The von Neumann entropy

We can give the von Neumann entropy $S(\rho_A)$ by using the formula (3.59) with the above results. Again we plot the von Neumann entropy $S(\rho_A)$ as a function of the entanglement temperature $1/\beta$ with fixing the operator insertion point $x^{\pm} = x_0^{\pm}$ in figures 25 and 26. As we increase the entanglement temperature, the location of the bifurcation surface approaches the asymptotic spatial infinity, so the black hole horizon expands, and the local operator is absorbed into the black hole. Thus, in this case, we can again observe the same physics as in the case that we vary x_0^-.

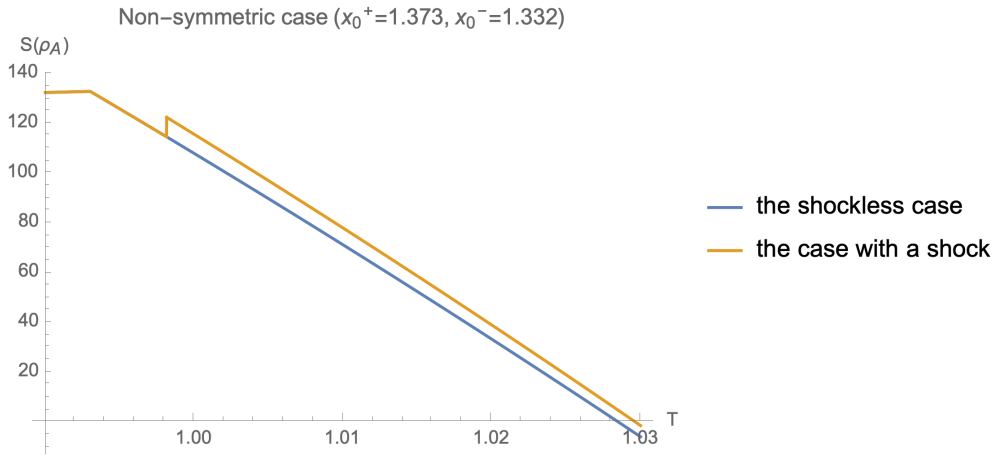

Figure 25: Plots of the Page curves corresponding to the shockless case (3.25) and the case with a shock wave (3.59) as the function of the entanglement temperature $T = 1/\beta$ with fixing the position of the operator, which is not on the reflection symmetric slice, ie $x_0^+ \neq x_0^-$, with the choice of parameters $\phi_0 = 1700$, $|\Lambda| = 500$, $c = 50$, $\Delta = 7$, $\varepsilon = 0.1$, $x_0^+ = 1.373$, $x_0^- = 1.332$. The island begins dominating at $T \simeq 0.993$ and the location of the corresponding QES is $x_H^+(0) = x_H^-(0) \simeq 1.328$. (These plots were also obtained in our paper [27] and we show them again.)

When we choose the operator insertion point and the conformal dimension of the local operator suitably, the behavior of the resulting von Neumann entropy becomes complicated as in figure 26. It is reasonable to compare this behavior with that of the von Neumann entropy for the shockless case (3.25). In the latter case where there is no shock wave, the transition between the no-island entropy $S_{\text{no-island}}$ and the island entropy S_{island} happens only once. However, in the former case, the transition between the no-island and island entropy can happen multiple times.

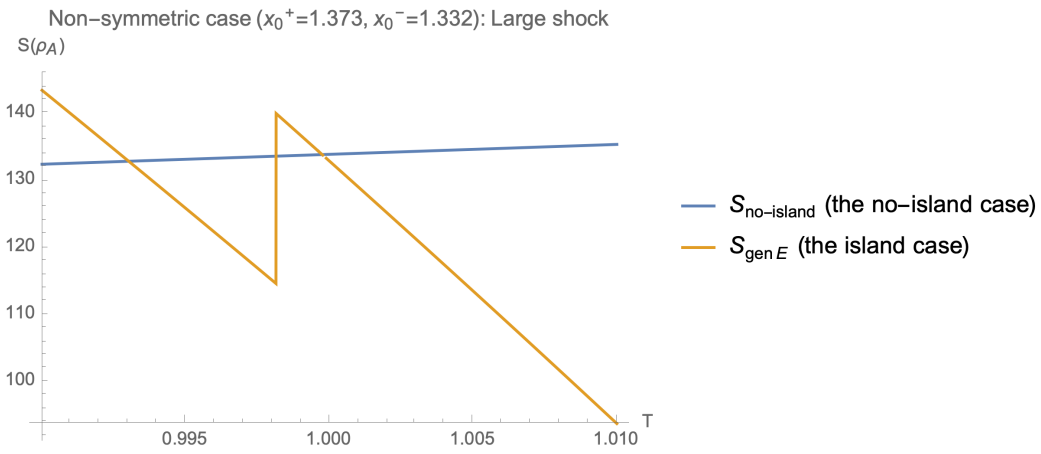

Figure 26: Similar plot to figure 25 but the shock wave has a larger energy than the previous case. We plot the Page curve only around the points at which the non-trivial dominance changes happen unlike the previous case (figure 25). The Page curve is given by the minimum between them. We set the parameters to be $\phi_0 = 1700$, $|\Lambda| = 500$, $c = 50$, $\Delta = 8$, $\varepsilon = 0.01$, $x_0^+ = 1.373$, $x_0^- = 1.332$. In this case, the transitions between them happen several times. The first transition is at $T \simeq 0.993$ and the location of the corresponding QES is $x_H^+(0) = x_H^-(0) \simeq 1.328$. (These plots were also obtained in our paper [27] and we show them again.)

Indeed, in figure 26, we can observe that at sufficiently low entanglement temperature, the no-island entropy $S_{\text{no-island}}$ dominates, and by increasing the entanglement temperature, the island entropy S_{island} becomes the dominant contribution like the behavior of the Page curve without the shock wave. However, this is not the end of the story. Namely, as we further increase the entanglement temperature, the black hole horizon expands, and thus the local operator is falling to the black hole horizon. This results in the size change of the black hole and the sudden increase of S_{island}. Now that the island entropy S_{island}, which is affected by the local operator, gets larger than the no-island entropy $S_{\text{no-island}}$, above this temperature the no-island entropy $S_{\text{no-island}}$ again dominates. Again as we further increase the entanglement temperature, the size of the black hole becomes smaller owing to the emissions of Hawking quanta, which corresponds to the increase of the entanglement temperature, thus eventually the island entropy S_{island} becomes smaller than the no-island one $S_{\text{no-island}}$, and it becomes dominant once again.

4 The Island formula and Baby Universes

In this section, we focus on the island formula in a setup that a AdS black hole is coupled to the bath CFT like in section 2 from a different perspective. In particular, we reconsider a treatment of the ensemble of quantum states that appears in a semi-classical description of a black hole by introducing new degrees of freedom, which we call the baby universe, and discuss the relationship between the island formula and the baby universe. We also discuss some physical implications of the baby universe. We note that the baby universe explained below is different from the non-gravitating universe A in previous section 3.

The introduction of the baby universe is related to the random fluctuations of an evaporating black hole. At first, we explain this relation briefly.

In principle, the evaporation process of a black hole is described by the bipartite system associated with the Hilbert space of the black hole H_{BH} and that for the Hawking radiation H_R. In this case, the state on this total system is given by an entangled state between the two systems H_{BH} and H_R. Of course, since the description of such an entangled state involves a quantum theory of gravity and such an entangled state depends on the detail of the quantum gravity, thus it seems impossible to study such a system efficiently. However, as was firstly discussed by Page [5], one can obtain a time variation of the von Neumann entropy of the Hawking radiation, which is consistent with the unitarity of quantum gravity, by taking the average of the entropy over the random fluctuations in the entangled state. This averaging operation enables us to have a *partially* fine-grained description of the evaporating black hole while maintaining semi-classical properties, to the extent of obtaining results, which is consistent with the principles of quantum theory. Indeed, in such a prescription, the island formula enables us to recover the Page curve within a semi-classical description of gravity. In particular, the Euclidean replica wormholes nicely capture the effects of these random fluctuations and their averaging geometrically.

We focus on a description of these random fluctuations in a Lorentzian spacetime in the semi-classical regime. We argue that the averaging over the random fluctuations can be "purified" by introducing an auxiliary system, which is often called a baby universe and entangled with the original spacetime. This new spacetime, the baby universe, is connected to the original spacetime with the black hole by an Einstein-Rosen (ER) bridge corresponding to the entanglement between the two spacetime. One can think of the baby universe as accommodating partially fine-grained information of the

evaporating black hole (see figure 29). It is enough to use such information to derive the Page curve.

Below we will see the above discussion in more detail and explain some physical implications.

4.1 Baby Universe and Ensemble nature of Semi-Classical Gravity

In this subsection, we explain the role of the baby universe in the evaluation of the von Neumann entropy of Hawking radiation through the island formula.

For this purpose, we begin with the fact that we have two distinct descriptions of a quantum theory of gravity. One of them is the fine-grained description, and the other is the coarse-grained one.

In the first full-fledged fine-grained description of quantum gravity, we have a sufficient number of observables (i.e., the complete set of operators of quantum gravity) to distinguish quantum states completely. Notice that, in this fine-grained, we can perform measurements with arbitrary precision. We focus on the gravitational system which has a black hole emitting Hawking quanta by the Hawking radiation. In the full-fledged fine-grained microscopic description, in the system a state has the following form,

$$|\Psi_M\rangle = \sum_{i=1}^{\mathcal{N}} \sum_{\alpha=1}^{k} F_{i\alpha}^{M} |\psi_i\rangle_{BH} |\alpha\rangle_R \,, \tag{4.1}$$

where $F_{i\alpha}^{M}$ is a *fixed number*. Here we introduced the orthonormal bases $|\psi_i\rangle_{BH}$ of the Hilbert space H_{BH} for micro-states for the black hole, and $|\alpha\rangle_R$ for the Hilbert space H_R for the Hawking quanta participating in the entanglement between the black hole and the Hawking radiation. $\mathcal{N}$ and k are the dimensions of their two Hilbert spaces.

The second description of the system is the coarse-grained one by using a semi-classical gravitational theory, where we have a limited number of observables, i.e., a subset of the complete set of observables of quantum gravity, or coarse-grained observables such as thermodynamical quantities. The spatial and time resolution of such observables are much worse than the Planck scale. In this description, the precise measurement of the coarse-grained observables can not fully specify the full quantum state of the full theory, but at best only specifies a set of states that have the same expectation values of the coarse-grained observables and correspond to the same semi-classical spacetime geometries.

Due to the limited number of observables and also to the fact that the resolution is much worse than the Planck scale, one is forced to describe the system in a coarse-grained way, in terms of a mixed state, i.e., an ensemble of states $\{p_M, |\Psi_M\rangle\}_M$, where p_M is a probability distribution, which we explain later. This ensemble includes the class of the states $|\Psi_M\rangle$ given by

$$|\Psi_M\rangle = \sum_{i=1}^{\mathcal{N}} \sum_{\alpha=1}^{k} C_{i\alpha}^M |\psi_i\rangle_{BH} |\alpha\rangle_R \,, \tag{4.2}$$

with the *random coefficient* matrix $C_{i\alpha}^M$.

Semi-classically we can not distinguish two such states $|\Psi_M\rangle, |\Psi_N\rangle$, which have different random coefficients C^M, C^N. This suggests that a coarse-grained observer describes the state by the mixed state as follows,

$$\rho_{BH\cup R} = \sum_M p_M |\Psi_M\rangle\langle\Psi_M| \,, \tag{4.3}$$

where p_M is the Gaussian probability distribution determined by the ensemble of states or random coefficient matrix $C_{i\alpha}^M$. Explicitly the probability distribution is given by (e.g., [61, 62])

$$p_M = \left(\frac{\mathcal{N}k}{\pi}\right)^{\mathcal{N}k} \exp\left(-\mathcal{N}k \,\mathrm{tr}(C^M C^{M\dagger})\right) , \tag{4.4}$$

and it satisfies the normalization condition $\sum_M p_M = 1$. See also (C.1)-(C.3) in appendix C. We also note that the coefficients $C_{i\alpha}$ are satisfying the following relationship,

$$\begin{aligned}
\langle 1 \rangle &= 1 \\
\langle C_{i\alpha} C_{\beta j}^\dagger \rangle &= \frac{1}{k\mathcal{N}} \delta_{ij} \delta_{\alpha\beta} \\
\langle C_{i\alpha} C_{\beta j}^\dagger C_{k\gamma} C_{\delta l}^\dagger \rangle &= \frac{1}{(k\mathcal{N})^2} \left(\delta_{ij}\delta_{\alpha\beta} \cdot \delta_{kl}\delta_{\gamma\delta} + \delta_{il}\delta_{\alpha\delta} \cdot \delta_{jk}\delta_{\beta\gamma}\right) \\
\langle (\Pi_{a=1}^n C_{i_a\alpha_a})(\Pi_{b=1}^n C_{\beta_b j_b}^\dagger) \rangle &= \frac{1}{(k\mathcal{N})^n} (\text{all possible contractions of indices}) \\
\langle (\Pi_{a=1}^n C_{i_a\alpha_a})(\Pi_{b=1}^m C_{\beta_b j_b}^\dagger) \rangle &= 0 \quad \text{for } m \neq n
\end{aligned} \tag{4.5}$$

where $\langle\cdot\rangle$ means the average over the random coefficient matrix $C_{i\alpha}^M$.

One can consider the randomness of the coefficient in the state (4.2) as the consequence of the highly chaotic dynamics of a black hole. More explicitly, the randomness can be understood as follows: Suppose that an observer tries

to determine the fine-grained state (4.1) by measurement of observables. To do so, the observer needs to perform a measurement with the Planck scale precision. However, for a coarse-grained observer, the measurement resolution is much worse than the Planck scale. Note that during the measurement time-scale, the microscopic state can time-evolve. Thus, if the measurement time-scale is much longer than the Planck scale, the microscopic state can time-evolve to almost all possible states of the form (4.2). In this way, a coarse-grained observer sees the black hole state as the state (4.2) with randomness. From the above discussion, we can intuitively understand why the randomness appears in the semi-classical description of the black hole dynamics.

Once we coarse-grain the system, we get the mixed state (4.2), not the pure state (4.1), and apparently we lose the microscopic details of the original state (4.1). However, within the coarse-grained description, we can compute some aspects of the *fine-grained* entropy, which is the von Neumann entropy calculated by using the fine-grained description, of Hawking radiation by purifying this mixed state (4.2) by introducing an auxiliary system H_{BU}, which we often call the baby universe. For instance, the recent understanding of the island formula suggests that by the purification, we can capture some part of fine-grained information of the Hawking radiation while using the semi-classical description. The related discussions on random fluctuations in black hole physics can be found in, e.g., [63–65]. We also note that Gaussian random fluctuations have a geometric interpretation in terms of the end-of-the-world branes in two-dimensional JT gravity [24].

We note that to purify the original system with the mixed state (4.3), we need to introduce an auxiliary system H_{BU} whose Hilbert space dimension is at least equal to or greater than that of the original system. In particular, the dimension of the baby universe Hilbert space H_{BU} depends on the coarse-graining procedure we consider. By using this baby universe Hilbert space, one can give the simplest purified state by

$$|\Phi\rangle_{BH\cup R\cup BU} = \sum_M \sqrt{p_M}|\Psi_M\rangle_{BH\cup R}|M\rangle_{BU}, \tag{4.6}$$

where $\{|M\rangle_{BU}\}$ are orthonormal baby universe states. A fine-grained observer can access to the auxiliary system, but a coarse-grain observer can not. We note that the coarse-grained description using the auxiliary system is not a full-fledged fine-grained description of the original system consisting of the black hole and the Hawking radiation. This is because we are artificially adding the degrees of freedom of the baby universe, which do not appear in the original Hilbert space $H_{BH} \otimes H_R$. In other words, in the fine-

grained (quantum gravitational) description, the actual fine-grained state realized in the system is one of the states in the ensemble, not the one with the baby universe. However, we consider the purified state (4.6) because it has an effective semi-classical gravitational description, on the contrary to the full-fledged fine-grained state (4.1) in quantum gravity. Moreover, as we will explain later, if we focus only on averaged properties of the fine-grained entropy, such as the Page curve, it is enough to consider the purified state by the baby universe.

We note that by tracing out the black hole degrees of freedom BH in the mixed state (4.3), we can get the reduced density matrix of the Hawking radiation ρ_R, but it gives an approximately thermal mixed state and its resulting von Neumann entropy $S(\rho_R)$ gives the Hawking's result

$$\begin{aligned} S(\rho_R) &= S(\ \langle \rho_{(M)R} \rangle_M\ ) \\ &= \log k, \end{aligned} \tag{4.7}$$

where we defined,

$$\rho_{(M)R} = \mathrm{tr}_{BH}\left[\, |\Psi_M\rangle\langle\Psi_M|_{BH\cup R}\,\right], \quad \langle \rho_{(M)R} \rangle_M = \sum_M p_M\ \rho_{(M)R}. \tag{4.8}$$

See the appendix C.1 for the derivation.

Next, we consider the von Neumann entropy of the Hawking radiation in the fine-grained description. For this purpose, firstly, we consider a geometric description of the purified state (4.6). In the purified state, the Hawking radiation H_R and the black hole H_{BH} are entangled with the auxiliary baby universe H_{BU}. From the viewpoint of ER=EPR (conjecture) [66], which states that the existence of the entanglement between two distant regions is related to that of a spatial wormhole connecting the two regions, it is expected that the entanglement between the baby universe H_{BU} and the original system $H_R \otimes H_{BU}$ is geometrically realized by an Einstein-Rosen bridge that connects the two systems (see figure 29). The detailed properties of the Einstein-Rosen bridge may depend highly on the choice of the ensemble. If this combined system is realized within the framework of the AdS/CFT correspondence, the auxiliary baby universe can be modeled by an additional boundary, and its gravity dual involves an Einstein-Rosen bridge connecting the new boundary. This purification process is the key in the finding of the island formula, which captures some aspects of fine-grained information of the quantum gravity states through non-perturbative contributions in the semi-classical gravitational description of gravity. For instance, when we describe an evaporation process of a black hole semi-classically, such non-perturbative

contributions are required to get a consistent result with quantum gravity. In such an evaporation process, the discreteness of the energy spectrum of the black hole micro-states is essential to ensure the unitarity of the process. However, in the coarse-grained description, typical energy differences between black hole micro-states are invisible since they are typically of order $\mathcal{O}(e^{-S_{BH}})$, where S_{BH} is the Bekenstein-Hawking entropy [67]. We can take the discrete energy spectrum into account after including non-perturbatively small contributions, which are provided by Euclidean wormholes [68, 69].

What the island formula suggests is that, after the Page time, one should identify the fine-grained Hilbert space of the Hawking radiation $H_{\mathbf{R}}$ with the tensor product of two Hilbert spaces $H_R \otimes H_{BU}$ in our formulation. On the other hand, before the Page time, $H_{\mathbf{R}}$ should be identified with just that of the Hawking radiation H_R, and correspondingly the fine-grained Hilbert space of the black hole should identify with the tensor product of the black hole and the baby universe $H_{BH} \otimes H_{BU}$. This difference between the radiation (and equivalently the black hole) Hilbert spaces before and after the Page time comes from the fact that the inequality between the Hilbert space dimensions of the Hawking radiation and that of the black hole changes. Indeed, before the Page time, since the total state (4.6) is pure, the von Neumann entropy of the union of the black hole and the baby universe $BH \cup BU$ equals to the previous von Neumann entropy (4.7) of the Hawking radiation R, i.e., $S(\rho_{BH\cup BU}) = S(\rho_R) = \log k$, which is consistent with the behavior of the Page curve before the Page time.

After the Page time, the reduced density matrix of the Hawking radiation and the baby universe $\rho_{R\cup BU}$ for the purified state (4.6) gives the the fined-grained entropy of the Hawking radiation $H_{\mathbf{R}}$, which is different from the von Neumann entropy (4.7) of the naive density matrix (4.3),

$$\begin{aligned} S(\rho_{\mathbf{R}}) &= S(\rho_{R\cup BU}) \\ &= \log \mathcal{N} \\ &= S_{BH}. \end{aligned} \tag{4.9}$$

In appendix C.2 we give details of this calculation. The above result (4.9) reproduces the behavior of the Page curve after the Page time, which gives the Bekenstein-Hawking entropy S_{BH} of the black hole. Thus by appropriately dividing the total system $BH \cup R \cup BU$ into two parts, we can obtain the von Neumann entropy which obeys the Page curve (see table 1).

We also know that the fine-grained entropy $S(\rho_{\mathbf{R}})$ of the Hawking radiation can be computed by using the island formula (2.56). In the calculations of the von Neumann entropy using the island formula, it was essential to

	Black Hole	Hawking Radiation	von Neumann Entropy
Before the Page time	$BH \cup BU$	R	$S(\rho_{BH\cup BU}) = S(\rho_R) = \log k$
After the Page time	BH	$R \cup BU$	$S(\rho_{BH}) = S(\rho_{R\cup BU}) = S_{BH}$

Table 1: How to divide the total system $BH \cup R \cup BU$ into two subsystems before and after the Page time, and the corresponding von Neumann entropies.

include the contribution of the island, which typically occupies a region behind a black hole horizon. Thus it is reasonable to identify the island region behind the black hole horizon with the Einstein-Rosen bridge of the purified state (4.6) connecting the original spacetime and the baby universe, which stores fine-grained information of the original spacetime.

One can naturally identify these baby universe states $\{|M\rangle_{BU}\}$ in the fine-grained Hilbert space with so-called α states [70–72] in the baby universe Hilbert space, which diagonalizes the baby universe creation operators [73]. Then each fine-grained state $|\Psi_M\rangle|M\rangle$ belongs to different super-selection sectors, since each α state does. In particular, this implies that off diagonal matrix elements $\langle\Psi_M|\langle M|(\mathcal{O}\otimes I)|\Psi_N\rangle|N\rangle$ for any operator $\mathcal{O}$ acting on the black hole and the Hawking radiation $H_{BH}\otimes H_R$ vanish, thus any local measurement on them can not distinguish the entangled pure state (4.6) with the following mixed state only with classical correlation

$$\rho = \sum_M p_M \, |\Psi_M\rangle\langle\Psi_M| \otimes |M\rangle\langle M|, \tag{4.10}$$

in the sense that

$$\mathrm{tr}\left[|\Phi\rangle\langle\Phi|\,(\mathcal{O}\otimes I)\right] = \mathrm{tr}\left[\rho\,(\mathcal{O}\otimes I)\right] = \sum_M p_M \langle\Psi_M|\mathcal{O}|\Psi_M\rangle. \tag{4.11}$$

To put it another way, LOCCs[22] acting only on the black hole BH and the Hawking radiation R, which can be available to a coarse-grained observer, can not distinguish the pure state (4.6) and the mixed state (4.10). However one can see that the von Neumann entropies of these two states (4.6) and (4.10) on $\mathbf{R} = R \cup BU$ are different. Indeed, the von Neumann entropy of the mixed state ρ (4.10), contains a classical Shannon term, meanwhile the von Neumann entropy of the pure state (4.6) does not. From another point of view, LOCCs on the original system $BH \cup R$ and the baby universe BU, which can only be available to a fine-grained observer, can distinguish the

[22]LOCC stands for local operation and classical communication, which are fundamental physical operations in quantum information theory, see, e.g., [60].

two states (4.6) and (4.10), because the equalities in (4.11) do not necessarily hold for general operators acting on the Hilbert space $H_{BH} \otimes H_R \otimes H_{BU}$.

In the following subsection, we discuss several implications of the baby universe and the Einstein-Rosen bridge connecting the baby universe and the original spacetime. The Einstein-Rosen bridge may depend on the geometric structure of the baby universe. We can not fully determine the geometry of the baby universe from the first principles of quantum gravity, but there is a canonical and minimal choice for such a baby universe; starting with the original system $|\Psi_M\rangle$, we prepare its copy $|\tilde{\Psi}_M\rangle$, and regard it as the purifier (the baby universe) $|M\rangle_{BU} = |\tilde{\Psi}_M\rangle_{\text{Puri.}}$. Then the state (4.6) becomes

$$\sum_M \sqrt{p_M} |\Psi_M\rangle_{BH\cup R} |\tilde{\Psi}_M\rangle_{\text{Puri.}}. \tag{4.12}$$

The existence of the boundaries in the original system $|\Psi_M\rangle$ implies that the purifier system $|M\rangle_{BU} = |\tilde{\Psi}_M\rangle_{\text{Puri.}}$ should also have similar boundaries. More generally, there are possibilities that we may choose multiple copies of the original system as the purifier (the baby universe) $|M\rangle_{BU} = |\tilde{\Psi}_M\rangle^{\otimes n}_{\text{Puri.}}$, and further choose their linear combinations as the purifier. Again from the ER=EPR, the entanglement between the original spacetime and the purifier (the baby universe) implies the existence of the Einstein-Rosen bridge connecting two island regions of the two spacetimes. This Einstein-Rosen bridge will affect the non-perturbative physics of this system.

4.2 Gauss Law modified by the Baby Universe

In this subsection, we discuss the physical implication of the existence of the baby universe sector introduced in the last subsection, which accommodates fine-grained information of the original system. We are mainly interested in how the baby universe helps to recover information of the interior of the black hole from the Hawking radiation. We will also briefly explain the relation between our formulation and the paradox discussed in the paper [30].

Before starting the discussion, we give a remark. In the light of the AdS/CFT correspondence, the introduction of a new additional boundary, i.e., the boundary of the baby universe sounds puzzling, since the AdS/CFT correspondence states that a theory of full quantum gravity in the bulk corresponds to a (non-gravitating) CFT on the boundary. This means that, in principle, we can read all the details of the bulk quantum gravity Hilbert space from the single CFT Hilbert space. Thus, naively we do not need to introduce the second copy of the CFT, as we did in the previous section, which results in the baby universe sector.

Nevertheless, we are forced to do so since we are considering a semi-classical description of the system. Then, to restore fine-grained information within the semi-classical regime, we need to introduce an auxiliary baby universe system and regard the new baby universe degrees of freedom as a part of the Hawking radiation degrees of freedom after the Page time. If we do not do this, this restriction amounts to that on the boundary, we are just accessible to a sub-Hilbert space H_{coarse} which characterizes coarse-grained degrees of freedom. To include the rest of the CFT Hilbert space, which we term H_{fine} just because it describes fine-grained degrees of freedom, we need to introduce a second copy of the CFT Hilbert space, and accommodate H_{fine} to it.

One can obtain the full Hilbert space on the single boundary by gluing two asymptotic boundaries of the two spacetime (see figure 27). In the resulting bulk spacetime, we have two homologically inequivalent paths, both of which connect a point in the interior of the black hole (and belong to the island region) to the boundary of the spacetime (see figure 27). The first path is the trivial one (the Path 1 (blue dotted line) in figure 27), which entirely lies within the original spacetime. This path necessarily intersects with the entanglement wedge of the black hole. However, in the presence of the baby universe, there is a second path (the Path 2 (green dotted line) in figure 27), which does not intersect with the entanglement wedge of the black hole. Instead, the second path crosses the Einstein-Rosen bridge, which connects the original spacetime to the baby universe, and ends on the second asymptotic boundary, which accommodates fine-grained degrees of freedom, as in the green dotted line in figure 27. Since these two boundaries of the original spacetime and the baby universe are glued together, the second path connects the island region and the conformal boundary without passing through the entanglement wedge of the black hole. As we will see later, in considering the gravitational dressing, it is natural to consider the second path instead of the first path.

4.2.1 The modification of Gauss Law

By the presence of the baby universe which has its own asymptotic boundary, the gravitational Gauss law is inevitably modified. We see this modification below.

Let Σ be a Cauchy slice of the spacetime, then the gravitational Gauss law relates the expectation value of the bulk stress-energy tensor $\langle T_{bulk} \rangle$ to

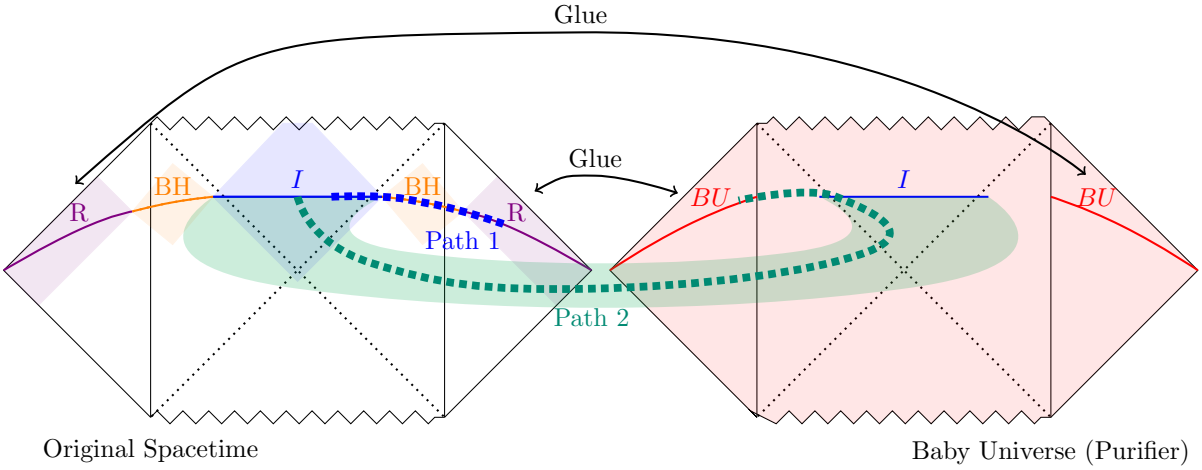

Figure 27: Schematic picture of the geometry of the AdS black hole coupled the bath CFT (left Penrose diagram) and the baby universe geometry (right red Penrose diagram) connected by the Einstein-Rosen bridge (transparent green shaded region), corresponding to the pure state (4.12). After the Page time, the fine-grained Hawking radiation $\mathbf{R}$ is the union of the Hawking radiation R (violet region) and the baby universe BU (red region). We regard the above spacetime describing this union by gluing two distinct asymptotic boundary regions BU and R. The island region I is connected to the fine-grained Hawking radiation $R \cup BU$ through two paths, Path 1 and Path 2. The Path 1 (thick blue dotted line) intersects with the entanglement wedge of the black hole BH (orange shaded region), but the Path 2 (thick green dotted line) does not.

the boundary energy $H_\partial[h]$ (the holographic stress-energy tensor) as follows

$$\langle T_{bulk} \rangle = H_\partial[h]. \tag{4.13}$$

Here the boundary energy $H_\partial[h]$ is given by the integration of the ADM current J^i over the conformal boundary $\partial\Sigma$ [74],

$$H_\partial[h] \equiv \frac{1}{2\kappa^2} \int_{\partial\Sigma} d^{d-1}x \sqrt{g}\, n_i J^i \qquad (\kappa = \sqrt{8\pi G_N}), \tag{4.14}$$

where n_i is the normal vector to the conformal boundary $\partial\Sigma$, and the ADM current J^i is defined by

$$J_i \equiv N\nabla^j \left(h_{ij} - h g^0_{ij}\right) - \nabla^j N \left(h_{ij} - h g^0_{ij}\right) \tag{4.15}$$

under the ADM decomposition

$$ds^2 = -N^2 dt^2 + g_{ij} \left(dx^i + N^i dt\right) \left(dx^j + N^j dt\right), \tag{4.16}$$

and the expansion from the background metric g^0_{ij} as follows $g_{ij} = g^0_{ij} + \kappa h_{ij}$. More precisely, the gravitational Gauss law in the form (4.13) is a perturbative version of the gravitational Gauss law which can be derived from the full Hamiltonian constraint

$$\mathcal{H}[\pi_{ij}, g_{ij}] = 2\kappa^2 g^{-1}\left(g_{ij}g_{kl}\pi^{ik}\pi^{jl} - \frac{1}{d-1}\left(g_{ij}\pi^{ij}\right)^2\right) - \frac{1}{2\kappa^2}(R - 2\Lambda) + \mathcal{H}^{\text{matter}} = 0, \tag{4.17}$$

where g_{ij} is the metric on the Cauchy slice, π_{ij} is the conjugate momentum, and $\mathcal{H}^{\text{matter}}$ is the matter Hamiltonian density. In the above constraint, by expanding (4.17) from the background metric, $g_{ij} = g^0_{ij} + \kappa h_{ij}$, and then at the second order of the expansion the constraint gives the relation (4.13). Details of the derivation can be found in, e.g., [74]. The boundary energy $H_\partial[h]$ should be understood as the change of the black hole mass, $H_\partial[h] = M_{BH}[g+h] - M_{BH}[g]$ owing to the back-reaction from the bulk stress-energy tensor $\langle T_{bulk}\rangle$.

In the paper [30], the authors argued that the gravitational Gauss law suggests an interesting puzzle on the island formula. Assume that we act a local operation on a state on the island region. Because information of the island region is encoded in the Hilbert space of the Hawking radiation H_R, we can regard the local operation as a local operation on the radiation Hilbert space H_R. This local operation changes the expectation value of the bulk stress-energy tensor. Then the gravitational Gauss law (4.13) relates the change of the expectation value of the bulk stress-energy tensor $\langle T_{bulk}\rangle$ on the island region behind the horizon to the change of the boundary energy $H_\partial[h]$. This implies that any change on the island region, no matter how it is small, is always detectable from the conformal boundary $\partial\Sigma$ according to the gravitational Gauss law. However, this sounds puzzling because $\partial\Sigma$ belongs to the entanglement wedge of the black hole. More explicitly, this means that in the bipartite system $H_R \otimes H_{BH}$, a local operation only on H_R can change the state of H_{BH}.

The above paradox is naturally resolved once we introduce the baby universe sector which admits the new boundary (see figure 27). In the presence of this new part of the spacetime, the gravitational Gauss law must be modified as follows

$$\langle T_{bulk}\rangle = H_{\partial BH}[h] + H_{\partial BU}[h], \tag{4.18}$$

where $H_{\partial BH}[h]$ denotes the boundary energy of the original spacetime with the black hole, and similarly $H_{\partial BU}[h]$ does the boundary energy of the baby universe.

The modified gravitational Gauss law (4.18) immediately suggests that,

in the presence of the baby universe, local operations on the island region need *not* to be detected on the conformal boundary of the black hole. To put it another way, $\langle T_{bulk} \rangle \neq 0$ does not necessarily mean $H_{\partial BH}[h] \neq 0$. Rather, it is reasonable to relate the non-trivial change $\langle T_{bulk} \rangle$ on the island region to the boundary energy of the baby universe $H_{\partial BU}[h]$ since the island region is encoded into the fine-grained Hawking radiation Hilbert space $H_{\mathbf{R}} = H_R \otimes H_{BU}$ after the Page time. Indeed, the island region holds fine-grained information of the Hawking radiation after the Page time, thus from the boundary point of view, such bulk operations on the island region should be encoded into the fine-grained part of the CFT Hilbert space H_{fine}, which coincides with the boundary Hilbert space of the baby universe H_{BU}.

One can interpret the above statement more intuitively as follows. Firstly we consider putting a local operator in the spacetime, which induces a small energy excitation in the bulk. The gravitational Gauss law means that by measuring the *total* flux for an appropriate closed surface, we can know the energy of the small excitation within the closed surface. The presence of the baby universe makes the measurement of the flux highly non-trivial. The Einstein-Rosen bridge connecting the original spacetime and the baby universe can release some part of the flux of the original spacetime into the baby universe (see figure 28). Here we note that because in our current setup, the baby universe has boundaries, flux lines can end on the boundaries of the baby universe as figure 28. That is, in measuring the *total* flux, we also need to consider the baby universe (right spacetime of figure 28) in addition to the original spacetime (left spacetime of figure 28). By the usual gravitational Gauss law, if we just measure only the flux of the original spacetime (left spacetime of figure 28), then we can not know the exact energy of the small excitation. This modification is not visible within the coarse-grained precision, but without the modification, we may encounter many problems, e.g., violation of the conservation law.

There are several other implications of the generalized gravitational Gauss law (4.18) as well. Firstly, the existence of the baby universe boundary energy term suggests that the gravitational Gauss law (4.18) does not precisely hold within the original black hole spacetime, $\langle T_{bulk} \rangle \neq H_{\partial BH}[h]$ generally. For instance, one way to treat the generalized Gauss law (4.18) is that it relates the spectrum of the fine-grained part $H_{\partial BU}[h]$ to that of the coarse-grained part $H_{\partial BH}[h]$. It is expected that the energy spectrum of the fine-grained part $H_{\partial BU}[h]$ is discrete, and the typical differences between two nearest energy eigenvalues are of order $e^{-S_{BH}}$. This forces the energy spectrum of the coarse-grained part $H_{\partial BH}[h]$ also discrete, which is necessary for the unitary time evolution of the black hole evaporation process.

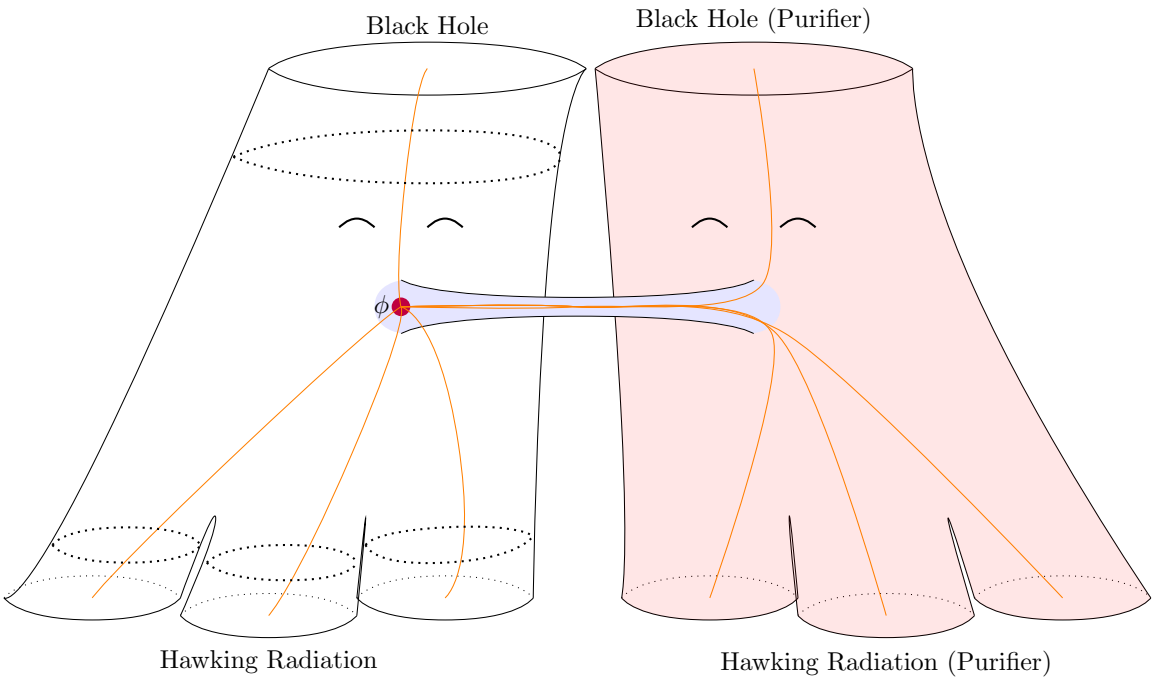

Figure 28: Schematic picture of flux lines on the geometry corresponding to (4.12) (, similar to the figure discussed in [75]). The dotted lines are horizons. A local operator ϕ (red dot) is put on the original spacetime (left region). The two spacetimes are connected by the Einstein-Rosen bridge (blue region). Some of flux lines (orange lines) escape into the baby universe (right red region) through the Einstein-Rosen bridge .

Now we estimate the magnitude of the violation of the gravitational Gauss law in the original spacetime. In order to obtain a unitary time evolution of an evaporating black hole, we need non-perturbative corrections of order $e^{-S_{BH}}$, where S_{BH} is the Bekenstein-Hawking entropy of the black hole. This implies that we need fine-grained states in a small energy window of order $e^{-S_{BH}}$, therefore $H_{\partial BU}$ is of the same order. This leads us to the following estimation

$$\langle T_{bulk} \rangle - H_{\partial BH}[h] = O(e^{-S_{BH}}), \tag{4.19}$$

i.e., the gravitational Gauss law (4.18) is violated only non-perturbatively in the original spacetime.

We note that such a baby universe is different from those appearing by cutting Euclidean wormholes into half, in the semi-classical gravitational path integral, see, e.g., [76]. The later baby universe is always closed, and thus does not have any asymptotic boundary. Such a closed baby universe

corresponds to an additional factor of the von Neumann algebra of the CFT [77]. On the other hand, our baby universe has an asymptotic boundary, which encodes fine-grained information of the state.

4.2.2 Comment on gravitational dressing

In a theory with dynamical gravity, local operators are not physical since they are not diffeomorphism invariant. One way to make them diffeomorphism invariant is to connect the local point P to an asymptotic boundary point P_∂, via a gravitational Wilson line, i.e., $\phi(P) \to \phi(P)W_{\text{gravity}}(P, P_\partial)$. Such a prescription is called gravitational dressing. In the paper [30], the authors argued that such a gravitational dressing of a local operator on the island region is inconsistent with the entanglement wedge reconstruction implicated by the island formula. This is because the gravitational Wilson line connects a point on the island to a point on the conformal boundary of the AdS black hole. However, this sounds troublesome, because whereas the island formula suggests that an operator locally acting on the island region can be expressed as that on the radiation Hilbert space according to the entanglement wedge reconstruction, the gravitational Wilson line attached to the operator intersects with the entanglement wedge of the black hole, thus it does change the state of the black hole Hilbert space H_{BH}.

From our point of view, the above paradox is naturally resolved because, in the presence of the baby universe with an asymptotic boundary, the gravitational Wilson line can end on the baby universe boundary (see figure 29). Moreover, because the new baby universe boundary belongs to the Hawking radiation degrees of freedom after the Page time, it is still an operator on the radiation Hilbert space, even after the gravitational dressing.

5 Summary and Future Directions

5.1 Summary

In this thesis, we studied the entropy of Hawking radiation and also black holes by using the island formula from two perspectives.

In section 3, in the framework of the disjoint setup, we studied the dynamics of a black hole in flat space, which is entangled with an auxiliary non-gravitational universe. As a result, due to the back-reaction of the entanglement between the two universes, the area of the black hole horizon

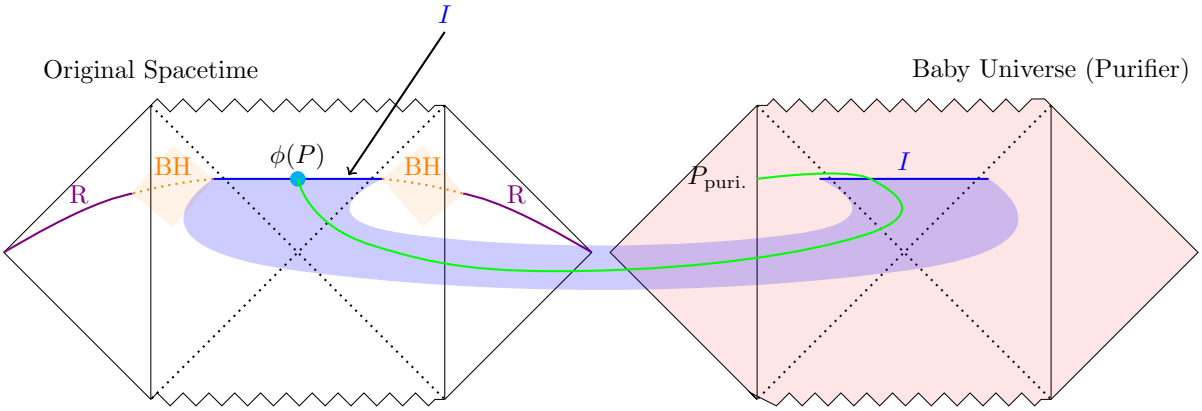

Figure 29: Schematic picture of the geometry of the AdS black hole coupled to the bath CFT (left Penrose diagram) and their copy (right Penrose diagram) connected to the original spacetime through the Einstein-Rosen bridge (blue region), corresponding to the state (4.12). The local operator ϕ in the island (cyan dot) can be gravitationally dressed with a gravitational Wilson line $W_{\text{gravity}}(P, P_{\text{puri.}})$ (green line) which ends on the baby universe (right Penrose diagram) without intersecting the entanglement wedge of the original black hole degrees of freedom (orange shaded region).

becomes smaller and the interior region becomes longer. Their changes can be understood in terms of the monogamy of entanglement [25]. Because the gravitating universe B contains two black hole horizons, the Hilbert space of the universe B naturally decomposes into two horizon Hilbert spaces $H_{B_L} \otimes H_{B_R}$. Both of these degrees of freedom are strongly entangled with the universe A, so according to the monogamy of entanglement, the entanglement between the two horizons should be suppressed. This suppression is geometrically manifested by the long interior region of the black hole. Then, we evaluated the von Neumann entropy of universe A, or equivalently the entanglement entropy between the two universes, and obtained the Page curve of an evaporating black hole in our setting.

We also investigated the effects of local operations on black holes. One can model such local operations by insertions of CFT local operators, which is called local operator quench. In our setting, it is natural to consider the insertions into the black hole interior as well as the insertions into the black hole exterior. Such insertions can back-react to the black hole through the stress-energy tensor expectation value for the state including the local operator. Some differences exist between the cases of interior and exterior insertions. When the local operator is inserted outside the black hole horizon,

the entanglement entropy does not change. In contrast, if the local operator is inserted inside the black hole horizon, the entanglement entropy decreases significantly. This disruption becomes stronger as the insertion point gets deeper into the black hole.

In section 4, we studied a partially fine-grained description of semi-classical evaporating black holes by introducing a new degree of freedom called a baby universe. We confirmed that the behavior of the Page curve can be obtained by introducing such a baby universe and properly dividing the system into two parts.

We also argued that in an ordinary consistent long-range gravity theory, the gravitational Gauss law must be modified by the introduction of the baby universe that is connected to the original spacetime, and when there is an island after Page time, this modification is essential to obtain results that are consistent with the idea of entanglement wedge reconstruction.

5.2 Future Directions

Local Quench outside the two universes

In the disjoint setup for a black hole in asymptotically flat space, we considered a local quench in universe B, where there is a black hole, but by considering the proper analytical connection of coordinates, we can consider a local quench that does not belong to both universes A and B. In that case, depending on where the local operator is inserted, the entanglement is expected to change even though there is no island. In this thesis, we did not deal with such a local quench because the treatment of the shock waves was unclear. However, we expect that investigating such a situation will be useful for further understanding the entanglement between black holes and Hawking radiation.

Entangled disjoint multi-universes

In the disjoint setup in this thesis, the entangled states that were mainly considered were those between two universes, A and B. However, entangled states between more universes, specifically between three or more universes, can be considered as well. It is a non-trivial question whether a similar argument can be made in such a situation, and it is expected to be an important issue in understanding the ER=EPR conjecture, which proposes a relationship between entanglement and spacetime.

The division of the baby universe which leads to the usual island formula

In this thesis, we considered von Neumann entropy with a division such that the baby universe always belongs to a black hole or Hawking radiation as listed in table 1, however, other possibilities of division exist.

For example, one may also consider the possibility of dividing the baby universe Hilbert space H_{BU} into two parts $H_{BU_{BH}} \otimes H_{BU_R}$, and then define the radiation Hilbert space as $H_{\mathbf{R}} = H_{BU_R} \otimes H_R$, instead of $H_{\mathbf{R}} = H_{BU} \otimes H_R$ which we do in the body of the thesis. In such a case, the states of the baby universe are given by $|M\rangle_{BU_{BH}} \otimes |M\rangle_{BU_R}$. In this case, assuming the orthogonality of the basis of $H_{BU_{BH}}$, we can check that the von Neumann entropy of the reduced density matrix $\rho_{BU_R \cup R}$ takes the following form

$$S(\rho_{BU_R \cup R}) = -\sum_M p_M \log p_M + \sum_M p_M S(\rho_{(M)R}),$$

where $\rho_{(M)R}$ is given in (4.8). Then it is natural to define the fine-grained entropy of Hawking radiation $S(\rho_{\mathbf{R}})$ as a conditional entropy of knowing the probability distribution p_M by subtracting the classical Shannon term $H(p_M) = -\sum_M p_M \log p_M$,

$$S(\rho_{\mathbf{R}}) = S(\rho_{BU_R \cup R}) - H(p_M) = \sum_M p_M \; S(\rho_{(M)R}).$$

This entropy coincides with the one discussed in, e.g., [61], giving the Page curve. However, we do not know the natural choice for such a dividing of the baby universe Hilbert space H_{BU}. Therefore, it would be interesting to investigate such directions further.

Multi-boundary Wormhole and Baby Universe

In the body of this thesis, we did not explicitly discuss the geometry of a system consisting of a black hole, Hawking radiation, and a baby universe. However, we can consider concrete geometric models to understand further detailed properties of the system.

A class of the candidate geometries is the multi-boundary wormhole solution of three-dimensional Einstein gravity with a negative cosmological constant. It is useful to consider the coordinates in which the AdS_3 metric takes the following form

$$ds^2 = -dt^2 + \cos^2 t d\Sigma_2^2, \tag{5.1}$$

where we denote by $d\Sigma_2^2$ the metric of two-dimensional hyperbolic space. We can construct these multi boundary wormholes by taking the appropriate quotient of the hyperbolic space by the isometry group $SL(2,R) \times SL(2,R)$ of AdS_3. Such a multi-boundary wormhole geometry has multiple conformal boundaries, on each of which we can define a CFT Hilbert space. In each asymptotic region, there is a horizon whose horizon area corresponds to the number of degrees of freedom in the boundary CFT Hilbert space.

For simplicity, we consider such a wormhole geometry with three asymptotic boundaries below. These three boundaries represent three Hilbert spaces of Hawking radiation H_R, the black hole $H_{\rm BH}$, and the baby universe $H_{\rm BU}$, see figure 30. Therefore, one can identify the horizon area of each asymptotic region with the von Neumann entropy of each Hilbert space computed in (C.8), (C.12), (C.16) in Appendix C. The interior region behind these horizons is identified with the Einstein-Rosen bridge, which connects the original black hole with the baby universe.

This geometric description manifests the entanglement structure of (4.6) as follows. When $k = \dim H_R$ is small, which models the early time of the black hole evaporation, this system is almost a bipartite system in which $H_{\rm BH}$ and $H_{\rm BU}$ are entangled (see left panel of figure 30). As we increase k, the cross-section of the Einstein-Rosen bridge gets larger, and at sufficiently late times $k \gg 1$, $H_{\rm BU}$ becomes mostly entangled with the Hawking radiation Hilbert space $H_{\rm R}$ (see right panel of figure 30).

It would be interesting to study the entanglement structure of the system by using this geometric model in detail.

Acknowledgement

I thank Tomonori Ugajin for collaborations and valuable discussions. I also thank Norihiro Iizuka for his collaborations and valuable discussions. This thesis is based on the results [27,29] in collaboration with them. Furthermore, I thank my supervisor, Mitsuhiro Kato. I also would like to thank all the members of Komaba particle theory group. Finally, I also would like to thank my family for their support.

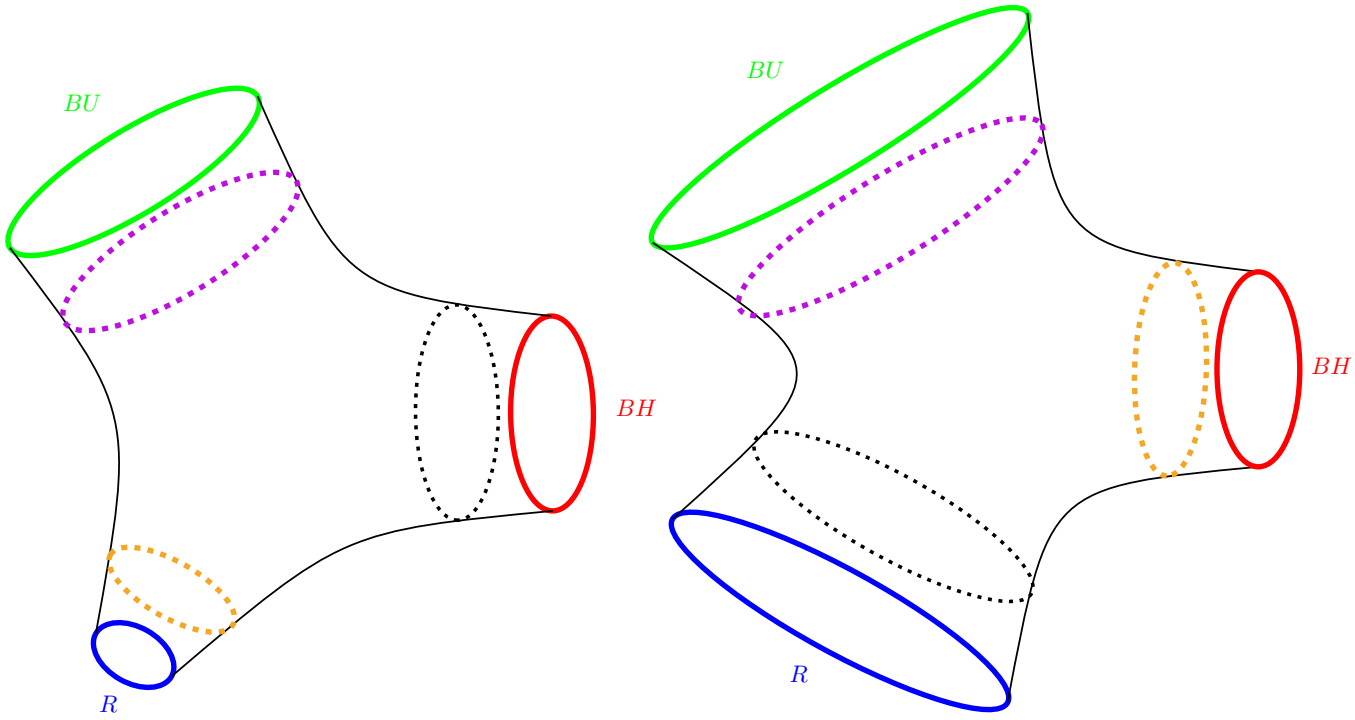

Figure 30: The three boundary wormhole, which models the black hole BH, the Hawking radiation R, and the baby universe BU. The dotted lines are horizons for three boundaries. The boundaries of the baby universe BU, the black hole BH, and the Hawking radiation R are represented by the green, red, and blue lines respectively. The actual (minimal) extremal surface, which divides the system into two parts as listed in table 1, is represented by the orange dotted line (horizon). The horizon area of the baby universe (purple dotted line) corresponds to the von Neumann entropy of the baby universe (C.16). **Left**: The three boundary wormhole which models the system at early times. In this case, the area of the actual extremal surface (orange dotted line) corresponds to the von Neumann entropy of the Hawking radiation, or equivalently that of the union of the black hole and the baby universe (C.8). **Right**: The three boundary wormhole which models the system at late times. In this case, the area of the actual extremal surface (orange dotted line) corresponds to the von Neumann entropy of the Hawking radiation and the baby universe, or equivalently that of the black hole (C.12).

A von Neumann Entropy in CFT_2

In this appendix, we briefly review the calculation of the von Neumann entropy in a two-dimensional conformal field theory with a central charge c and present some results, which we use in the main sections. In appendix B, we explain the von Neumann entropy in the case that we consider a local quench.

At first, let $|\Psi\rangle$ denote a normalized state on the system, and $H_A \otimes H_{A^c}$ denote the Hilbert space of the system, which is given by the tensor product of two Hilbert spaces associated to regions (sub-systems) A and A^c. We assume that the metric is flat, and the region A consists of a single interval, and A^c is its complement. The reduced density matrix associated with the subsystem A is given by tracing out the remaining degrees of freedom

$$\rho_A = \mathrm{tr}_{A^c} |\Psi\rangle \langle\Psi| . \tag{A.1}$$

Then the von Neumann entropy of the reduced density matrix ρ_A is given by

$$S(\rho_A) = -\,\mathrm{tr}_A\, \rho_A \log \rho_A, \tag{A.2}$$

and this von Neumann entropy is called the entanglement entropy frequently. We can consider the von Neumann entropy for the reduced density matrix ρ_{A^c} similarly. In the case that the total state is pure, not a mixed state, the von Neumann entropy has the property $S(\rho_A) = S(\rho_A^c)$. The von Neumann entropy measures the quantum entanglement between the two sub-systems A and A^c.

Since, in general, it is difficult to evaluate the right-hand side of the von Neumann entropy (A.2), instead we use the replica trick, consider the Rényi entropy given by

$$S^{(n)}[A] \equiv \frac{1}{1-n} \log \mathrm{tr}\, \rho_A^n, \tag{A.3}$$

and through the $n \to 1$ limit we get the von Neumann entropy

$$S(\rho_A) \equiv S[A] = \lim_{n\to 1} S^{(n)}[A]. \tag{A.4}$$

Thus to get the von Neumann entropy we consider $\mathrm{tr}\, \rho_A^n$.

In evaluating the quantity $\mathrm{tr}\, \rho_A^n$, by using a conformal symmetry, we can associate it with the two point function of the twist and anti-twist operates [40, 78]

$$\mathrm{tr}\, \rho_A^n = \langle \sigma_n \sigma_{-n} \rangle , \tag{A.5}$$

where σ_n and σ_{-n} are inserted into the endpoints of the region A. Here the conformal dimension of the twist and anti-twist operators is given by $2H_n = \frac{c}{12}\left(n - \frac{1}{n}\right)$. Then by evaluating the two point function we can compute $\mathrm{tr}\,\rho_A^n$ and the Rényi entropy, and by taking the $n \to 1$ limit we obtain the von Neumann entropy.

Below we present some results on the von Neumann entropy for some cases [40, 78].

von Neumann entropy of an interval on a system with infinite size

When the system size is infinite and the system is at zero temperature, the von Neumann entropy of the interval, whose size is given by l, is given by

$$S(\rho_A) = \frac{c}{3}\log\frac{l}{\varepsilon_{UV}}, \tag{A.6}$$

where ε_{UV} is the UV cutoff.

For the system is at finite temperature $1/\beta$, the von Neumann entropy is given by

$$S(\rho_A) = \frac{c}{3}\log\left(\frac{\beta}{\pi\varepsilon_{UV}}\sinh\left(\frac{\pi l}{\beta}\right)\right). \tag{A.7}$$

von Neumann entropy of an interval on a system with finite size

When the system size is finite and given by L, and the system is at zero temperature and with periodic boundary conditions, the von Neumann entropy of the interval, whose size is given by l, is given by

$$S(\rho_A) = \frac{c}{3}\log\left(\frac{L}{\pi\varepsilon_{UV}}\sin\left(\frac{\pi l}{L}\right)\right), \tag{A.8}$$

where ε_{UV} is the UV cutoff.

A.1 The vacuum entropy formula

In this subsection, we derive the vacuum entropy formula (2.36) holographically by using the Ryu-Takayanagi formula [6]

$$S_{\mathrm{RT}}[w_1, w_2] = \mathrm{Min}_\gamma \frac{\mathrm{Area}(\gamma)}{4G_N^{(3)}}, \tag{A.9}$$

where $G_N^{(3)}$ is the three-dimensional Newton constant. The above quantity (A.9) calculated in AdS_3 is equal to the von Neumann entropy in CFT_2,

$S_{\rm CFT}\left[w_1, w_2\right]$. Here, after the minimization, the resulting γ is the minimal surface homologous to the interval between the two points w_1, w_2 like the discussion of (1.2). The interval between the two points w_1, w_2 corresponds to the boundary region A in the discussion of (1.2). Since we consider CFT_2, the bulk dual is AdS_3. In this case, the minimal surface γ is given by the geodesic connecting the points w_1, w_2, and its area Area(γ) is given by the geodesic length between the points.

At first we derive a (space-like) geodesic length in the Poincare AdS_3 coordinates, which corresponds to the vacuum state in CFT_2 with the w coordinates. In such a case it it sufficient to consider the following AdS_3 Poincare metric

$$\begin{aligned} ds^2_{\text{Poincar } AdS_3} &= \frac{dz^2 + dx^2 - dt_P^2}{z^2} \\ &= \frac{dz^2 + ds^2}{z^2}, \end{aligned} \tag{A.10}$$

where we introduced the coordinates satisfying $ds^2 = dx^2 - dt_P^2$ in the second line. Later we will relate the Poincare AdS_3 coordinates to the w coordinates, where the metric is given by $ds^2 = \Omega^{-2} dw^+ dw^-$, and give expressions by using the w coordinates. For notational convenience, we call w_1 and w_2 the point 1 and 2 respectively.

In the (Poincare) coordinates (z, s), geodesics are given by semi-circles whose centers are at $z = 0$,

$$z^2 + (s - s_0)^2 = \left(\frac{d(1,2)}{2}\right)^2 \tag{A.11}$$

where s_0 and $d(1,2) > 0$ are determined by the location of the two points 1 and 2. The conditions for s_0 and $d(1,2)$ are given by

$$\begin{aligned} z_{b1}^2 + (s_1 - s_0)^2 &= \left(\frac{d(1,2)}{2}\right)^2 \\ z_{b2}^2 + (s_2 - s_0)^2 &= \left(\frac{d(1,2)}{2}\right)^2, \end{aligned} \tag{A.12}$$

where the coordinate z_{b1}, s_1 (z_{b2}, s_2) is the coordinates of the point 1 (2) in the (Poincare) coordinates (z, s). As we will see later, we are interested in the case that z_{b1}, z_{b2} are very small, which implies the points 1 and 2 are very closed to the AdS_3 boundary $z = 0$. In such a case, from the above conditions we get the following expressions

$$s_0 \approx \frac{s_1 + s_2}{2}, \tag{A.13}$$

and

$$\begin{aligned} d(1,2)^2 &\approx |s_2 - s_1|^2 \\ &= \left| \int_1^2 ds \right|^2 \\ &= \left| (x_2 - x_1)^2 - (t_{P2} - t_{P1})^2 \right|. \end{aligned} \tag{A.14}$$

To evaluate the geodesic length, it is convenient to introduce a new parameter by

$$\begin{aligned} z &= \frac{d(1,2)}{2} \sin\xi \\ s &= s_0 + \frac{d(1,2)}{2} \cos\xi. \end{aligned} \tag{A.15}$$

The boundary condition for the geodesic γ, which ends on the two points 1 and 2, gives the upper and lower value for ξ

$$\begin{aligned} 1 \gg z_{b1} &= \frac{d(1,2)}{2} \sin\xi_{b1} \\ &\approx \frac{d(1,2)}{2} \xi_{b1}, \\ 1 \gg z_{b2} &= \frac{d(1,2)}{2} \sin\xi_{b2} \\ &\approx \frac{d(1,2)}{2} (\pi - \xi_{b2}) \end{aligned} \tag{A.16}$$

where we assumed the relation $s_1 < s_2$. By using the above parameter, we get the geodesic length

$$\begin{aligned} \text{Area}(\gamma) &= \int_1^2 ds_{\text{Poincar } AdS_3} \\ &= \int_{\xi_{b1}}^{\xi_{b2}} \frac{ds_{\text{Poincar } AdS_3}}{d\xi} d\xi \\ &= \log\left(\frac{\tan\frac{\xi_{b2}}{2}}{\tan\frac{\xi_{b1}}{2}} \right) \\ &\approx \log\left(\frac{d(1,2)^2}{z_{b1} z_{b2}} \right) \\ &= \log\left(\frac{(x_2 - x_1)^2 - (t_{P2} - t_{P1})^2}{z_{b1} z_{b2}} \right), \end{aligned} \tag{A.17}$$

Next we relate the Poincare AdS_3 coordinates to the w coordinates in AdS_3 boundary, i.e., CFT_2, following the techniques discussed in [14].

Near the Poincare AdS_3 boundary $z \ll 1$, we consider the w coordinates given by the following relation

$$ds^2_{\text{Poincar } AdS_3} = \frac{dz^2 - dt_P^2 + dx^2}{z^2} \underset{z=z_b \ll 1}{\Longrightarrow} -\frac{dw^+ dw^-}{z_b^2} = -\frac{1}{\varepsilon_{UV}^2} dy^+ dy^- \quad \text{(A.18)}$$

where we defined $w^\pm \equiv t_P \pm x$, and ε_{UV} is the UV cutoff. From the above relation, we obtain

$$\begin{aligned} z_b &= \varepsilon_{UV} \sqrt{\frac{dw^+}{dy^+}\frac{dw^-}{dy^-}} \\ &= \varepsilon_{UV}\ \Omega(w^+, w^-), \end{aligned} \quad \text{(A.19)}$$

where in the second line we defined $\Omega(w^+, w^-) = \sqrt{\frac{dw^+}{dy^+}\frac{dw^-}{dy^-}}$.

By substituting the above result (A.19) into the expression for the geodesic length (A.17) in the AdS_3 Poincare coordinate , we get

$$\text{Area}(\gamma) = \log\left[\frac{|(w_2^+ - w_1^+)(w_2^- - w_1^-)|}{\varepsilon_{UV}^2 \Omega(w_1^+, w_1^-)\Omega(w_2^+, w_2^-)}\right] \quad \text{(A.20)}$$

As a result from the Ryu-Takayanagi formula we obtain

$$\begin{aligned} S_{\text{CFT}}\left[w_1, w_2\right] = S_{\text{RT}}\left[w_1, w_2\right] &= \frac{\text{Area}(\gamma)}{4G_N^{(3)}} \\ &= \frac{c}{6}\log\left[\frac{|(w_2^+ - w_1^+)(w_2^- - w_1^-)|}{\varepsilon_{UV}^2 \Omega(w_1^+, w_1^-)\Omega(w_2^+, w_2^-)}\right], \end{aligned} \quad \text{(A.21)}$$

where in the second line we used the Brown-Henneaux's central charge $c = \frac{3\ell_{AdS_3}}{2G_N^{(3)}}$ [79]. Here ℓ_{AdS_3} is the AdS_3 length scale, which we set to be unity $\ell_{AdS_3} = 1$.

B von Neumann entropy and local quench for two disjoint intervals

In this appendix we will derive the expressions appearing in 3.3.3 and 3.3.3 for the CFT von Neumann entropy with a local operator insertion, by following the argument of [50]. We focus on the state (3.26) of the total system AB, and the reduced density matrix on the two intervals $\bar{C}$ in the universe B.

We denote by $\rho_{\bar{C}}$ the reduced density matrix on two intervals $\bar{C} = \bar{C}_1 \cup \bar{C}_2$, whose endpoints are given by $x_2^\pm$ and $x_3^\pm$ ($x_2^\pm \leq x_3^\pm$) for $\bar{C}_1$ and $x_5^\pm$ and $x_6^\pm$

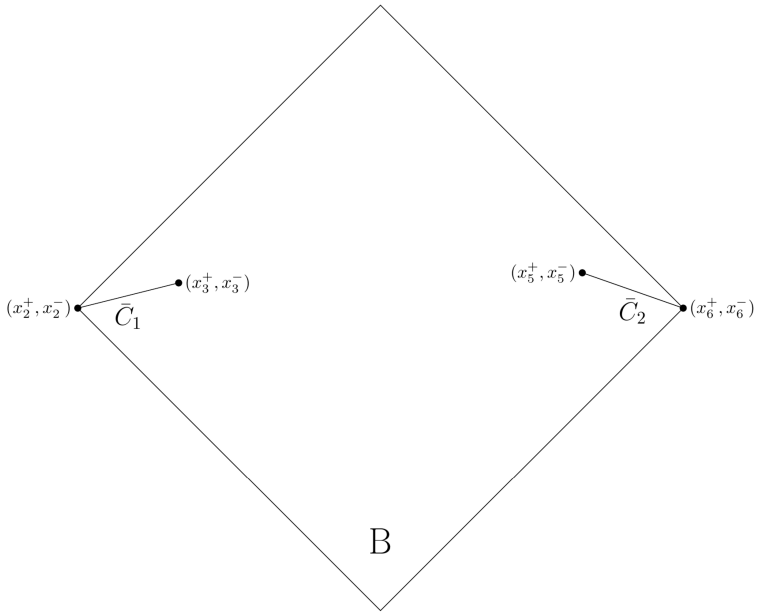

Figure 31: The two intervals in the universe B

$(x_3^\pm < x_5^\pm \leq x_6^\pm)$ for $\bar{C}_2$ respectively (see figure 31), i.e., $\rho_{\bar{C}} = \mathrm{tr}_C\, \rho$. Here we give the density matrix ρ by the reduced density matrix of the universe B (3.28). We can calculate the CFT von Neumann entropy of this density matrix by using the replica trick. To do so, at first we consider the n-th Rényi entropy

$$S^{(n)}[\bar{C}] = \frac{1}{1-n} \log \mathrm{tr}\, \rho_{\bar{C}}^n \tag{B.1}$$

and, by taking the limit

$$S[\bar{C}] = \lim_{n \to 1} S^{(n)}[\bar{C}], \tag{B.2}$$

we can get the CFT von Neumann entropy.

To calculate $\mathrm{tr}\, \rho_{\bar{C}}^n$, we need to consider a normalized $2n$-point function on an n-sheeted replica manifold branched along the region $\bar{C}$. Because this reduced density matrix $\rho_{\bar{C}}$ has the thermal form, each replica sheet is given by a cylinder with the thermal periodicity β. The $2n$-point function is equal to the normalized six-point function which includes twist operators on a (no-replicated) manifold (which is the thermal cylinder), in the cyclic orbifold theory $CFT^{\otimes n}/\mathbb{Z}_n$. We use the later description and evaluate the six-point

function given by

$$\mathrm{tr}\,\rho_{\tilde{C}}^n = \frac{\langle \mathcal{O}^{\otimes n}(x_1^+,x_1^-)\sigma_n(x_2^+,x_2^-)\sigma_{-n}(x_3^+,x_3^-)\sigma_n(x_5^+,x_5^-)\sigma_{-n}(x_6^+,x_6^-)\mathcal{O}^{\dagger\otimes n}(x_4^+,x_4^-)\rangle_\beta}{(\langle \mathcal{O}(x_1^+,x_1^-)\mathcal{O}^\dagger(x_4^+,x_4^-)\rangle_\beta)^n}, \tag{B.3}$$

where $\langle\cdots\rangle_\beta$ denote the thermal trace $\mathrm{tr}[\,\rho_\beta\ \cdots]$.

In the above expression, we introduced the UV regulator ε in the location of the local operators by

$$\begin{cases} x_1^\pm = x_0^\pm \mp i\varepsilon, \\ x_4^\pm = x_0^\pm \pm i\varepsilon; \end{cases} \tag{B.4}$$

$\mathcal{O}^{\otimes n}$ and $\mathcal{O}^{\dagger\otimes n}$ denote the products of the local operators $\mathcal{O}_i$ and $\mathcal{O}_i^\dagger$ which are the i-th copies of the local operators in the cyclic orbifold theory $CFT^{\otimes n}/\mathbb{Z}_n$,

$$\begin{aligned} \mathcal{O}^{\otimes n} &= \mathcal{O}_1\mathcal{O}_2\ldots\mathcal{O}_n, \\ \mathcal{O}^{\dagger\otimes n} &= \mathcal{O}_1^\dagger\mathcal{O}_2^\dagger\ldots\mathcal{O}_n^\dagger. \end{aligned} \tag{B.5}$$

which have conformal dimension $nh_{\mathcal{O}}$; σ_n and σ_{-n} are twist and anti-twist fields respectively, which have conformal dimension $2H_n$ given by

$$H_n = \frac{c}{24}\left(n - \frac{1}{n}\right). \tag{B.6}$$

We will evaluate the six-point function (B.3) in a holographic CFT. Such a CFT has a large central charge and a sparse spectrum. In this class of theories, one can approximate the six-point function function by a six-point Virasoro vacuum conformal block with an appropriate choice of branch cut [50]. To introduce the conformal block, it is useful to map the thermal cylinder to a plane by

$$w^\pm(x^\pm) = \exp\left(\frac{2\pi}{\beta}\left(x^\pm - x_0^\pm\right)\right), \tag{B.7}$$

and further consider the conformal map

$$z^\pm(w^\pm) = \frac{\left(w_1^\pm - w^\pm\right)w_{34}^\pm}{w_{13}^\pm\left(w^\pm - w_4^\pm\right)}, \tag{B.8}$$

where we introduced the notation $w_{ij}^\pm = w_i^\pm - w_j^\pm$. Through the conformal map $w^\pm \to z^\pm$, one can map $\mathrm{tr}\,\rho_{\tilde{C}}^n$ in the six-point function (B.3) to the

following one on the plane,

$$\begin{aligned}\operatorname{tr}\rho_C^n =&((1-z^+)(1-z^-))^{2H_n}(z_{65}^+z_{65}^-)^{2H_n}\\ &\times\left\{\left(\frac{\beta}{\pi\varepsilon_{UV}}\right)^4\sinh\left(\frac{\pi}{\beta}x_{65}^+\right)\sinh\left(\frac{\pi}{\beta}x_{65}^-\right)\sinh\left(\frac{\pi}{\beta}x_{32}^+\right)\sinh\left(\frac{\pi}{\beta}x_{32}^-\right)\right\}^{-2H_n}\\ &\times\langle\mathcal{O}^{\otimes n}\left|\sigma_n\left(z^+,z^-\right)\sigma_{-n}(1,1)\sigma_n\left(z_5^+,z_5^-\right)\sigma_{-n}\left(z_6^+,z_6^-\right)\right|\mathcal{O}^{\otimes n}\rangle,\end{aligned} \tag{B.9}$$

where we introduced the UV cutoff ε_{UV} different from the UV regulator in (B.4), and the notation

$$\begin{aligned}&\langle\mathcal{O}^{\otimes n}\left|\sigma_n\left(z^+,z^-\right)\sigma_{-n}(1,1)\sigma_n\left(z_5^+,z_5^-\right)\sigma_{-n}\left(z_6^+,z_6^-\right)\right|\mathcal{O}^{\otimes n}\rangle\\ &\equiv\lim_{z_4^+,z_4^-\to\infty}\left(z_4^+z_4^-\right)^{2nh_{\mathcal{O}}}\langle\mathcal{O}^{\dagger\otimes n}(z_4^+,z_4^-)\sigma_n(z^+,z^-)\sigma_{-n}(1,1)\sigma_n(z_5^+,z_5^-)\sigma_{-n}(z_6^+,z_6^-)\mathcal{O}^{\otimes n}(0,0)\rangle.\end{aligned} \tag{B.10}$$

Next, we evaluate (B.10) with an insertion of a complete set as follows

$$\begin{aligned}&\langle\mathcal{O}^{\otimes n}\left|\sigma_n\left(z^+,z^-\right)\sigma_{-n}(1,1)\sigma_n\left(z_5^+,z_5^-\right)\sigma_{-n}\left(z_6^+,z_6^-\right)\right|\mathcal{O}^{\otimes n}\rangle\\ &=\sum_\alpha\langle\mathcal{O}^{\otimes n}\left|\sigma_n\left(z^+,z^-\right)\sigma_{-n}(1,1)|\alpha\rangle\langle\alpha|\sigma_n\left(z_5^+,z_5^-\right)\sigma_{-n}\left(z_6^+,z_6^-\right)\right|\mathcal{O}^{\otimes n}\rangle,\end{aligned} \tag{B.11}$$

where the sum runs over all possible intermediate states. However, in the $\varepsilon\to 0$ limit, $z^\pm$ approach 1, and since the OPE $\sigma_n(z)\sigma_{-n}(1)$ starts from the identity, one can consider the approximation of the six-point function as a product of four-point functions as follows

$$\begin{aligned}&\langle\mathcal{O}^{\otimes n}\left|\sigma_n\left(z^+,z^-\right)\sigma_{-n}(1,1)\sigma_n\left(z_5^+,z_5^-\right)\sigma_{-n}\left(z_6^+,z_6^-\right)\right|\mathcal{O}^{\otimes n}\rangle\\ &\simeq\langle\mathcal{O}^{\otimes n}\left|\sigma_n\left(z^+,z^-\right)\sigma_{-n}(1,1)|\mathcal{O}^{\otimes n}\rangle\langle\mathcal{O}^{\otimes n}|\sigma_n\left(z_5^+,z_5^-\right)\sigma_{-n}\left(z_6^+,z_6^-\right)\right|\mathcal{O}^{\otimes n}\rangle,\end{aligned} \tag{B.12}$$

in the $\varepsilon\to 0$ limit. Further by considering the conformal map

$$\tilde{z}^\pm\left(z^\pm\right)=\frac{\left(z_1^\pm-z^\pm\right)z_{64}^\pm}{z_{16}^\pm\left(z^\pm-z_4^\pm\right)} \tag{B.13}$$

to the second four-point function in (B.12), we obtain

$$\begin{aligned}
&\operatorname{tr}\rho_{\bar{C}}^{n}(t) \\
&= \left\{\left(\frac{\beta}{\pi\varepsilon_{UV}}\right)^{4}\sinh\left(\frac{\pi}{\beta}x_{65}^{+}\right)\sinh\left(\frac{\pi}{\beta}x_{65}^{-}\right)\sinh\left(\frac{\pi}{\beta}x_{32}^{+}\right)\sinh\left(\frac{\pi}{\beta}x_{32}^{-}\right)\right\}^{-2H_n} \\
&\quad\times\left((1-z^{+})(1-z^{-})\right)^{2H_n}\left\langle\mathcal{O}^{\otimes n}\left|\sigma_n\left(z^{+},z^{-}\right)\sigma_{-n}(1,1)\right|\mathcal{O}^{\otimes n}\right\rangle \\
&\quad\times\left(\left(1-\tilde{z}_5^{+}\right)\left(1-\tilde{z}_5^{-}\right)\right)^{2H_n}\left\langle\mathcal{O}^{\otimes n}\left|\sigma_n\left(\tilde{z}_5^{+},\tilde{z}_5^{-}\right)\sigma_{-n}(1,1)\right|\mathcal{O}^{\otimes n}\right\rangle .
\end{aligned} \tag{B.14}$$

In general, it is not easy to obtain a full analytic expression of the above four-point functions because they depend on the details of the dynamics of the CFT which we consider. Nevertheless, since we focus on the holographic CFT that has the large central charge $c \gg 1$ and the sparse spectrum, one can approximate the four-point functions by the vacuum Virasoro conformal block.

Furthermore, when we compute the von Neumann entropy by taking $n \to 1$ limit of the twist operators in the correlation function (B.14), it is enough to consider the Heavy-Heavy-Light-Light Virasoro block, since the conformal dimension of the twist and anti-twist operators approaches to 0, i.e., $H_n/c \to 0$ as $n \to 1$. In taking the limit, we fix the conformal dimension $h_{\mathcal{O}}$ of the local operator $\mathcal{O}$, which is assumed to be proportional to the central charge c. Under the limit, the dominant contribution of such a four-point function is given by [80]

$$\begin{aligned}
&\left(\left(1-z^{+}\right)\left(1-z^{-}\right)\right)^{2H_n}\left\langle\mathcal{O}^{\otimes n}\left|\sigma_n\left(z^{+},z^{-}\right)\sigma_{-n}(1,1)\right|\mathcal{O}^{\otimes n}\right\rangle \\
&\quad\simeq\left(\frac{(z^{+})^{\frac{1-\alpha}{2}}\left(1-(z^{+})^{\alpha}\right)(z^{-})^{\frac{1-\alpha}{2}}\left(1-(z^{-})^{\alpha}\right)}{\alpha^{2}(1-z^{+})(1-z^{-})}\right)^{-2H_n},
\end{aligned} \tag{B.15}$$

where $\alpha=\sqrt{1-\frac{24h_{\mathcal{O}}}{c}}=\sqrt{1-\frac{12\Delta}{c}}$. By substituting this result into (B.14) and taking the $n \to 1$ limit, we obtain the expression for the CFT von Neumann entropy $S[\bar{C}] = S_{\beta}[\bar{C}] + \Delta S[\bar{C}]$ with

$$
\begin{aligned}
S_\beta[\bar{C}] &= \frac{c}{6}\log\left[\left(\frac{\beta}{\pi\varepsilon_{UV}}\right)^4 \sinh\left(\frac{\pi}{\beta}x_{65}^+\right)\sinh\left(\frac{\pi}{\beta}x_{65}^-\right)\sinh\left(\frac{\pi}{\beta}x_{32}^+\right)\sinh\left(\frac{\pi}{\beta}x_{32}^-\right)\right] \\
\Delta S[\bar{C}] &= \frac{c}{6}\log\left[\frac{(z^+)^{\frac{1-\alpha}{2}}\left(1-(z^+)^\alpha\right)(z^-)^{\frac{1-\alpha}{2}}\left(1-(z^-)^\alpha\right)}{\alpha^2\left(1-z^+\right)\left(1-z^-\right)}\right] \\
&\quad + \frac{c}{6}\log\left[\frac{\left(\tilde{z}_5^+\right)^{\frac{1-\alpha}{2}}\left(1-\left(\tilde{z}_5^+\right)^\alpha\right)\left(\tilde{z}_5^-\right)^{\frac{1-\alpha}{2}}\left(1-\left(\tilde{z}_5^-\right)^\alpha\right)}{\alpha^2\left(1-\tilde{z}_5^+\right)\left(1-\tilde{z}_5^-\right)}\right].
\end{aligned}
\tag{B.16}
$$

$S_\beta[\bar{C}]$ is the CFT von Neumann entropy of the two intervals $\bar{C}_1 \cup \bar{C}_2$ at finite temperature $T = 1/\beta$, and $\Delta S[\bar{C}]$ is the contribution to the CFT von Neumann entropy from the perturbation by the local operator $\mathcal{O}$ [23].

The right-hand side of the expression (B.16) includes branch cuts, thus in order to make it well-defined, we need to choose the branch appropriately. One can archive this by demanding that the resulting von Neumann entropy is consistent with causality and positivity of the non-trivial part $\Delta S[\bar{C}]$. In imposing such conditions, it is helpful to consider the quasi-particle picture [51,56,57] for the time evolution of the von Neumann entropy under the local quench. The quasi-particle picture states the following: By the local quench, a pair of entangled quasi-particles is created at the operator insertion point, one of which propagates along one spatial direction at the speed of light, and the other does the opposite direction.

The non-trivial part of the CFT von Neumann entropy $\Delta S[\bar{C}]$ can be non-zero only in the case that one of such particles enters in the region $\bar{C}$ while the other does not [48–59]. This condition constrains branches which we should choose, because vanishing of the non-trivial part $\Delta S[\bar{C}] = 0$ is equivalent to choose the branch where $(z, z_5) \to 1$ in the $\varepsilon \to 0$ limit . If we have multiple branches which satisfy the above condition, the physical intuition coming from the holographic dual setup suggests that one should choose the one giving the minimal value of $\Delta S[\bar{C}]$ among candidates.

In our current setup, the causality condition requires that the CFT von Neumann entropy is vanishing in the following three cases: (1) the local operator is inserted in the domain of dependence of the intervals, i.e., $x_0 \in D[\bar{C}_1]$ or $x_0 \in D[\bar{C}_2]$ (2) the local operator is not inserted in these domains of dependence, but the right moving particle created by the local quench enters into the region $D[\bar{C}_2]$ and the left-moving one does in the region $D[\bar{C}_1]$. (3)

[23] Note that if we choose the other channel, then $S_\beta[\bar{C}]$ and $\Delta S[\bar{C}]$ take a different form.

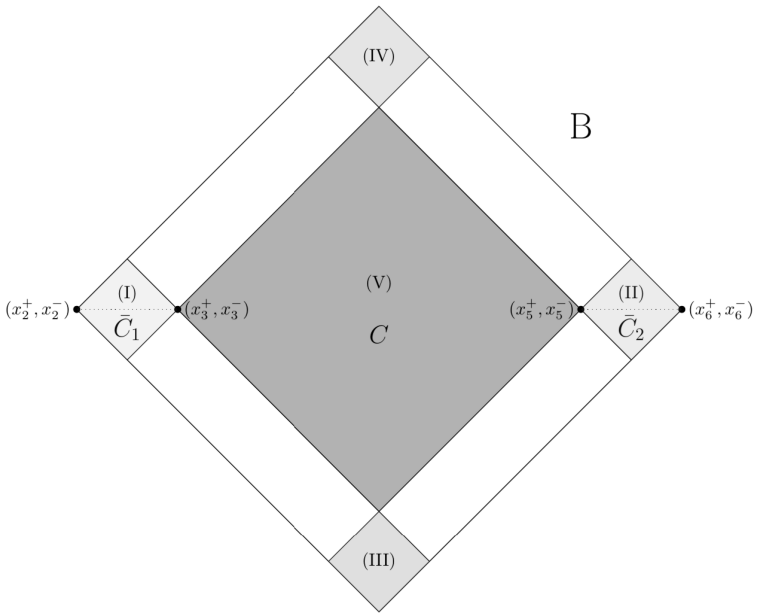

Figure 32: The regions in which $\Delta S[\bar{C}]$ must vanish. The shaded regions correspond to $(I) - (V)$.

the local operator is inserted in $D[C]$, where C is the complement region of $\bar{C}$.

More concretely, the conditions that the CFT von Neumann entropy should vanish in the above regions suggests that we should choose the branch $(z^+, z^-) \to (1, 1)$ and $(\tilde{z}_5^+, \tilde{z}_5^-) \to (1, 1)$ when the operator $\mathcal{O}$ is inserted in the below regions

(I) $D[\bar{C}_1]$: $x_0^+ < x_3^+$, $x_0^- < x_3^-$,

(II) $D[\bar{C}_2]$: $x_5^+ < x_0^+$, $x_5^- < x_0^-$,

(III) Union of the causal pasts of $D[\bar{C}_1]$ and $D[\bar{C}_2]$: $x_0^+ < x_3^+$, $x_5^- < x_0^-$,

(IV) Union of the causal futures of $D[\bar{C}_1]$ and $D[\bar{C}_2]$: $x_5^+ < x_0^+$, $x_0^- < x_3^-$,

(V) $D[C]$: $x_3^+ < x_0^+ < x_5^+$, $x_3^- < x_0^- < x_5^-$.

(See figure 32.) When the local operator is inserted in other regions, the expression of $\Delta S[\bar{C}]$ is given by suitable analytic continuations of (B.16) with respect to x_0 from the above regions $(I) - (V)$. By using the above standard

choices, we can specify branches on the other regions from the consistency of analytic continuation of $x_0^{\pm}$.

Let us take the region $x_0^+ < x_3^+$ and $x_3^- < x_0^- < x_5$ as an example of such a calculation and specify possible branch choices in the region. Starting from the three regions (I), (III) and (V) which are adjacent to the region $x_0^+ < x_3^+$ and $x_3^- < x_0^- < x_5^-$, we move the local operator $\mathcal{O}$ to the region $x_0^+ < x_3^+$ and $x_3^- < x_0^- < x_5^-$. We expand $z^{\pm}$ and $\tilde{z}_5^{\pm}$ to the first order in ε, which is very small compared to the inverse temperature β, and consider the change of their imaginary parts under the move. For the case (I), the imaginary part of z^- changes sign from plus to minus at $x_0^- = x_3^-$, but the others remain unchanged. In such a case, we choose the branches as $(z^+, z^-) \to (1, e^{2\pi i})$ and $(\tilde{z}_5^+, \tilde{z}_5^-) \to (1, 1)$. For the case (III), the imaginary part of $\tilde{z}_5^-$ changes sign from plus to minus $x_0^- = x_5^-$, but the others not. Similarly, we choose the branches as $(z^+, z^-) \to (1, 1)$ and $(\tilde{z}_5^+, \tilde{z}_5^-) \to (1, e^{2\pi i})$. For the case (V), the imaginary part of z^+ changes sign from minus to plus at $x_0^+ = x_3^+$, but the others not. In this case, we choose the branches as $(z^+, z^-) \to (e^{2\pi i}, 1)$ and $(\tilde{z}_5^+, \tilde{z}_5^-) \to (1, 1)$. From the above calculation, we have finished specifying possible branch choices in the region $x_0^+ < x_3^+$ and $x_3^- < x_0^- < x_5^-$.

Now that we have determined the branches in the region, we can get the analytic expression for $\Delta S[\bar{C}]$ in the region. Because each branch gives a different non-trivial part $\Delta S[\bar{C}]$ and as noted above we should choose the dominant contribution corresponding to the minimum $\Delta S[\bar{C}]$ among candidates in the region [53]. For example, we consider the region $x_0^+ < x_3^+$ and $x_3^- < x_0^- < x_5$, and evaluate $\Delta S[\bar{C}]$. In this region, $x_0^+ < x_3^+$ and $x_3^- < x_0^- < x_5^-$, we must compare the above three branch choices obtained from analytic continuation from the three regions (I), (III) and (V), and pick up the minimum among the three choices. As a result we get

$$\Delta S[\bar{C}] = \frac{c}{6} \log \left[\frac{\beta}{\pi\varepsilon} \frac{\sin \pi\alpha}{\alpha} \frac{\sinh\left(\frac{\pi}{\beta}\left(x_3^+ - x_0^+\right)\right) \sinh\left(\frac{\pi}{\beta}\left(x_0^+ - x_2^+\right)\right)}{\sinh\left(\frac{\pi}{\beta}\left(x_3^+ - x_2^+\right)\right)} \right] \quad \text{for the region } : x_0^+ < x_3^+ \text{ and } x_3^- < x_0^- < x_5^-. \tag{B.17}$$

By similar discussions, we can also obtain the expression of $\Delta S[\bar{C}]$ for the other regions. By combining all the results and $S_\beta[\bar{C}]$, we get the full expression for the entire region in the universe B.

Until now, we have considered the CFT von Neumann entropy of the two intervals. However, one can easily apply the above analysis to the single interval case by removing either region $\bar{C}_1$ or $\bar{C}_2$ and following similar discussions.

C The von Neumann Entropy of the naive Hawking Radiation, the Black hole and the Baby Universe

In this appendix, we evaluate the von Neumann entropy of various subsystems for the states (4.6) and (4.3) by using the relationship (4.5). In particular, we consider the following von Neumann entropy: (i) the naive Hawking radiation or the union of the black hole and the baby universe, $S(\rho_R) = S(\rho_{BH\cup BU})$; (ii) the naive Hawking radiation and the baby universe or the black hole $S(\rho_{R\cup BU}) = S(\rho_{BH})$; (iii) the baby universe or the union of the black hole and the naive Hawking radiation $S(\rho_{BU}) = S(\rho_{BH\cup R})$.

Before evaluating them, we note the relation between the pure state (4.6) and the mixed state (4.3), which are given by

$$\begin{aligned}\rho_{BH\cup R} &= \mathrm{tr}_{BU}\left[|\Phi\rangle\langle\Phi|_{BH\cup R\cup BU}\right] \\ &= \sum_M p_M |\Psi_M\rangle\langle\Psi_M|_{BH\cup R}.\end{aligned} \tag{C.1}$$

We also note that the probability distribution p_M is given by (e.g., [61, 62])

$$p_M = \left(\frac{\mathcal{N}k}{\pi}\right)^{\mathcal{N}k} \exp\left(-\mathcal{N}k\,\mathrm{tr}(C^M C^{M\dagger})\right), \tag{C.2}$$

and this probability distribution is normalized

$$\begin{aligned}\sum_M p_M &\to \left(\frac{\mathcal{N}k}{\pi}\right)^{\mathcal{N}k} \int \prod_{i,j=1}^{\mathcal{N}} \prod_{\alpha,\beta=1}^{k} dC^M_{i\alpha} dC^{\dagger M}_{\beta j} \ \exp\left(-\mathcal{N}k\,\mathrm{tr}(C^M C^{M\dagger})\right) \\ &= 1\end{aligned} \tag{C.3}$$

and gives the relationship (4.5). We give the above probability distribution explicitly, but in calculating the von Neumann entropy below, we do not use the relation (4.5) rather than the explicit form (C.2), .

C.1 The entropy of the naive Hawking radiation $S(\rho_R) = S(\rho_{BH\cup BU})$

In order to evaluate the von Neumann entropy of the naive Hawking radiation R, we focus on the reduced density matrix for the naive Hawking radiation.

It is given by

$$\begin{aligned}\rho_R &= \sum_M p_M \,\mathrm{tr}_{BH}\left[|\Psi_M\rangle\langle\Psi_M|_{BH\cup R}\right] \\ &= \sum_M p_M \,\rho_{(M)R} \\ &\equiv \langle\rho_{(M)R}\rangle_M,\end{aligned} \tag{C.4}$$

where in the second line we defined the following reduced density matrix

$$\begin{aligned}\rho_{(M)R} &= \mathrm{tr}_{BH}\left[|\Psi_M\rangle\langle\Psi_M|_{BH\cup R}\right] \\ &= \sum_{i=1}^{\mathcal{N}} \sum_{\alpha,\beta=1}^{k} C^M_{i\alpha} C^{\dagger M}_{\beta i} |\alpha\rangle\langle\beta|_R\end{aligned} \tag{C.5}$$

and in the last line to emphasize the ensemble average of the reduced density matrix $\rho_{(M)R}$ we introduced the notation $\langle\rho_{(M)R}\rangle_M$, which is defined by the second line. We note that such average operations are given by the relation (4.5).

Next we consider the following quantity of the above reduced density matrix

$$\begin{aligned}\mathrm{tr}_R\,\rho_R^n &= \sum_{M_1,M_2,\cdots,M_n} p_{M_1}p_{M_2}\cdots p_{M_n}\,\mathrm{tr}_R[\rho_{(M_1)R}\,\rho_{(M_2)R}\cdots\rho_{(M_n)R}] \\ &= \sum_{M_1,M_2,\cdots,M_n} p_{M_1}p_{M_2}\cdots p_{M_n} \\ &\qquad\qquad \times \sum_{i_1,i_2,\cdots,i_n=1}^{\mathcal{N}} \sum_{\alpha_1,\alpha_2,\cdots,\alpha_n=1}^{k} C^{M_1}_{i_1\alpha_1} C^{\dagger M_1}_{\alpha_2 i_1} C^{M_2}_{i_2\alpha_2} C^{\dagger M_2}_{\alpha_3 i_2}\cdots C^{M_n}_{i_n\alpha_n} C^{\dagger M_n}_{\alpha_1 i_n} \\ &= \sum_{i_1,i_2,\cdots,i_n=1}^{\mathcal{N}} \sum_{\alpha_1,\alpha_2,\cdots,\alpha_n=1}^{k} \langle C^{M_1}_{i_1\alpha_1} C^{\dagger M_1}_{\alpha_2 i_1}\rangle_{M_1} \langle C^{M_2}_{i_2\alpha_2} C^{\dagger M_2}_{\alpha_3 i_2}\rangle_{M_2}\cdots\langle C^{M_n}_{i_n\alpha_n} C^{\dagger M_n}_{\alpha_1 i_n}\rangle \\ &= \sum_{i_1,i_2,\cdots,i_n=1}^{\mathcal{N}} \sum_{\alpha_1,\alpha_2,\cdots,\alpha_n=1}^{k} \frac{1}{(k\mathcal{N})^n}\delta_{i_1 i_1}\delta_{\alpha_1\alpha_2}\delta_{i_2 i_2}\delta_{\alpha_2\alpha_3}\cdots\delta_{i_n i_n}\delta_{\alpha_n\alpha_1} \\ &= \frac{1}{k^{n-1}},\end{aligned} \tag{C.6}$$

where in the third line the labels $M_1,\cdots,M_n$ are distinguished, and we take the ensemble average for each factor, which consists of the same label M_s, and in the forth line we used the relation (4.5).

Thus we get the von Neumann entropy (4.7)

$$\begin{aligned} S(\rho_R) &= S(\langle \rho_{(M)R} \rangle_M) \\ &= -\lim_{n \to 1} \partial_n \operatorname{tr}_R \rho_R^n \\ &= \log k. \end{aligned} \tag{C.7}$$

This von Neumann entropy is equal to the Hawking's result, and it means the information paradox.

We note that since the total state (4.6) is pure, the above von Neumann entropy is equal to that of the the union of the black hole and the baby universe $BH \cup BU$

$$\begin{aligned} S(\rho_{BH \cup BU}) &= S(\rho_R) \\ &= \log k. \end{aligned} \tag{C.8}$$

C.2 The entropy of the naive Hawking radiation and the baby universe $S(\rho_{R \cup BU}) = S(\rho_{BH})$

Next, to obtain the von Neumann entropy of the union of the naive Hawking radiation and the baby universe $R \cup BU (= \mathbf{R})$, we focus on the reduced density matrix given by

$$\begin{aligned} \rho_{R \cup BU} &= \operatorname{tr}_{BH} \left[|\Phi\rangle\langle\Phi|_{BH \cup R \cup BU} \right] \\ &= \sum_{MN} \sqrt{p_M p_N} \left(\operatorname{tr}_{BH} |\Psi_M\rangle\langle\Psi_N|_{BH \cup R} \right) \otimes |M\rangle\langle N|_{BU} \\ &= \sum_{MN} \sqrt{p_M p_N} \sum_{i=1}^{\mathcal{N}} \sum_{\alpha,\beta=1}^{k} C_{i\alpha}^{M} C_{\beta i}^{\dagger N} |\alpha\rangle\langle\beta|_R \otimes |M\rangle\langle N|_{BU}. \end{aligned} \tag{C.9}$$

As in the previous case, we focus on the following quantity

$$\begin{aligned}
\mathrm{tr}_{R\cup BU}\,\rho_{R\cup BU}^n &= \sum_{M_1,M_2,\cdots,M_n} p_{M_1}p_{M_2}\cdots p_{M_n} \\
&\quad\times \mathrm{tr}_R\left[(\mathrm{tr}_{BH}\,|\Psi_{M_1}\rangle\langle\Psi_{M_2}|)(\mathrm{tr}_{BH}\,|\Psi_{M_2}\rangle\langle\Psi_{M_3}|)\cdots(\mathrm{tr}_{BH}\,|\Psi_{M_n}\rangle\langle\Psi_{M_1}|)\right] \\
&= \sum_{M_1,M_2,\cdots,M_n} p_{M_1}p_{M_2}\cdots p_{M_n} \\
&\qquad\times \sum_{i_1,i_2,\cdots,i_n=1}^{\mathcal{N}} \sum_{\alpha_1,\alpha_2,\cdots,\alpha_n=1}^{k} C_{i_1\alpha_1}^{M_1} C_{\alpha_2 i_1}^{\dagger M_2} C_{i_2\alpha_2}^{M_2} C_{\alpha_3 i_2}^{\dagger M_3}\cdots C_{i_n\alpha_n}^{M_n} C_{\alpha_1 i_n}^{\dagger M_1} \\
&= \sum_{i_1,i_2,\cdots,i_n=1}^{\mathcal{N}} \sum_{\alpha_1,\alpha_2,\cdots,\alpha_n=1}^{k} \\
&\quad\times \langle C_{\alpha_1 i_n}^{\dagger M_1} C_{i_1\alpha_1}^{M_1}\rangle_{M_1}\langle C_{\alpha_2 i_1}^{\dagger M_2} C_{i_2\alpha_2}^{M_2}\rangle_{M_2}\langle C_{\alpha_3 i_2}^{\dagger M_3} C_{i_3\alpha_3}^{M_3}\rangle_{M_3}\cdots\langle C_{\alpha_n i_{n-1}}^{\dagger M_n} C_{i_n\alpha_n}^{M_n}\rangle_{M_n} \\
&= \sum_{i_1,i_2,\cdots,i_n=1}^{\mathcal{N}} \sum_{\alpha_1,\alpha_2,\cdots,\alpha_n=1}^{k} \frac{1}{(k\mathcal{N})^n}\delta_{i_n i_1}\delta_{\alpha_1\alpha_1}\delta_{i_1 i_2}\delta_{\alpha_2\alpha_2}\cdots\delta_{i_{n-1}i_n}\delta_{\alpha_n\alpha_n} \\
&= \frac{1}{\mathcal{N}^{n-1}},
\end{aligned} \tag{C.10}$$

where in the fourth line we used the relation (4.5). We note that $\mathcal{N} = e^{S_{BH}}$.

From the above result, we get the von Neumann entropy of the union of the naive Hawking radiation and the baby universe (4.9)

$$\begin{aligned}
S(\rho_{R\cup BU}) &= -\lim_{n\to 1}\partial_n\,\mathrm{tr}_{R\cup BU}\,\rho_{R\cup BU}^n \\
&= \log\mathcal{N} \\
&= S_{BH}.
\end{aligned} \tag{C.11}$$

We note that the above von Neumann entropy is also equal to that of the black hole BH

$$\begin{aligned}
S(\rho_{BH}) &= S(\rho_{R\cup BU}) \\
&= S_{BH}.
\end{aligned} \tag{C.12}$$

C.3 The entropy of the baby universe $S(\rho_{BU}) = S(\rho_{BH\cup R})$

Finally, to obtain the von Neumann entropy of the baby universe BU, we focus on the reduced density matrix given by

$$\begin{aligned}\rho_{BU} &= \mathrm{tr}_{BH\cup R}\left[|\Phi\rangle\langle\Phi|_{BH\cup R\cup BU}\right] \\ &= \sum_{MN}\sqrt{p_M p_N}\left(\mathrm{tr}_{BH\cup R}\,|\Psi_M\rangle\langle\Psi_N|_{BH\cup R}\right)\otimes|M\rangle\langle N|_{BU} \\ &= \sum_{MN}\sqrt{p_M p_N}\sum_{i=1}^{\mathcal{N}}\sum_{\alpha=1}^{k} C^{M}_{i\alpha}C^{\dagger N}_{\alpha i}|M\rangle\langle N|_{BU}.\end{aligned} \tag{C.13}$$

Then we get

$$\begin{aligned}\mathrm{tr}_{BU}\,\rho^n_{BU} &= \sum_{M_1,M_2,\cdots,M_n} p_{M_1}p_{M_2}\cdots p_{M_n} \\ &\qquad\times\sum_{i_1,i_2,\cdots,i_n=1}^{\mathcal{N}}\sum_{\alpha_1,\alpha_2,\cdots,\alpha_n=1}^{k} C^{M_1}_{i_1\alpha_1}C^{\dagger M_2}_{\alpha_1 i_1}C^{M_2}_{i_2\alpha_2}C^{\dagger M_3}_{\alpha_2 i_2}\cdots C^{M_n}_{i_n\alpha_n}C^{\dagger M_1}_{\alpha_n i_n} \\ &= \sum_{i_1,i_2,\cdots,i_n=1}^{\mathcal{N}}\sum_{\alpha_1,\alpha_2,\cdots,\alpha_n=1}^{k} \\ &\qquad\times\langle C^{\dagger M_1}_{\alpha_n i_n}C^{M_1}_{i_1\alpha_1}\rangle_{M_1}\langle C^{\dagger M_2}_{\alpha_1 i_1}C^{M_2}_{i_2\alpha_2}\rangle_{M_2}\langle C^{\dagger M_3}_{\alpha_2 i_2}C^{M_3}_{i_3\alpha_3}\rangle_{M_3}\cdots\langle C^{\dagger M_n}_{\alpha_{n-1}i_{n-1}}C^{M_n}_{i_n\alpha_n}\rangle_{M_n} \\ &= \sum_{i_1,i_2,\cdots,i_n=1}^{\mathcal{N}}\sum_{\alpha_1,\alpha_2,\cdots,\alpha_n=1}^{k}\frac{1}{(k\mathcal{N})^n}\delta_{i_n i_1}\delta_{\alpha_n\alpha_1}\delta_{i_1 i_2}\delta_{\alpha_1\alpha_2}\cdots\delta_{i_{n-1}i_n}\delta_{\alpha_{n-1}\alpha_n} \\ &= \frac{1}{(k\mathcal{N})^{n-1}},\end{aligned} \tag{C.14}$$

where in the third line we used the rule (4.5).

From the above result, we obtain the von Neumann entropy of the baby universe

$$\begin{aligned}S(\rho_{BU}) &= -\lim_{n\to 1}\partial_n\,\mathrm{tr}_{BU}\,\rho^n_{BU} \\ &= \log(k\mathcal{N}) \\ &= S_{BH}+\log k.\end{aligned} \tag{C.15}$$

This is equal to the von Neumann entropy of the union of the black hole and the Hawking radiation $BH\cup R$

$$\begin{aligned}S(\rho_{BH\cup R}) &= S(\rho_{BU}) \\ &= S_{BH}+\log k.\end{aligned} \tag{C.16}$$

References

[1] S. W. Hawking, *Black hole explosions*, *Nature* **248** (1974) 30–31.

[2] S. W. Hawking, *Particle Creation by Black Holes*, *Commun. Math. Phys.* **43** (1975) 199–220. [Erratum: Commun.Math.Phys. 46, 206 (1976)].

[3] J. D. Bekenstein, *Black holes and entropy*, *Phys. Rev. D* **7** (1973) 2333–2346.

[4] J. D. Bekenstein, *Generalized second law of thermodynamics in black hole physics*, *Phys. Rev. D* **9** (1974) 3292–3300.

[5] D. N. Page, *Information in black hole radiation*, *Phys. Rev. Lett.* **71** (1993) 3743–3746, [hep-th/9306083].

[6] S. Ryu and T. Takayanagi, *Holographic derivation of entanglement entropy from AdS/CFT*, *Phys. Rev. Lett.* **96** (2006) 181602, [hep-th/0603001].

[7] S. Ryu and T. Takayanagi, *Aspects of Holographic Entanglement Entropy*, *JHEP* **08** (2006) 045, [hep-th/0605073].

[8] V. E. Hubeny, M. Rangamani, and T. Takayanagi, *A Covariant holographic entanglement entropy proposal*, *JHEP* **07** (2007) 062, [arXiv:0705.0016].

[9] T. Faulkner, A. Lewkowycz, and J. Maldacena, *Quantum corrections to holographic entanglement entropy*, *JHEP* **11** (2013) 074, [arXiv:1307.2892].

[10] N. Engelhardt and A. C. Wall, *Quantum Extremal Surfaces: Holographic Entanglement Entropy beyond the Classical Regime*, *JHEP* **01** (2015) 073, [arXiv:1408.3203].

[11] J. M. Maldacena, *The Large N limit of superconformal field theories and supergravity*, *Adv. Theor. Math. Phys.* **2** (1998) 231–252, [hep-th/9711200].

[12] G. Penington, *Entanglement Wedge Reconstruction and the Information Paradox*, *JHEP* **09** (2020) 002, [arXiv:1905.08255].

[13] A. Almheiri, N. Engelhardt, D. Marolf, and H. Maxfield, *The entropy of bulk quantum fields and the entanglement wedge of an evaporating black hole*, *JHEP* **12** (2019) 063, [arXiv:1905.08762].

[14] A. Almheiri, R. Mahajan, J. Maldacena, and Y. Zhao, *The Page curve of Hawking radiation from semiclassical geometry*, *JHEP* **03** (2020) 149, [arXiv:1908.10996].

[15] A. Almheiri, T. Hartman, J. Maldacena, E. Shaghoulian, and A. Tajdini, *The entropy of Hawking radiation*, *Rev. Mod. Phys.* **93** (2021), no. 3 035002, [arXiv:2006.06872].

[16] D. L. Jafferis, A. Lewkowycz, J. Maldacena, and S. J. Suh, *Relative entropy equals bulk relative entropy*, *JHEP* **06** (2016) 004, [arXiv:1512.06431].

[17] X. Dong, D. Harlow, and A. C. Wall, *Reconstruction of Bulk Operators within the Entanglement Wedge in Gauge-Gravity Duality*, *Phys. Rev. Lett.* **117** (2016), no. 2 021601, [arXiv:1601.05416].

[18] A. Hamilton, D. N. Kabat, G. Lifschytz, and D. A. Lowe, *Local bulk operators in AdS/CFT: A Boundary view of horizons and locality*, *Phys. Rev. D* **73** (2006) 086003, [hep-th/0506118].

[19] A. Hamilton, D. N. Kabat, G. Lifschytz, and D. A. Lowe, *Holographic representation of local bulk operators*, *Phys. Rev. D* **74** (2006) 066009, [hep-th/0606141].

[20] J. Cotler, P. Hayden, G. Penington, G. Salton, B. Swingle, and M. Walter, *Entanglement Wedge Reconstruction via Universal Recovery Channels*, *Phys. Rev. X* **9** (2019), no. 3 031011, [arXiv:1704.05839].

[21] C.-F. Chen, G. Penington, and G. Salton, *Entanglement Wedge Reconstruction using the Petz Map*, *JHEP* **01** (2020) 168, [arXiv:1902.02844].

[22] T. Faulkner and A. Lewkowycz, *Bulk locality from modular flow*, *JHEP* **07** (2017) 151, [arXiv:1704.05464].

[23] T. Faulkner, M. Li, and H. Wang, *A modular toolkit for bulk reconstruction*, *JHEP* **04** (2019) 119, [arXiv:1806.10560].

[24] G. Penington, S. H. Shenker, D. Stanford, and Z. Yang, *Replica wormholes and the black hole interior*, arXiv:1911.11977.

[25] V. Balasubramanian, A. Kar, and T. Ugajin, *Entanglement between two disjoint universes*, *JHEP* **02** (2021) 136, [arXiv:2008.05274].

[26] V. Balasubramanian, A. Kar, and T. Ugajin, *Islands in de Sitter space*, *JHEP* **02** (2021) 072, [arXiv:2008.05275].

[27] A. Miyata and T. Ugajin, *Evaporation of black holes in flat space entangled with an auxiliary universe*, arXiv:2104.00183.

[28] C. G. Callan, Jr., S. B. Giddings, J. A. Harvey, and A. Strominger, *Evanescent black holes*, *Phys. Rev. D* **45** (1992), no. 4 R1005, [hep-th/9111056].

[29] N. Iizuka, A. Miyata, and T. Ugajin, *A comment on a fine-grained description of evaporating black holes with baby universes*, arXiv:2111.07107.

[30] H. Geng, A. Karch, C. Perez-Pardavila, S. Raju, L. Randall, M. Riojas, and S. Shashi, *Inconsistency of Islands in Theories with Long-Range Gravity*, arXiv:2107.03390.

[31] A. Almheiri, R. Mahajan, and J. Maldacena, *Islands outside the horizon*, arXiv:1910.11077.

[32] A. Almheiri, T. Hartman, J. Maldacena, E. Shaghoulian, and A. Tajdini, *Replica Wormholes and the Entropy of Hawking Radiation*, *JHEP* **05** (2020) 013, [arXiv:1911.12333].

[33] T. J. Hollowood and S. P. Kumar, *Islands and Page Curves for Evaporating Black Holes in JT Gravity*, *JHEP* **08** (2020) 094, [arXiv:2004.14944].

[34] K. Goto, T. Hartman, and A. Tajdini, *Replica wormholes for an evaporating 2D black hole*, *JHEP* **04** (2021) 289, [arXiv:2011.09043].

[35] J. Maldacena, D. Stanford, and Z. Yang, *Conformal symmetry and its breaking in two dimensional Nearly Anti-de-Sitter space*, *PTEP* **2016** (2016), no. 12 12C104, [arXiv:1606.01857].

[36] I. Heemskerk, J. Penedones, J. Polchinski, and J. Sully, *Holography from Conformal Field Theory*, *JHEP* **10** (2009) 079, [arXiv:0907.0151].

[37] A. Almheiri and J. Polchinski, *Models of AdS_2 backreaction and holography*, *JHEP* **11** (2015) 014, [arXiv:1402.6334].

[38] R. B. Mann, *Conservation laws and 2-D black holes in dilaton gravity*, *Phys. Rev. D* **47** (1993) 4438–4442, [hep-th/9206044].

[39] A. Kitaev, "A simple model of quantum holography.." http://online.kitp.ucsb.edu/online/entangled15/kitaev/,http://online.kitp.ucsb.edu/online/entangled15/kitaev2/.

[40] P. Calabrese and J. Cardy, *Entanglement entropy and conformal field theory*, *J. Phys. A* **42** (2009) 504005, [arXiv:0905.4013].

[41] H. Casini, C. D. Fosco, and M. Huerta, *Entanglement and alpha entropies for a massive Dirac field in two dimensions*, *J. Stat. Mech.* **0507** (2005) P07007, [cond-mat/0505563].

[42] F. F. Gautason, L. Schneiderbauer, W. Sybesma, and L. Thorlacius, *Page Curve for an Evaporating Black Hole*, *JHEP* **05** (2020) 091, [arXiv:2004.00598].

[43] T. Anegawa and N. Iizuka, *Notes on islands in asymptotically flat 2d dilaton black holes*, *JHEP* **07** (2020) 036, [arXiv:2004.01601].

[44] K. Hashimoto, N. Iizuka, and Y. Matsuo, *Islands in Schwarzschild black holes*, *JHEP* **06** (2020) 085, [arXiv:2004.05863].

[45] T. Hartman, E. Shaghoulian, and A. Strominger, *Islands in Asymptotically Flat 2D Gravity*, *JHEP* **07** (2020) 022, [arXiv:2004.13857].

[46] Y. Chen, V. Gorbenko, and J. Maldacena, *Bra-ket wormholes in gravitationally prepared states*, *JHEP* **02** (2021) 009, [arXiv:2007.16091].

[47] T. Hartman, Y. Jiang, and E. Shaghoulian, *Islands in cosmology*, *JHEP* **11** (2020) 111, [arXiv:2008.01022].

[48] P. Caputa, M. Nozaki, and T. Takayanagi, *Entanglement of local operators in large-N conformal field theories*, *PTEP* **2014** (2014) 093B06, [arXiv:1405.5946].

[49] J. R. David, S. Khetrapal, and S. P. Kumar, *Universal corrections to entanglement entropy of local quantum quenches*, *JHEP* **08** (2016) 127, [arXiv:1605.05987].

[50] P. Caputa, J. Simón, A. Štikonas, T. Takayanagi, and K. Watanabe, *Scrambling time from local perturbations of the eternal BTZ black hole*, *JHEP* **08** (2015) 011, [arXiv:1503.08161].

[51] P. Calabrese and J. Cardy, *Entanglement and correlation functions following a local quench: a conformal field theory approach*, *J. Stat. Mech.* **0710** (2007), no. 10 P10004, [arXiv:0708.3750].

[52] M. Nozaki, T. Numasawa, and T. Takayanagi, *Holographic Local Quenches and Entanglement Density*, *JHEP* **05** (2013) 080, [arXiv:1302.5703].

[53] C. T. Asplund, A. Bernamonti, F. Galli, and T. Hartman, *Holographic Entanglement Entropy from 2d CFT: Heavy States and Local Quenches*, *JHEP* **02** (2015) 171, [arXiv:1410.1392].

[54] T. Ugajin, *Two dimensional quantum quenches and holography*, arXiv:1311.2562.

[55] C. T. Asplund and A. Bernamonti, *Mutual information after a local quench in conformal field theory*, *Phys. Rev. D* **89** (2014), no. 6 066015, [arXiv:1311.4173].

[56] M. Nozaki, T. Numasawa, and T. Takayanagi, *Quantum Entanglement of Local Operators in Conformal Field Theories*, *Phys. Rev. Lett.* **112** (2014) 111602, [arXiv:1401.0539].

[57] M. Nozaki, *Notes on Quantum Entanglement of Local Operators*, *JHEP* **10** (2014) 147, [arXiv:1405.5875].

[58] P. Caputa, J. Simón, A. Štikonas, and T. Takayanagi, *Quantum Entanglement of Localized Excited States at Finite Temperature*, *JHEP* **01** (2015) 102, [arXiv:1410.2287].

[59] T. Hartman, S. Jain, and S. Kundu, *Causality Constraints in Conformal Field Theory*, *JHEP* **05** (2016) 099, [arXiv:1509.00014].

[60] M. A. Nielsen and I. L. Chuang, *Quantum Computation and Quantum Information*. Cambridge University Press, 2000.

[61] J. Kudler-Flam, V. Narovlansky, and S. Ryu, *Distinguishing Random and Black Hole Microstates*, *PRX Quantum* **2** (2021), no. 4 040340, [arXiv:2108.00011].

[62] J. Kudler-Flam, *Relative Entropy of Random States and Black Holes*, *Phys. Rev. Lett.* **126** (2021), no. 17 171603, [arXiv:2102.05053].

[63] E. Verlinde and H. Verlinde, *Black Hole Entanglement and Quantum Error Correction*, *JHEP* **10** (2013) 107, [arXiv:1211.6913].

[64] K. Langhoff and Y. Nomura, *Ensemble from Coarse Graining: Reconstructing the Interior of an Evaporating Black Hole*, *Phys. Rev. D* **102** (2020), no. 8 086021, [arXiv:2008.04202].

[65] Y. Nomura, *Black Hole Interior in Unitary Gauge Construction*, *Phys. Rev. D* **103** (2021), no. 6 066011, [arXiv:2010.15827].

[66] J. Maldacena and L. Susskind, *Cool horizons for entangled black holes*, *Fortsch. Phys.* **61** (2013) 781–811, [arXiv:1306.0533].

[67] V. Balasubramanian, D. Marolf, and M. Rozali, *Information Recovery From Black Holes*, *Gen. Rel. Grav.* **38** (2006) 1529–1536, [hep-th/0604045].

[68] J. M. Maldacena, *Eternal black holes in anti-de Sitter*, *JHEP* **04** (2003) 021, [hep-th/0106112].

[69] P. Saad, S. H. Shenker, and D. Stanford, *JT gravity as a matrix integral*, arXiv:1903.11115.

[70] S. R. Coleman, *Black Holes as Red Herrings: Topological Fluctuations and the Loss of Quantum Coherence*, *Nucl. Phys. B* **307** (1988) 867–882.

[71] S. B. Giddings and A. Strominger, *Loss of Incoherence and Determination of Coupling Constants in Quantum Gravity*, *Nucl. Phys. B* **307** (1988) 854–866.

[72] S. B. Giddings and A. Strominger, *Baby Universes, Third Quantization and the Cosmological Constant*, *Nucl. Phys. B* **321** (1989) 481–508.

[73] D. Marolf and H. Maxfield, *Observations of Hawking radiation: the Page curve and baby universes*, *JHEP* **04** (2021) 272, [arXiv:2010.06602].

[74] C. Chowdhury, V. Godet, O. Papadoulaki, and S. Raju, *Holography from the Wheeler-DeWitt equation*, arXiv:2107.14802.

[75] C. Akers, N. Engelhardt, and D. Harlow, *Simple holographic models of black hole evaporation*, *JHEP* **08** (2020) 032, [arXiv:1910.00972].

[76] D. Marolf and H. Maxfield, *Transcending the ensemble: baby universes, spacetime wormholes, and the order and disorder of black hole information*, *JHEP* **08** (2020) 044, [arXiv:2002.08950].

[77] E. Gesteau and M. J. Kang, *Holographic baby universes: an observable story*, arXiv:2006.14620.

[78] P. Calabrese and J. L. Cardy, *Entanglement entropy and quantum field theory*, *J. Stat. Mech.* **0406** (2004) P06002, [hep-th/0405152].

[79] J. D. Brown and M. Henneaux, *Central Charges in the Canonical Realization of Asymptotic Symmetries: An Example from Three-Dimensional Gravity*, *Commun. Math. Phys.* **104** (1986) 207–226.

[80] A. L. Fitzpatrick, J. Kaplan, and M. T. Walters, *Universality of Long-Distance AdS Physics from the CFT Bootstrap*, *JHEP* **08** (2014) 145, [arXiv:1403.6829].